

Linköping Studies in Science and Technology
Dissertations, No. 1669

Evaluation, Generation, and Transformation of Driving Cycles

Peter Nyberg



Linköping University
INSTITUTE OF TECHNOLOGY

Department of Electrical Engineering
Linköping 2015

Linköping Studies in Science and Technology
Dissertations, No. 1669

Peter Nyberg
`peter.nyberg@liu.se`
`www.vehicular.isy.liu.se`
Division of Vehicular Systems
Department of Electrical Engineering
Linköping University
SE-581 83 Linköping, Sweden

Copyright © 2015 Peter Nyberg, unless otherwise noted.
All rights reserved.

Nyberg, Peter
Evaluation, Generation, and Transformation of Driving Cycles
ISBN 978-91-7519-065-5
ISSN 0345-7524

Cover photo by Ryan McGuire. Available at pixabay.com and bound to the Creative Commons Deed CC0.

Typeset with L^AT_EX 2_ε
Printed by LiU-Tryck, Linköping, Sweden 2015

To Eva

ABSTRACT

Driving cycles are important components for evaluation and design of vehicles. They determine the focus of vehicle manufacturers, and indirectly they affect the environmental impact of vehicles since the vehicle control system is usually tuned to one or several driving cycles. Thus, the driving cycle affects the design of the vehicle since cost, fuel consumption, and emissions all depend on the driving cycle used for design. Since the existing standard driving cycles cannot keep up with the changing road infrastructure, the changing vehicle fleet composition, and the growing number of vehicles on the road, which do all cause changes in the driver behavior, the need to get new and representative driving cycles are increasing. A research question is how to generate these new driving cycles so that they are both representative and at the same time have certain equivalence properties, to make fair comparisons of the performance results. Besides generation, another possibility to get more driving cycles is to transform the existing ones into new, different, driving cycles considering equivalence constraints.

With the development of new powertrain concepts the need for evaluation will increase, and an interesting question is how to utilize new developments in dynamometer technology together with new possibilities for connecting equipment. Here a pedal robot is developed to be used in a vehicle mounted in a chassis dynamometer and the setup is used for co-simulation together with a moving base simulator that is connected with a communication line. The results show that the co-simulation can become a realistic driving experience and a viable option for dangerous tests and a complement to tests on a dedicated track or on-road tests, if improvements on the braking and the vehicle feedback to the driver are implemented.

The problem of generating representative driving cycles, with specified excitation at the wheels, is approached with a combined two-step method. A Markov chain approach is used to generate candidate driving cycles that are then transformed to equivalent driving cycles with respect to the mean tractive force components, which are the used measures. Using an optimization methodology the transformation of driving cycles is formulated as a nonlinear program with constraints and a cost function to minimize. The nonlinear program formulation can handle a wide range of constraints, e.g., the mean tractive force components, different power measures, or available energy for recuperation, and using the vehicle jerk as cost function gives good drivability.

In conclusion, methods for driving cycle design have been proposed where new driving cycles can either be generated from databases, or given driving cycles can be transformed to fulfill certain equivalence constraints, approaching the important problem of similar but not the same. The combination of these approaches yields a stochastic and general method to generate driving cycles with equivalence properties that can be used at several instances during the product development process of vehicles. Thus, a powerful and effective engineering tool has been developed.

POPULÄRVETENSKAPLIG SAMMANFATTNING

Enligt världshälsoorganisationen, WHO, dör miljontals människor i förtid till följd av luftföroreningar och en betydande del av dessa föroreningar kommer från utsläpp från transportsektorn. En förbättring av emissionsutsläppen och även bränsleförbrukningen för fordon ger således renare luft att andas och samtidigt kommer fordon att kunna köras längre mellan tankningarna.

Under en bilresa mellan hemmet och jobbet kommer bilen ha olika hastigheter vid olika tidpunkter. Denna hastighetsprofil kallas för en körcykel och för att säkerställa att biltillverkarna följer emissionslagstiftningen i Europa så behöver olika biltyper testas i en förutbestämd körcykel. Under ett sådant test mäts bland annat bränsleförbrukningen och den används av bilförsäljare, samt för beräkning av den årliga fordonsskatten. Hur körcykeln ser ut spelar stor roll för vilken bränsleförbrukning som fås i mätningen. Olika körcykler är olika krävande och ju mer krävande en körcykel är, desto högre blir bränsleförbrukningen. Detta innebär också att det i dagsläget är svårt att jämföra körcykler med varandra eftersom de påverkar fordonet på olika sätt.

Om en körcykel speglar hur människor normalt kör sina bilar på vägen kallas körcykeln för representativ. Körbeteendet påverkas av att nya vägar byggs, vi får snabbare fordon, nya koncept som hybrid- och elbilar utvecklas samt att det i stora delar av världen kommer allt fler fordon ut i trafiken. Detta innebär att även om en viss körcykel är representativ idag, så behöver den inte vara det i framtiden. Ett annat problem är då biltillverkarna använder sig av en specifik körcykel i en allt för stor utsträckning vid utveckling av styrsystemet. Detta kan leda till att fordonet blir mer anpassat till själva körcykeln än den verkliga användningen. Om körcykeln dessutom inte är representativ så finns det en överhängande risk att bilen får högre bränsleförbrukning vid verklig körning än vad testerna visar.

För att angripa dessa problem har det i denna avhandling tagits fram metoder dels för att generera nya körcykler och dels för att transformera de befintliga körcyklerna på ett sådant sätt att de nya körcyklerna både är representativa, samt har vissa egenskaper som gör att testresultat från de enklare kan jämföras med varandra. Kombinationen av dessa metoder ger fordonstillverkare nya möjligheter att skapa nya körcykler som kan användas vid utvecklingen av framtidens fordon.

I takt med att nya tekniska lösningar på fordonssidan presenteras ökar behovet av tester. Om till exempel en bil utrustas med ett specifikt förarstödsystem så är det viktigt att föraren känner förtroende för systemet. Ett nytt sätt att utvärdera sådana stödsystem på ett realistiskt sätt i en kontrollerad miljö som är säker för föraren och ger möjlighet till upprepade experiment, är att använda sig av en avancerad körsimulator hos VTI som är kopplad till en chassidynamometer med monterad bil i fordonslaboratoriet vid Linköpings universitet. Detta innebär att föraren upplever en riktig drivlina istället för en modell av den. En annan fördel av en sådan uppställning är att fordonet kommer att uppleva realistiska krafter eftersom körupplevelsen i körsimulatorens är nära verklig körning. Detta kan till exempel utnyttjas vid utvärdering av nya styrningsalgoritmer i fordonet.

ACKNOWLEDGMENTS

This work has been carried out at the Division of Vehicular Systems at the Department of Electrical Engineering, Linköping University.

First of all, I would like to express my gratitude to my supervisors Lars Nielsen and Erik Frisk for the guidance and invaluable support during my Ph.D. studies.

I would like to thank Lars Eriksson for his inspiration in the field of research, it sparked an interest which finally led me to apply for a Ph.D. position. I am also grateful to Lars Nielsen for letting me join the Vehicular Systems group. A special thank of mine goes to my colleagues who have created a pleasant atmosphere at work, and you never know what kind of discussion topics that will pop up during the coffee breaks.

Per Öberg and Erik Frisk are acknowledged for all the computer-related support and the administrators Maria Hammér and her predecessor Maria Hoffstedt both have been a helping hand during my time here. My thanks also goes to my roommate Kristoffer Lundahl for the company and all the discussions we have had. Åse Johansson and Eva Broman are acknowledged for proofreading parts of the thesis.

The financial support from the Swedish Hybrid Vehicle Centre, the Linnaeus Center CADICS, and the industrial partners are acknowledged. I would like to thank Tomas Nilsson, Christofer Sundström, Erik Frisk, and Mattias Krysander for our joint work related to the usage of wheel loaders. My thanks also go to Anders Andersson, Håkan Sehammar, and Per Öberg for their work in our joint paper.

I would like to express my warm thanks to my family and friends for all the good times we have had, and I hope we will continue to have many good times in the future. All of you mean a lot to me!

Last but definitely not least, I would like to express my greatest gratitude to the love of my life Eva for letting me know that there is more to life than just to work and write papers. Your support, encouragement, and love means everything to me and I will always be by your side.

Peter Nyberg
April 2015
Linköping, Sweden

Contents

1	Introduction	1
1.1	Generation and Transformation of Driving Cycles	4
1.2	Test Platforms for Evaluation of Vehicles	6
1.3	Contributions	9
1.4	Publications	10
1.5	Outlook	11
1.6	Concluding Remark	12
	References	13
	Papers	19
A	A New Chassis Dynamometer Laboratory for Vehicle Research	21
1	Introduction	24
2	Background	25
3	Laboratory Overview	26
3.1	The Vehicle Propulsion Laboratory	27
3.2	Equipment	28
4	Dynamometer System	30
4.1	System Description	30
4.2	Dynamometer Performance	31
4.3	Mounting Procedure	33
4.4	Test Modes	33
5	Performed Studies	36
5.1	Modeling of Engine and Driveline Related Disturbances on the Wheel Speed in Passenger Cars	37
5.2	Modeling and Control of Co-Surge in Bi-Turbo Engines	37
5.3	Formula Student, Mapping	40
5.4	Chassis Dynamometer Road Force Co-Simulation with a Moving Base Simulator	40
6	Future Projects Aims and Goals	42
7	Summary	43
	References	44

B	Vehicle Powertrain Test Bench Co-Simulation with a Moving Base Simulator Using a Pedal Robot	45
1	Introduction	48
2	Experimental Setup	48
2.1	Chassis Dynamometer Lab	49
2.2	VTI Simulator III	53
2.3	Pedal Robot	54
2.4	Connection Between Facilities	57
2.5	Synchronizing Vehicle Models	57
2.6	Driving Mission	59
3	Results	60
3.1	Network Performance	60
3.2	Step Response Tests of Pedal Robot	61
3.3	Running the Complete System	62
4	Conclusions	67
	References	68
C	Using Real-World Driving Databases to Generate Driving Cycles with Equivalence Properties	69
1	Introduction	72
1.1	Related Work	72
1.2	Outline of Ideas and Paper	74
2	Mean Tractive Force	75
3	Equivalent Driving Cycles	77
4	Fuel Consumption Investigation	78
4.1	Experimental Setup	78
4.2	Correlation of the MTF Components to Fuel Consumption	81
5	Driving Cycle Generation	84
5.1	Real-World Driving Cycles	85
5.2	Markov Chains and the Transition Probability Matrix	86
5.3	Selection Criterion	89
5.4	Transformation to Equivalent Driving Cycles	90
5.5	Method Summary	91
6	Results	91
6.1	Discussion	94
7	Conclusions	95
	References	97
D	Driving Cycle Equivalence and Transformation	99
1	Introduction	102
1.1	Related Work	103
1.2	Outline	104
2	Characterization of Driving Cycles	105
2.1	Vehicle Model	105
2.2	Vehicle Operating Modes	106

- 2.3 Mean Tractive Force Components 106
- 2.4 Power and Energy Demand 108
- 3 Driving Cycle Equivalence 108
- 4 Problem Formulation 109
 - 4.1 Transformable and Invariant Sets of the Driving Cycle . . 109
 - 4.2 Fundamental Problem and Three Problem Instances . . . 110
- 5 Method: Numerical Optimization Approach 111
 - 5.1 Constraints for Keeping the Traction and Non-Traction Regions 112
 - 5.2 Constraints from Maximum Acceleration 113
 - 5.3 Constraints from Vehicle Excitation 114
 - 5.4 Power and Energy Recuperation Constraints 115
 - 5.5 Constraints on the Speed Profile 116
 - 5.6 Cost Function 116
 - 5.7 Method Summary and Discussion 116
- 6 Results 117
 - 6.1 Incorporating a Speed Profile - P1 118
 - 6.2 Transformation to Equivalent Driving Cycles - P2 119
 - 6.3 Changing the Power and Energy in a Driving Cycle - P3 . 122
- 7 Conclusions 123
- References 125

Chapter 1

Introduction

A driving cycle, or driving schedule, is represented by vehicle speed versus time. One important example is the European certification driving cycle for light-duty vehicles, the New European Driving Cycle, NEDC, shown in Figure 1.1. Other certification driving cycles that are used for test approval to control that the vehicle manufacturers follow the legislation are, e.g., the FTP75 used in the United States and the JC08 driving cycle which is used in Japan.

Driving cycles are important components for evaluating vehicles and play a fundamental role in vehicle design since the driving cycle affects the cost, fuel consumption, and the emissions of vehicles (Liaw and Dubarry, 2007; André and Rapone, 2009; Ericsson, 2000). In the past driving cycles have mainly been used to assess exhaust gas emissions of vehicles (André, 2004; André et al., 2006; Wang et al., 2000; Fontaras et al., 2009; Wang et al., 2008; Zervas and Bikas, 2008; Pelkmans and Debal, 2006) but they can also be used to evaluate different control strategies for vehicles as in (Pisu and Rizzoni, 2007; Koot et al., 2005; Manzie et al., 2007; Park et al., 2009; Gao et al., 2009; Stockar et al., 2011). Driving cycles have also been used in vehicle design and sizing of components (Maxoulis et al., 2004; Hellgren and Jonasson, 2007; Smith et al., 2011; Souffran et al., 2012; Murgovski et al., 2012; Jaafar et al., 2013; Pourabdollah et al., 2013; Hu et al., 2014).

The certification driving cycles are sometimes criticized to not be representative of real-world driving (Zaccardi and Le Berr, 2012; Souffran et al., 2012; Ashtari et al., 2014) which means that using them for evaluation and design could be questioned. A representative driving cycle usually means that several statistical measures, e.g., mean speed or proportion of time in cruising mode, of the driving cycle are close to real-world driving conditions. Even if a driving cycle is representative today there is no guarantee that it is still representative in the future since the development of the road network, changes in vehicle fleet composition, and the growing number of vehicles on the road causes changes

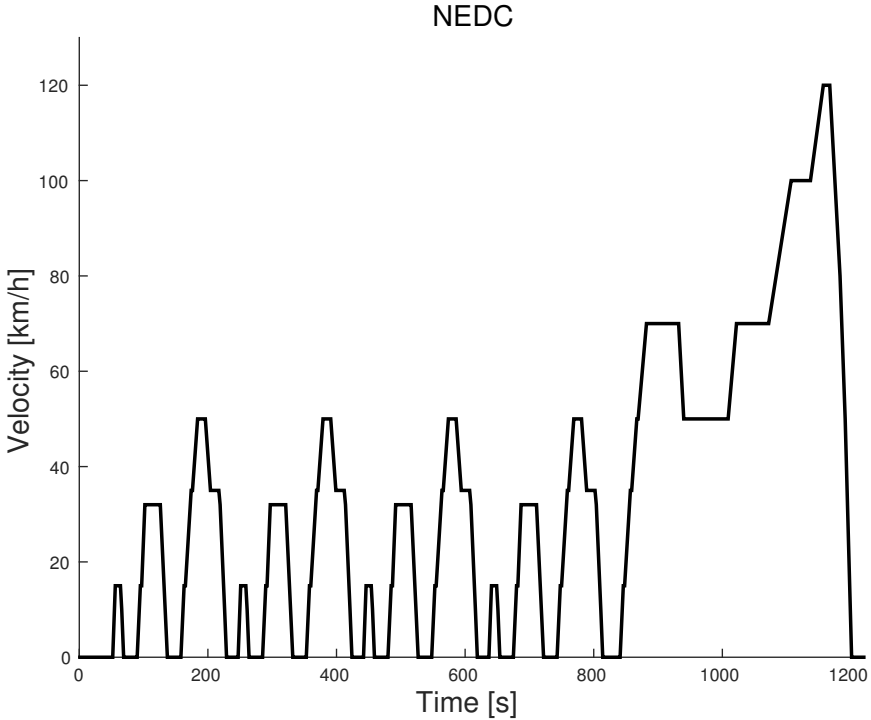


Figure 1.1: European certification driving cycle NEDC.

in the driving behavior, which also varies from region to region (André et al., 2006; Wang et al., 2008; Tong et al., 2011). Thus, there will always be a need for getting new representative driving cycles.

By using only a single driving cycle when designing a vehicle there is a considerable risk that the vehicle is optimized for this specific driving cycle and the resulting design may be non-robust and have sub-optimal performance for other driving cycles (Tazelaar et al., 2009; Schwarzer and Ghorbani, 2013). The vehicle manufacturers need then only to focus on limited operating regions of the engine (Pelkmans and Debal, 2006) and since other driving cycles may excite different regions of the engine, different exhaust gas emissions and fuel consumption characteristics are obtained. For example, Figure 1.2 shows the NO_x emissions for diesel cars for both the NEDC and the Common Artemis Driving Cycles, CADC, (André, 2004) driving cycles (T&E Bulletin). The CADC reflects more of real-world driving compared to the NEDC and while the NO_x level in the NEDC is lower for each new generation of the legislation, the same is not true for the CADC. Further, the lower emission limit value in Euro 5 has not resulted in a reduction of NO_x emissions for diesel cars for real-world driving and it is not expected that these emissions will be close to

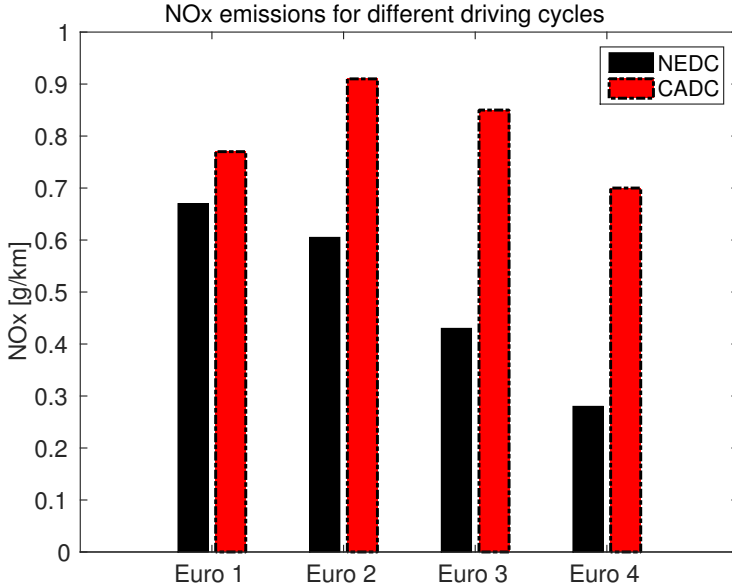


Figure 1.2: Comparison of NO_x emissions of diesel cars in the NEDC and CADC driving cycles for different European emission legislation.

the emission limit value of the NEDC in Euro 6 (Legerink et al., 2013). Thus, focusing on the NEDC is no guarantee that the controls are good in real-world driving conditions.

A common usage of driving cycles is to have different vehicles follow the same driving cycle, and then compare the results to, e.g., rank vehicles with respect to emission levels or fuel consumption. The fuel consumption figures from the certification driving cycles like the NEDC is one such comparison. Another use of driving cycles is to evaluate and compare certain control strategies (Koot et al., 2005; Pisu and Rizzoni, 2007; Tulpule et al., 2010). However, a direct comparison between driving cycles is not always a fair comparison (Zervas and Bikas, 2008). The reason for this is that different driving cycles excites the vehicle differently and the vehicle parameters determine the impact a certain driving cycle has on the vehicle. Figure 1.3 illustrates six different driving cycles with a corresponding fuel consumption shown. The low fuel consumption in the third driving cycle may be the result of a driving cycle which is less demanding to follow than, e.g., the fifth driving cycle which has the highest fuel consumption. Thus, one can not separate between the control and efficiency of the components and the vehicle parameters which can result in different power demand on the vehicle. However, if all driving cycles have similar vehicle excitation, a comparison of driving cycles would be more fair since then the effect of the vehicle parameters on the driving cycle demand would be similar. In such a case, the vehicle control

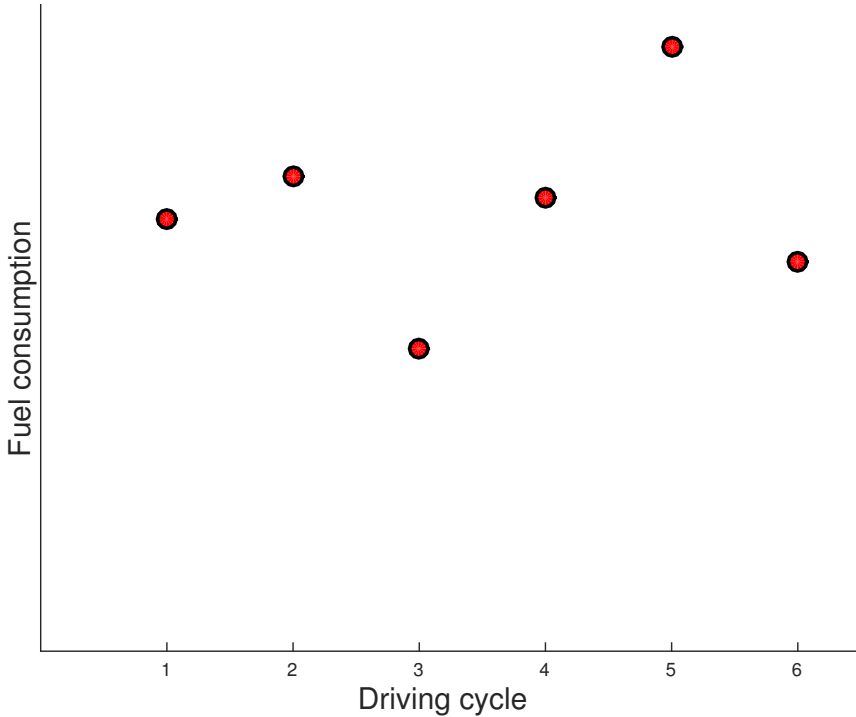


Figure 1.3: Illustration of fuel consumption for six different driving cycles.

and component efficiency can be evaluated to see which driving cycles that the control or the components are especially suited for, and in which driving cycles they perform poorly. This can be an indication on sub-optimal control and it can be further analyzed why a certain driving cycle is better, or worse, compared to other driving cycles. For example, assume that the third driving cycle is the NEDC and all driving cycles have similar vehicle excitation, one could suspect that the vehicle is well adapted to the NEDC and not well suited for the fifth driving cycle.

1.1 GENERATION AND TRANSFORMATION OF DRIVING CYCLES

From the previous section three problems were identified and these are regarding the representativeness of driving cycles, sub-optimization issues, and also how to perform a fair comparison of driving cycles. To solve the two former problems more representative driving cycles are needed to both increase the robustness and reduce the risk for sub-optimization. Today the vehicle manufacturers use several

different driving cycles with the objective that they will cover and represent real-world driving, however, the abovementioned changing driving behavior results in a need to get more driving cycles. There are several approaches to generate new driving cycles that are representative for a certain region of interest, e.g., the Markov chain approaches in (Lee and Filipi, 2011; Gong et al., 2011; Souffran et al., 2012) that extract typical behavior from large amounts of operational data. There have been many proposals of new driving cycles that are representative of a certain region of interest, see, e.g., (Kent et al., 1978; Lin and Niemeier, 2002; Kamble et al., 2009; Shahidinejad et al., 2010; Tong et al., 2011). Another approach (Zaccardi and Le Berr, 2012) compared the existing standard driving cycles with objective methods, e.g., correlation analysis or automatic clustering, and chooses a combination of driving cycles that can be representative. However, comparison of driving cycles is still difficult to perform and the lack of a definition of representative driving cycles enables subjective judgments on how close these statistical measures need to be compared to real-world driving.

To make a fair comparison of the performance results obtained from different driving cycles it is important that the vehicle have similar excitation, e.g., regarding the forces acting on the vehicle in the different driving cycles. A driving cycle generation approach based on Markov chains combined with an equivalence transformation algorithm, is presented in Paper C. The Markov chain is parameterized using real-world driving cycles. The equivalence measures used are the mean tractive force components which are found to be correlated with the fuel consumption.

Another approach to get more driving cycles, besides generation of new driving cycles, is to transform existing ones into new, different, driving cycles. A motivational example is during a concept study where a new powertrain has substantial lower performance and the existing driving cycles cannot be used due to the required power exceeds the maximum power the new powertrain can deliver. Can the driving cycle be transformed in such a way that a performance comparison of the results between the driving cycles is fair and at the same time the vehicle is able to follow the new driving cycles? How to transform a given driving cycle into either a more demanding driving cycle or to a less demanding driving cycle is non-trivial if there are additional constraints that need to be considered. In (Carlson et al., 2009) the vehicle speed and time in the UDDS driving cycle (Kruse and Huls, 1973) was scaled by different factors resulting in an increase both in vehicle speed and acceleration while the traveled distance remained the same. Such an approach enables some control on certain measures but the level of control on other measures, e.g., the average power, are low. Paper D presents a general and systematic methodology for driving cycle transformation where a wide range of constraints can be handled and by using a cost function the vehicle jerk can be decreased simultaneously.

A flowchart on how to generate new driving cycles is shown in Figure 1.4. Here it is assumed that there exists a database of real-world driving cycles, which have been tagged with certain attributes regarding the measurement, e.g., vehicle

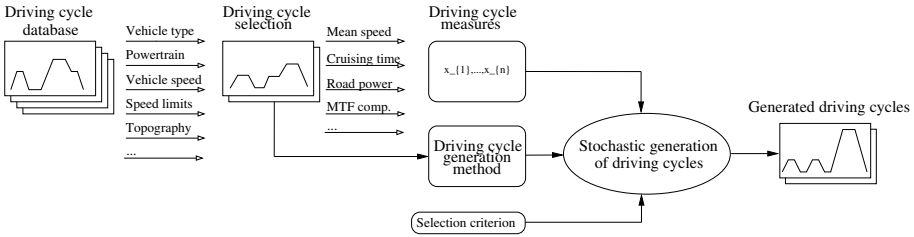


Figure 1.4: Schematic overview of a flowchart for driving cycle generation.

type, speed limits, or topography. From this database certain driving cycles are selected, e.g., all driving cycles driven in a certain region or only highway driving cycles with high mean speed. These driving cycles can be characterized by different measures, e.g., mean speed or road power. Using a certain driving cycle generation method together with a specified selection criterion, stochastic driving cycles with certain wanted properties can be generated. These driving cycle have different properties depending on which application they are used in. Figure 1.4 illustrates the approach used in Paper C where the driving cycle generation method uses Markov chains and as an additional step the generated driving cycles are transformed using an algorithm by Nyberg et al. (2013). The driving cycle transformation methodology in Paper D is more general and could be used instead.

These driving cycles that have either been measured, generated or transformed are used to evaluate and test vehicles. The vehicle evaluation can be performed in computer simulation software as in (Koot et al., 2005; Pisu and Rizzoni, 2007; Tulpule et al., 2010; Stockar et al., 2011) but for type approval the vehicle needs to follow the driving cycle in a chassis dynamometer. Another type of test platform is a moving base simulator and tests are also conducted on dedicated tracks and in real-traffic. In the next section a moving base simulator is combined with a chassis dynamometer to form a new hardware-in-the-loop test platform for vehicle evaluation.

1.2 TEST PLATFORMS FOR EVALUATION OF VEHICLES

With increasing environmental concern, new powertrain technologies, e.g., hybrid electric vehicles and electric vehicles, with the objective to reduce the environmental footprint of vehicles, have been proposed and developed. How vehicles with these technologies are perceived by the drivers is important and it is furthermore vital to be able to conclude if a certain technology is better in practice and not just in a certain driving cycle. With the development of new experimental equipment, these kinds of questions can be addressed in a more systematic and repeatable way.

For evaluating the driver perception of the vehicle, a moving base simulator

is a well-established technique and with improvements in power electronics and electrical drives new chassis dynamometer concepts have given opportunities to improve the existing usage and also enables possibilities to even connect such setups in a hardware-in-the-loop. Paper B presents a co-simulation of the chassis dynamometer in the vehicle propulsion laboratory (presented in Paper A) at Linköping University and the moving base simulator, Sim III, at the Swedish National Road and Transport Research Institute, VTI. These two setups are separated by a distance of 500 meter and are connected with a dedicated fiber link.

Sim III, the moving base driving simulator used in Paper B, is seen in Figure 1.5. It simulates the road conditions for vehicles (Bolling et al., 2011) and has in previous studies been used for, e.g., studying the effects of yaw stability at side impact in (Andersson and Jansson, 2011). The linear motion system of Sim III has four degrees of freedom and offers both linear and tilt motion. By linking the cradle motion to the vehicle's lateral position realistic lateral motions are obtained. Six projectors are used to give the driver a field of vision of 120 degrees. Road unevenness, which has high frequency, can be simulated by the vibration table and a Saab 9-3 cabin is currently used in Sim III.

Driving cycles are usually performed in chassis dynamometers (Kent et al., 1978) to, e.g., test the effect of different fuel types as in (Wang et al., 2000), or measuring tailpipe emissions for light-duty vehicles or trucks as in (Durbin et al., 2002; André, 2004; Pelkmans and Debal, 2006). Chassis dynamometer experiments are good alternatives to tests on a dedicated track or on-road tests since they give a higher repeatability, lower cost, and better experimental control and supervision. In the past chassis dynamometers usually meant rolls of different dimensions where the surfaces of the rolls are in direct contact with the tires of the vehicle, see, e.g., (Wang et al., 2000; Brace and Moffa, 2009; Carlson et al., 2009). However, in Paper A, a vehicle propulsion laboratory is presented that uses a different type of chassis dynamometer that is mounted directly to the wheel hubs, with the help of adapter plates. Thus, the wheel torques are extracted directly from the driven wheel hub connection instead from the friction between the tire and roll. The chassis dynamometer is shown in Figure 1.6 and consists of four mobile dynamometers which can operate both as motors and as generators depending on system mode, and can thus both brake and propel the vehicle. The outputs of the dynamometer are wheel torques and rotational wheel speeds but also vehicle speed and other quantities that can be calculated using the internal vehicle model.

Paper B develops and evaluates a co-simulation of a chassis dynamometer and a moving base simulator. The purpose of such a setup is to try to improve the driving experience in Sim III and at the same time the vehicle mounted in the chassis dynamometer is experiencing more realistic loads due to that the driver's perception of the simulation is closer to reality. Previous work used an internet-distributed hardware-in-the-loop simulation of an engine test bench and



Figure 1.5: Moving base simulator Sim III.



Figure 1.6: Volkswagen Passat mounted in the chassis dynamometer in the vehicle propulsion laboratory.

a ride motion simulator (Ersal et al., 2011). The co-simulation is made possible with the development of a pedal robot that actuates the driver's input in the moving base simulator to the mounted vehicle. In the experiment a front-wheel-driven Volkswagen Passat Ecofuel DSG from 2009 was used. The vehicle, shown in Figure 1.6, has an automatic transmission meaning no gear-shifting robot was required.

The vehicle model in Sim III was modified to accept inputs from the vehicle propulsion laboratory. This means that the chassis dynamometer at the propulsion laboratory controls the propulsion of the vehicle during the co-simulation but the other parts of the simulator are intact providing a realistic environment to the driver in the Sim III. During a driving mission the driver, in Sim III, actuates the accelerator and brake pedal both in Sim III and also in the mounted vehicle in the chassis dynamometer via the pedal robot. The resulting wheel torques, from the powertrain, are measured and both torques and wheel speeds are sent to the Sim III and forms a loop. Using this new laboratory setup, new powertrain technologies can be tested in a controlled and realistic setting and can be a complement to on-road tests.

The resulting vehicle speed trace of such an experiment could be compared to, e.g., on-road tests, to determine if there are any differences in driver behavior in the co-simulation compared to real-world driving. Such an evaluation of the setup has the benefit of being objective compared to subjective answers from test persons in the study.

1.3 CONTRIBUTIONS

The main contributions of Papers A - D are summarized below.

PAPER A

Paper A presents the vehicle propulsion laboratory for vehicle research where a chassis dynamometer is used to test light-duty vehicles. The contribution is the development of a new chassis dynamometer laboratory and its design choices. The laboratory hardware such as data acquisition, network infrastructure, and the chassis dynamometer, its performance, and possible usage are discussed. The vehicle propulsion laboratory is a requirement for the co-simulation study in Paper B. The author of this thesis contributed with equal amount of work compared to the first author of Paper A and it includes design, conducting the experiments, implementation, and the written presentation.

PAPER B

Paper B presents a new engineering tool for vehicle testing in a controlled environment by connecting the chassis dynamometer in the vehicle propulsion

laboratory to the moving base simulator Sim III. The contribution is a proof-of-concept that the configuration works and with some improvements can be a realistic environment for vehicle testing. The author of this thesis contributed with equal amount of work compared to his co-authors of Paper B and it includes design, conducting the experiments, implementation, and the written presentation.

PAPER C

Paper C presents an approach to generate driving cycles with certain desired equivalence properties from a database of real-world driving cycles. The contribution is the experimental investigation that shows a gain in using the individual components of the mean tractive force, MTF, compared of the aggregated MTF, as an indication of the fuel consumption in the driving cycle. The experiments were conducted in a hardware-in-the-loop setup with a real engine. A second contribution is the combination of using a Markov chain approach to generate candidate driving cycle and then use a transformation algorithm in (Nyberg et al., 2013) to get driving cycles with the same vehicle excitation regarding the mean tractive force components. The author of this thesis contributed with the majority of this work including design and the implementation. Paper C relies partly on work presented in (Nyberg et al., 2013, 2014).

PAPER D

Paper D presents a methodology for transforming driving cycles. The contribution is a methodology that can be used to transform a given driving cycle into a new, different, driving cycle considering general constraints. An evaluation of the method shows that all tested problems are solved swiftly and it can handle a wide range of constraints on the driving cycle. The method is straightforward to use and gives an effective new engineering tool for driving cycle design. The author of this thesis contributed with the majority of this work including design and the implementation. Paper D relies partly on the ideas in (Nyberg et al., 2013).

1.4 PUBLICATIONS

The research work leading to this thesis is presented in the following publications.

JOURNAL PAPERS

- P. Öberg, P. Nyberg, and L. Nielsen. A new chassis dynamometer laboratory for vehicle research. *SAE International Journal of Passenger Cars - Electronic and Electrical Systems*, 6(1):152–161, 2013 (**Paper A**)

- A. Andersson, P. Nyberg, H. Sehammar, and P. Öberg. Vehicle powertrain test bench co-simulation with a moving base simulator using a pedal robot. *SAE International Journal of Passenger Cars - Electronic and Electrical Systems*, 6(1):169–179, 2013 (**Paper B**)
- T. Nilsson, P. Nyberg, C. Sundström, E. Frisk, and M. Krysander. Robust driving pattern detection and identification with a wheel loader application. *International Journal of Vehicle Systems Modelling and Testing*, 9(1):56–76, 2014

SUBMITTED

- P. Nyberg, E. Frisk, and L. Nielsen. Using real-world driving databases to generate driving cycles with equivalence properties. 2015a. Submitted for journal publication (**Paper C**)
- P. Nyberg, E. Frisk, and L. Nielsen. Driving cycle equivalence and transformation. 2015b. Submitted for journal publication (**Paper D**)

CONFERENCE PAPERS

- P. Nyberg, E. Frisk, and L. Nielsen. Driving cycle adaption and design based on mean tractive force. In *Proceedings of 7th IFAC Symposium on Advances in Automotive Control*, volume 7, pages 689–694, Tokyo, Japan, 2013
- P. Nyberg, E. Frisk, and L. Nielsen. Generation of equivalent driving cycles using markov chains and mean tractive force components. In *Proceedings of 19th IFAC World Congress*, volume 19, pages 8787–8792, Cape Town, South Africa, 2014

1.5 OUTLOOK

The methodology presented in Paper D enables transformation of driving cycles in a controlled and systematic way, and yields possibilities to increase both the robustness and the sensitivity of the control of vehicles. For example, the sensitivity of the sizing of the energy buffer or the fuel consumption in a hybrid electric vehicle, of the recuperation energy can be evaluated by changing the available recuperation energy in the driving cycle. Combining a driving cycle generation tool, e.g., the Markov chain approach used in Paper C, with the general driving cycle transformation methodology presented in Paper D yields a powerful tool that can be used at several instances during the product development process of vehicles.

An interesting continuation would be to include the road slope as an extra state. In the Markov chain approach of generation of driving cycles this corresponds to use three states; vehicle speed, acceleration, and road slope as in

(Souffran et al., 2012). The transformation methodology in Paper D would have to be extended to also consider the road slope and not just the vehicle speed points as optimization variables.

The performance of the fiber link between the two laboratories in Paper A and B was not an issue. However, an interesting continuation would be to conduct studies for examining the effect of delays and lost packages on the driving experience. For example, what is an acceptable delay, both for the driver and the system, in such a setup can be a research question.

1.6 CONCLUDING REMARK

Previously, changing how demanding a driving cycle is to follow for a vehicle usually consisted of either changing the vehicle speed and time by scaling as in (Carlson et al., 2009), or by just extending the driving cycle by consecutive repetitions of itself as in (Tulpule et al., 2010). The former case enables some control on the vehicle speed and acceleration but other measures such as average power can not be directly included. Consecutive repetitions of the same driving cycle increases the length and thus the required total energy but keeps the speed and acceleration characteristics.

Now, using the methodology presented in Paper D the transformation of a driving cycle is controlled and target measures such as mean tractive force components, average power, and available energy for recuperation can be formulated as constraints. Thus, a general and systematic methodology for changing the driving cycle demand on the vehicle has been developed.

REFERENCES

- A. Andersson and J. Jansson. A moving base simulator investigation of effects of a yaw stability system caused by a side impact. *ASME/Journal of Computing and Information Science in Engineering*, 11(4), 2011.
- A. Andersson, P. Nyberg, H. Sehammar, and P. Öberg. Vehicle powertrain test bench co-simulation with a moving base simulator using a pedal robot. *SAE International Journal of Passenger Cars - Electronic and Electrical Systems*, 6(1):169–179, 2013.
- M. André and M. Rapone. Analysis and modelling of the pollutant emissions from European cars regarding the driving characteristics and test cycles. *Atmospheric Environment*, 43(5):986–995, 2009.
- M. André. The ARTEMIS European driving cycles for measuring car pollutant emissions. *Science of The Total Environment*, 334-335(0):73–84, 2004.
- M. André, R. Joumard, R. Vidon, P. Tassel, and P. Perret. Real-world European driving cycles, for measuring pollutant emissions from high- and low-powered cars. *Atmospheric Environment*, 40(31):5944–5953, 2006. 13th International Symposium on Transport and Air Pollution (TAP-2004).
- A. Ashtari, E. Bibeau, and S. Shahidinejad. Using large driving record samples and a stochastic approach for real-world driving cycle construction: Winnipeg driving cycle. *Transportation Science*, 48(2):170–183, 2014.
- A. Bolling, J. Jansson, M. Hjort, M. Lidström, S. Nordmark, H. Sehammar, and L. Sjögren. An approach for realistic simulation of real road condition in a moving base driving simulator. *ASME/Journal of Computing and Information Science in Engineering*, 11(4), 2011.
- C. J. Brace and J. Moffa. Increasing accuracy and repeatability of fuel consumption measurement in chassis dynamometer testing. *Journal of Automobile Engineering*, 223(9):1163–1177, 2009.
- R. Carlson, H. Lohse-Busch, M. Douba, and N. Shidore. Drive cycle fuel consumption variability of plug-in hybrid electric vehicles due to aggressive driving. In *SAE Technical paper 2009-01-1335*, Detroit, USA, 2009.
- T. D. Durbin, R. D. Wilson, J. M. Norbeck, J. Miller, T. Huai, and S. H. Rhee. Estimates of the emission rates of ammonia from light-duty vehicles using standard chassis dynamometer test cycles. *Atmospheric Environment*, 36(9):1475–1482, 2002.
- E. Ericsson. Variability in urban driving patterns. *Transportation Research Part D: Transport and Environment*, 5(5):337–354, 2000.

- T. Ersal, M. Brudnak, A. Salvi, J. Stein, Z. Filipi, and H. Fathy. Development and model-based transparency analysis of an internet-distributed hardware-in-the-loop simulation platform. *Mechatronics*, 21:22–29, 2011.
- G. Fontaras, G. Karavalakis, M. Kousoulidou, T. Tzamkiozis, L. Ntziachristos, E. Bakeas, S. Stournas, and Z. Samaras. Effects of biodiesel on passenger car fuel consumption, regulated and non-regulated pollutant emissions over legislated and real-world driving cycles. *Fuel*, 88(9):1608–1617, 2009.
- J.-P. Gao, G.-M. G. Zhu, E. G. Strangas, and F.-C. Sun. Equivalent fuel consumption optimal control of a series hybrid electric vehicle. *Proceedings of the Institution of Mechanical Engineers, Part D: Journal of Automobile Engineering*, 223(8):1003–1018, 2009.
- Q. Gong, S. Midlam-Mohler, V. Marano, and G. Rizzoni. An iterative markov chain approach for generating vehicle driving cycles. *SAE International Journal of Engines*, 4(1):1035–1045, 2011.
- J. Hellgren and E. Jonasson. Maximisation of brake energy regeneration in a hybrid electric parallel car. *International Journal of Electric and Hybrid Vehicles*, 1(1):95–121, 2007.
- X. Hu, N. Murgovski, L. Johannesson, and B. Egardt. Comparison of three electrochemical energy buffers applied to a hybrid bus powertrain with simultaneous optimal sizing and energy management. *IEEE Transactions on Intelligent Transportation Systems*, 15(3):1193–1205, 2014.
- A. Jaafar, B. Sareni, and X. Roboam. A systemic approach integrating driving cycles for the design of hybrid locomotives. *IEEE Transactions on Vehicular Technology*, 62(8):3541–3550, 2013.
- S. Kamble, T. Mathew, and G. Sharma. Development of real-world driving cycle: Case study of Pune, India. *Trans. Research Part D*, 14(2):132–140, 2009.
- J. Kent, G. Allen, and G. Rule. A driving cycle for Sydney. *Transportation Research*, 12(3):147–152, 1978.
- M. Koot, J. Kessels, B. de Jager, W. Heemels, P. van den Bosch, and M. Steinbuch. Energy management strategies for vehicular electric power systems. *IEEE Transactions on Vehicular Technology*, 54(3):771–782, May 2005.
- R. E. Kruse and T. A. Huls. Development of the federal urban driving schedule. In *SAE Technical Paper 730553*, 1973.
- T.-K. Lee and Z. Filipi. Synthesis of real-world driving cycles using stochastic process and statistical methodology. *International Journal of Vehicle Design*, 57(1):17–36, 2011.

- N. Legerink, G. Kadijk, P. van Mensch, S. Hausberger, and M. Rexeis. Investigations and real world emission performance of Euro 6 light-duty vehicles. Technical report, TNO, 2013.
- B. Liaw and M. Dubarry. From driving cycle analysis to understanding battery performance in real-life electric hybrid vehicle operation. *Journal of Power Sources*, 174(1):76–88, 2007.
- J. Lin and D. Niemeier. An exploratory analysis comparing a stochastic driving cycle to California’s regulatory cycle. *Atmospheric Environment*, 36(38):5759–5770, 2002.
- C. Manzie, H. Watson, and S. Halgamuge. Fuel economy improvements for urban driving: Hybrid vs. intelligent vehicles. *Transportation Research Part C: Emerging Technologies*, 15(1):1–16, 2007.
- C. N. Maxoulis, D. N. Tsinoglou, and G. C. Koltsakis. Modeling of automotive fuel cell operation in driving cycles. *Energy Conversion and Management*, 45(4):559–573, 2004.
- N. Murgovski, L. Johannesson, J. Sjöberg, and B. Egardt. Component sizing of a plug-in hybrid electric powertrain via convex optimization. *Mechatronics*, 22(1):106–120, 2012.
- T. Nilsson, P. Nyberg, C. Sundström, E. Frisk, and M. Krysander. Robust driving pattern detection and identification with a wheel loader application. *International Journal of Vehicle Systems Modelling and Testing*, 9(1):56–76, 2014.
- P. Nyberg, E. Frisk, and L. Nielsen. Driving cycle adaption and design based on mean tractive force. In *Proceedings of 7th IFAC Symposium on Advances in Automotive Control*, volume 7, pages 689–694, Tokyo, Japan, 2013.
- P. Nyberg, E. Frisk, and L. Nielsen. Generation of equivalent driving cycles using markov chains and mean tractive force components. In *Proceedings of 19th IFAC World Congress*, volume 19, pages 8787–8792, Cape Town, South Africa, 2014.
- P. Nyberg, E. Frisk, and L. Nielsen. Using real-world driving databases to generate driving cycles with equivalence properties. 2015a. Submitted for journal publication.
- P. Nyberg, E. Frisk, and L. Nielsen. Driving cycle equivalence and transformation. 2015b. Submitted for journal publication.
- P. Öberg, P. Nyberg, and L. Nielsen. A new chassis dynamometer laboratory for vehicle research. *SAE International Journal of Passenger Cars - Electronic and Electrical Systems*, 6(1):152–161, 2013.

- J. Park, Z. Chen, L. Kiliaris, M. Kuang, M. Masrur, A. Phillips, and Y. Murphey. Intelligent vehicle power control based on machine learning of optimal control parameters and prediction of road type and traffic congestion. *IEEE Transactions on Vehicular Technology*, 58(9):4741–4756, 2009.
- L. Pelkmans and P. Debal. Comparison of on-road emissions with emissions measured on chassis dynamometer test cycles. *Transportation Research Part D: Transport and Environment*, 11(4):233–241, 2006.
- P. Pisu and G. Rizzoni. A comparative study of supervisory control strategies for hybrid electric vehicles. *IEEE Transactions on Control Systems Technology*, 15(3):506–518, May 2007.
- M. Pourabdollah, N. Murgovski, A. Grauers, and B. Egardt. Optimal sizing of a parallel PHEV powertrain. *IEEE Transactions on Vehicular Technology*, 62(6):2469–2480, 2013.
- V. Schwarzer and R. Ghorbani. Drive cycle generation for design optimization of electric vehicles. *IEEE Transactions on Vehicular Technology*, 62(1):89–97, 2013.
- S. Shahidinejad, E. Bibeau, and S. Filizadeh. Statistical development of a duty cycle for plug-in vehicles in a North American urban setting using fleet information. *IEEE Transactions on Vehicular Technology*, 59(8):3710–3719, 2010.
- R. Smith, S. Shahidinejad, D. Blair, and E. Bibeau. Characterization of urban commuter driving profiles to optimize battery size in light-duty plug-in electric vehicles. *Transportation Research Part D: Transport and Environment*, 16(3):218–224, 2011.
- G. Souffran, L. Miegerville, and P. Guerin. Simulation of real-world vehicle missions using a stochastic markov model for optimal powertrain sizing. *IEEE Transactions on Vehicular Technology*, 61(8):3454–3465, 2012.
- S. Stockar, V. Marano, M. Canova, G. Rizzoni, and L. Guzzella. Energy-optimal control of plug-in hybrid electric vehicles for real-world driving cycles. *IEEE Transactions on Vehicular Technology*, 60(7):2949–2962, 2011.
- E. Tazelaar, J. Bruinsma, B. Veenhuizen, and P. van den Bosch. Driving cycle characterization and generation, for design and control of fuel cell buses. *World Electric Vehicle Journal*, 3(1), 2009.
- T&E Bulletin. Who adds pressure for stricter Euro-5 standards. Number 146, March 2006.
- H. Tong, H. Tung, W. Hung, and H. Nguyen. Development of driving cycles for motorcycles and light-duty vehicles in Vietnam. *Atmospheric Environment*, 45(29):5191–5199, 2011.

- P. Tulpule, V. Marano, and G. Rizzoni. Energy management for plug-in hybrid electric vehicles using equivalent consumption minimisation strategy. *International Journal of Electric and Hybrid Vehicles*, 2(4):329–350, 2010.
- Q. Wang, H. Huo, K. He, Z. Yao, and Q. Zhang. Characterization of vehicle driving patterns and development of driving cycles in Chinese cities. *Transportation Research Part D: Transport and Environment*, 13(5):289–297, 2008.
- W. Wang, D. Lyons, N. Clark, M. Gautam, and P. Norton. Emissions from nine heavy trucks fueled by diesel and biodiesel blend without engine modification. *Environmental Science and Technology*, 34(6):933–939, 2000.
- J.-M. Zaccardi and F. Le Berr. Analysis and choice of representative drive cycles for light duty vehicles - Case study for electric vehicles. *Proceedings of the Institution of Mechanical Engineers, Part D: Journal of Automobile Engineering*, 2012.
- E. Zervas and G. Bikas. Impact of the driving cycle on the NO_x and particulate matter exhaust emissions of diesel passenger cars. *Energy and Fuels*, 22(3): 1707–1713, 2008.

Papers

A New Chassis Dynamometer Laboratory for
Vehicle Research*

A

*Published in *SAE International Journal of Passenger Cars - Electronic and Electrical Systems*, 6(1):152-161, 2013.

A New Chassis Dynamometer Laboratory for Vehicle Research

Per Öberg, Peter Nyberg, and Lars Nielsen

*Vehicular Systems, Department of Electrical Engineering,
Linköping University, SE-581 83 Linköping, Sweden.*

ABSTRACT

In recent years the need for testing, calibration and certification of automotive components and powertrains have increased, partly due to the development of new hybrid concepts. At the same time, the development within electrical drives enables more versatile chassis dynamometer setups with better accuracy at a reduced cost. We are developing a new chassis dynamometer laboratory for vehicle research, aiming at extending a recently commercially available dynamometer, building a new laboratory around it, and applying the resulting facility to some new challenging vehicle research problems. The projects are enabled on one hand by collaboration with the dynamometer manufacturer, and on the other hand on collaboration with automotive industry allowing access to relevant internal information and equipment. The test modes of the chassis dynamometer are under development in a joint collaboration with the manufacturer. The laboratory has been operational since September 2011 and has already been used for NVH-analysis for a tire pressure indication application, chassis dynamometer road force co-simulation with a moving base simulator, co-surge modeling and control for a 6-cylinder bi-turbo engine, and traditional engine mapping. We are also looking at projects with focus on look-ahead control, as well as clutch and transmission modeling and control, and driving cycle related research.

1 INTRODUCTION

Testing, calibration and certification are vital parts for the development of new automotive technologies. With the development of new hybrid concepts the need for it have also increased. To be able to perform large scale vehicle experiments a chassis dynamometer is an option to use.

This paper presents our new chassis dynamometer laboratory, the design choices that are made and the unique opportunities that are made possible by the implementation. The test modes of the equipment, some of which are newly developed, and some of the projects that have already been performed are discussed together with future projects that we foresee possible having access to our new laboratory. The basis for the laboratory is the development within electrical drives, power electronics and precision motion control of electrical machines also for high torques and powers. This progress has enabled a reduced cost and a versatile setup. In our case the basis for the system is ABB technology, applied by Rototest for vehicle applications. A first glance of the laboratory is seen in Figure 1.

The development of our new facility is exciting since it utilizes, combines and enhances new state-of-the-art commercial technology made possible by tech-



Figure 1: Glance of the new chassis dynamometer lab. A Golf V with a 1.4l multifuel engine has been mounted to the dynamometer units in a 4WD configuration.

nological development with several timely automotive research and development projects. On one hand it is curiosity driven, and on the other hand there is substantial interest from our automotive collaborators since they are facing more and more complex development tasks, and are with interest looking at new possibilities.

2 BACKGROUND

Chassis dynamometer experiments are good alternatives to road tests since they give a higher repeatability, lower cost, and better experimental control and supervision. Another benefit is that the body of the vehicle does not need to be mounted, which yields, a possibility to test different configurations of the powertrain before a complete vehicle is constructed. Using a chassis dynamometer it is possible to test the whole powertrain of a vehicle as opposed to engine tests benches. In the past chassis dynamometers usually meant rolls of different dimensions where the surface of the rolls was in direct contact with the tire of the tested vehicle. They were expensive and required complex facilities, and the time to change vehicles is often long. With the use of absorption, and possibly a drive unit, the rolls can be controlled to brake and propel the vehicle while measuring e.g. the speed of the roll and the transferred torque from the tire to the roll.

There are many examples of work where chassis dynamometers have been used. For example, to get an estimate of the pollutant emissions from light-duty trucks, test or driving cycles have frequently been used while measuring the emissions (André, 2004). These driving cycles, which are speed profiles, are mainly performed at a chassis dynamometer. The legislative certification driving cycle in Europe is the NEDC driving cycle, and in (Pelkmans and Debal, 2006) on-road emissions and emissions for chassis dynamometer driving NEDC are compared. Another work used transportable chassis dynamometers to compare alternative fuel and diesel fuel heavy-duty vehicles emissions (Wang et al., 1997). The chassis dynamometer used in that study used rolls for the driven wheels, but the power was extracted directly from the vehicle hubs instead of extracting power from the rolls that usually is the case. During emission measurements a common practice is to measure the related fuel consumption at the same time. In (Brace and Moffa, 2009) a statistical approach is used for identifying factors that influence the fuel consumption of a vehicle. Here a 48 inch chassis dynamometer is used and the largest effect was recognized to be a discharged battery.

Except for conducting legislative certification driving cycles for emissions, a chassis dynamometer can also be used for other experiments or tests such as performance tests of the powertrain and noise tests, of vibration and harshness (NVH) to mention a few. In the latter case usually larger diameters of the rolls are required to ensure that the contact surface between the tire and roll are large enough.

3 LABORATORY OVERVIEW

The vehicle propulsion laboratory is housed in the facility L-huset at Linköping University which was finished mid 2011. The L-huset can be viewed in Figure 2 and contains in total approximately 220 m² laboratory space and also some office space. The focus of this paper is on the vehicle propulsion laboratory being one of three labs in the building. The chassis dynamometer in the propulsion laboratory was chosen because of its flexibility, simplicity, and cost of ownership and installation. Nevertheless, during construction of the lab, some criteria had to be fulfilled to support the chassis dynamometer installation. The main specific criterion during the construction of the lab-building was that the electrical power transmission had to be dimensioned to support the four 160 A 230 V three phase power supplies for the regenerative motor drives and the 125 A power supply for the head wind fan. The second criterion was that the exhaust gases need to be taken care of with suitable ventilation. Other than that, the laboratory building is simply a regular building with garage.



Figure 2: Building L-huset where the vehicle propulsion laboratory is housed.

3.1 THE VEHICLE PROPULSION LABORATORY

The vehicle propulsion laboratory consists of an 80 m² lab area divided between a control room and the actual lab space. An overview picture of the vehicle propulsion laboratory can be seen to the left in Figure 3. The usable ceiling height is approximately 5 m and the garage doors are of a height of 4 m. This way even light-duty-trucks can be brought into the laboratory. The panoramic window in



Figure 3: Left: View of the vehicle propulsion laboratory with four mobile dynamometers, head wind fan and exhaust ventilation. Right: View from the corridor.

the corridor, which can be seen to the right in Figure 3, gives spectators and staff a view of the laboratory and yields the possibility to easily demonstrate the facility for visitors. In the control room, which can be seen in Figure 4, a supervisor can control the experiments and at the same time have a visual supervision of the activity in the laboratory.

Due to that the wheels need to be removed during the mounting of the dynamometers a jack or preferable a lift needs to be used to lift the vehicle. Because the dynamometer units are mobile the choice of lift requires some consideration. The laboratory is currently equipped with a movable hydraulic scissor lift (not shown in the figures) that can be used and stowed away easily, maintaining the flexibility of the dynamometers. One drawback with the current solution is, however, that not all cars have enough ground clearance for the lift.

Because the dynamometer can be used at high vehicle loads for long time measurements the exhaust gases can reach high temperatures. To cope with the high temperatures the ventilation system is dimensioned to suck excess air, thus diluting the hot exhaust gases at the source. Currently a selection of pipes with different lengths and shapes are used to fit the ventilation to vehicles with different exhaust pipe layouts but a more flexible solution is sought for.



Figure 4: View of the vehicle propulsion laboratory control room.

3.2 EQUIPMENT

The propulsion laboratory is equipped with a chassis dynamometer, as well a data acquisition hardware, network infrastructure, and communication software. Pictures of the laboratory can be seen in Figure 3 and a schematic overview of the system can be seen in Figure 5. The main parts of the equipment are

The chassis dynamometer which is the main equipment of the vehicle propulsion laboratory and consists of four mobile units, as well as other control and supply components. The chassis dynamometer is thoroughly described further down.

A PC for measurement and control located in the control room. This computer is currently running a standard Linux distribution that can be adapted to running real time software, e.g. for look-ahead-control purposes. Measurements are either performed directly at the dynamometer systems Control PC or by this measurement computer through CAN, serial port OBDII or UDP. This way data that is measured by other means than by the dynamometer or vehicle control systems can easily be forwarded to the measurement computer.

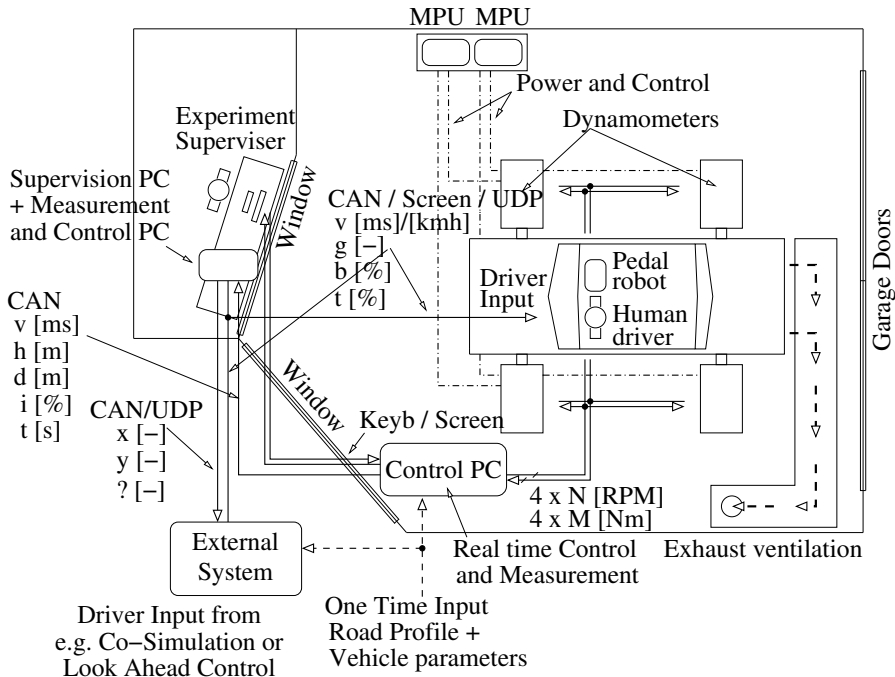


Figure 5: Lab area, where the dynamometer units are located, and a control room, from where an experiment supervisor controls the experiment, are separated with a large panoramic window. The garage doors, shown in the right part of the picture, are large enough to allow full size trucks to enter the lab area.

A supervision PC located in the control room. This computer is used for supervision and communication using Confero (Johanson, 2010) which is a teleconference software which can be used independently without an external Internet connection.

Ethernet connections to a local switch room with single mode fiber to neighboring facilities. The Ethernet network is separated between a local high speed measurement network, also available from the offices, a dedicated single mode fiber extension currently connected to the moving base simulator facility at the Swedish National Road and Transport Research Institute, VTI, as well as a number of standard university networks for use with regular research and student activities.

Direct cable connections between the control room and the lab area for Ethernet, CAN, serial RS232 connections or other equipment suitable for CAT5e cables, e.g. keyboard video and mouse extenders, USB extenders or OBDII adapters.

The power supply of the laboratory, which consists of

- A 125 A 230 V three phase European power socket for the head wind fan.
- Four 160 A 230 V three phase power supplies for the regenerative motor drives.
- Two 16 A 230 V three phase European power sockets for use with the vehicle lift and other typical tools.

Finally, for personal safety the laboratory is equipped with a hand-carried CO₂ sensor as well as CO₂ and CO sensors connected to an emergency evacuation fan.

4 DYNAMOMETER SYSTEM

4.1 SYSTEM DESCRIPTION

The chassis dynamometer equipment consists of

- Four mobile dynamometer units, (Rototest Energy 230 4WD).
- Two main power units housing the regenerative motor drives. These are placed in a protective cabinet which is vented with outside air to avoid smoke damages in case of a small fire.
- A mobile control rack consisting of the master control unit, a real time control system, as well as a user interface module which is built on an ordinary PC.
- A mobile head wind fan capable of wind speed up to 100 km/h (about 62 mph)

Depending on the system mode the dynamometer units can operate as either motors or generators, and can thus both brake and propel the vehicle. This can for example be used when simulating downhill driving where the vehicle is accelerated even if the engine does not provide any tractive force.

The dynamometer units are mobile and can be moved to fit different vehicle sizes and configurations, such as 1WD (motorcycles), 2WD, or 4WD vehicles. The vehicle is fitted to the dynamometer by removing the driven wheels and mounting the vehicle to the dynamometer using adapter plates directly on the wheel hubs. Switching vehicles can be performed in less than 30 minutes which enables the use of the laboratory for parallel projects.

CONFIGURATION FOR COMPONENT TESTING

Because of the system's flexibility it is also tempting to use the system for other purposes than as a chassis dynamometer. An application is to use the dynamometer units as parts of a transmission test rig which can be used in early stages of for example clutch and transmission control evaluation.

HEAD WIND FAN

A head wind fan is used to simulate the head wind which cools the engine and its components. The headwind fan, which can be seen in the left part in Figure 3, can either be manually controlled or it can be set to follow the simulated vehicle velocity in the interval 0-100 km/h. One benefit with the dynamometer equipment is that the noise is relatively low. The single noisiest component is the head wind fan with a peak noise level of 120 dBA at full speed. In the speed range 0-70 km/h the noise is low enough to hear the powertrain components as one would in a normal driving situation. This way, experiments where drivetrain noise is important can be performed.

SENSORS

The outputs of the dynamometer are wheel torques and speeds but also vehicle speed and other quantities that can be calculated using the internal vehicle model. The torques are measured using string gauges fitted to the drive suspension of the dynamometer units and the torque measurement accuracy is within 0.1% of measured value.

SETUP

Before starting an experiment a number of vehicle parameters are needed. Depending on operation mode they are

- Axle weight, m_a , and effective wheel diameter, d_w , for calculation of safety limits.
- Gear ratios, $r_{g,i}$, for all gears including the final drive, for calculation of engine speed.
- Vehicle mass, m_v , front area, A_f , drag coefficient, c_d , and rolling resistance, c_r , for driving resistance calculation in the road force simulation mode.

For the road profile simulation mode an elevation map, including turn radii, for the road is also needed.

In a typical test setup the driver steps into the vehicle as would be the case for a normal driving mission. Because of the mobile dynamometer setup the driver can turn the steering wheel. In another scenario a pedal robot is used, e.g. when connected to an external system as discussed below. In both setups the experiments are directed from the control room, and the dynamometer is controlled either through the Control PC or via CAN remote control which adds for extra safety when connected to an external systems.

4.2 DYNAMOMETER PERFORMANCE

The performance of the chassis dynamometer equipment is in the speed range 0 – 1000 rpm limited to an axle torque of 1180 Nm continuous and up to 2200 Nm

momentarily. In the speed range 1000 – 2100 rpm the torque is limited by the power. The continuous power that the equipment can output is 124 kW (166 bhp) and up to 230 kW (308 bhp) momentarily per axle. Thus, for four wheel driven vehicles the continuous power that the vehicle can either be braked or propelled by is 248 kW. In Figure 6 the continuous and momentarily limitations are shown together with the modeled required power to overcome the rolling and aerodynamic resistance at a flat road for different speeds of a typical car. The operating points (torque vs speed) from three tests with different drivers are also shown. For these tests the drivers were instructed to drive at highway speeds on a simulated highway with moderate traffic. This indicates the possibility of interesting investigations of driver behavior.

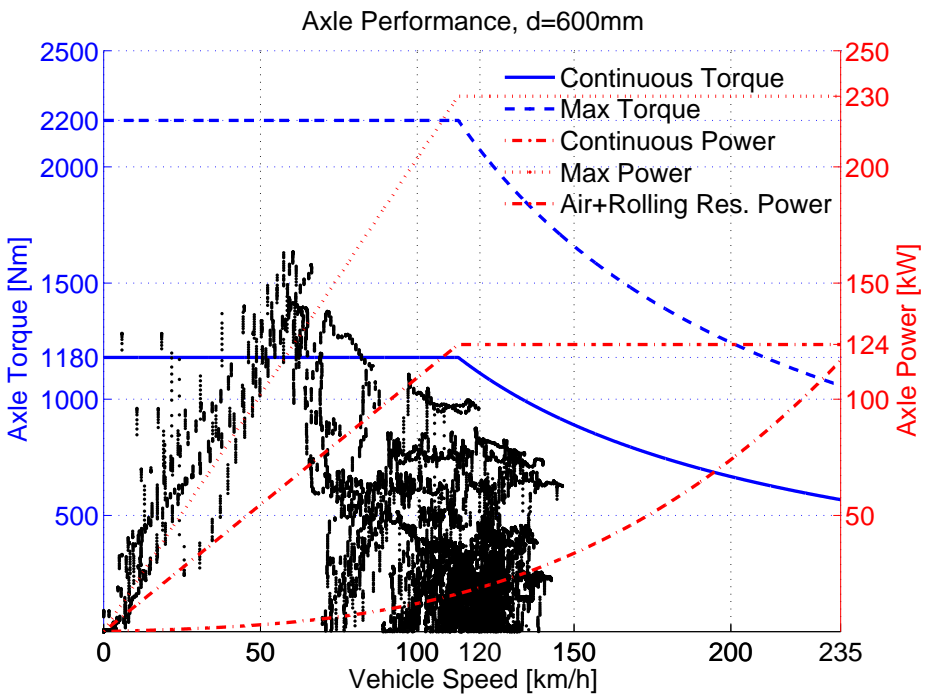


Figure 6: In the speed range 0 – 1000 rpm the dynamometer can deliver 1180 Nm of continuous torque and up to 2200 Nm momentarily per axle. In the speed range 1000 – 2100 rpm the power is the limiting factor. The continuous power is 124 kW and up to 230 kW momentarily can be exerted per axle. A reference trajectory of the required steady-state power for a typical 2WD car is shown together with measured torque from three experiments.

4.3 MOUNTING PROCEDURE

To mount a vehicle in the laboratory a vehicle is driven into the lab through the garage doors and the vehicle is then raised with either a jack or a lift. The vehicle is connected to the dynamometer units by removing the driven wheels, and with the help of adapter plates the vehicle is fitted to the equipment. The adapter plates are bolted on the wheels hubs and are then connected to the dynamometer unit for each wheel hub. After the bolts are tightened the vehicle is lowered and the vehicle then rests on the dynamometer. The connection to the dynamometer is similar to (Wang et al., 1997), where the car wheel rests on small rolls while the torque is extracted from the wheel hubs, but here the driven wheels are removed so that the driven wheel hubs are resting on the dynamometer units instead.

4.4 TEST MODES

The chassis dynamometer equipment can be used in a variety of ways depending on the purpose of the experiments. One test mode is constant speed while measuring the torque exerted by the powertrain. In another test mode the forces a vehicle is exposed to during normal driving are simulated, e.g. used when simulating driving cycles. This is also the foundation for the road profile test mode, a product from the ongoing joint collaboration. In this mode the system is pre-programmed with an elevation map. In the next sections the different test modes of the equipment are explained.

CONSTANT SPEED

In constant speed tests the chassis dynamometer are set to achieve a pre-defined velocity of the vehicle. The dynamometer units act as motors or generators to maintain the vehicle at this speed. A typical example is performance test where the vehicle manufacturer/owner want to measure how much power/torque the vehicle is producing at certain speeds. In Figure 7 the maximum torque and power for different vehicle speeds and gears have been measured. The tested vehicle was a Golf V with a 1.4l multifuel engine.

ROAD FORCES SIMULATION

An alternative to on-road tests is the use the chassis dynamometer in the road forces simulation mode. In this mode the simulated forces that a vehicle has to overcome at the wheels are the aerodynamic drag force F_{air} , the rolling resistance, F_{roll} , the gravitational resistance, F_{grav} , in case that the simulated road is not flat, i.e. has non-zero incline. If the propulsion force at the wheels, F_{prop} , produced by the powertrain exceeds these modeled losses the mounted vehicle will accelerate with an acceleration, a , according to

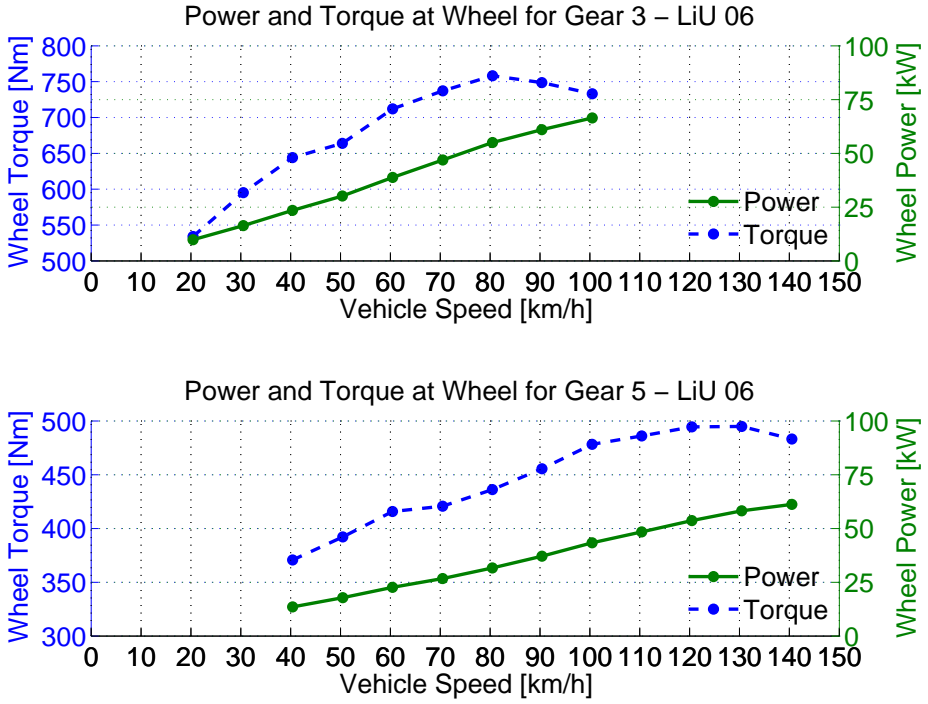


Figure 7: Measurements of the maximum torque and power that can be exerted at the wheels for a Golf V with a 1.4l multifuel engine. The upper figure is for the 3rd gear and the lower figure is for the 5th gear engaged.

$$m \cdot a = F_{\text{prop}} - F_{\text{res}}$$

$$F_{\text{prop}} = \sum_i \frac{T_{\text{wheel},i}}{r_{\text{wheel}}},$$

where m is the vehicle mass, F_{prop} the propulsion force calculated from the measured torque on each driven wheel, $T_{\text{wheel},i}$, and the wheel radius constant, r_{wheel} . The resistance force F_{res} can either be a polynomial function in vehicle speed or a standard model for driving resistance

$$F_{\text{res}} = F_{\text{roll}} + F_{\text{air}} + F_{\text{grav}}$$

$$F_{\text{roll}} = c_r \cdot m \cdot g$$

$$F_{\text{air}} = \frac{1}{2} \cdot \rho_a \cdot c_d \cdot A_f \cdot (v + v_0)^2$$

$$F_{\text{grav}} = m \cdot g \cdot p,$$

where c_r is the rolling friction coefficient, g the gravitational constant, ρ_a the density of air, c_d drag coefficient, A_f the frontal area of the vehicle, p incline of the road, and v_0 is the relative wind speed during the experiment. In case a polynomial function is used the air drag and rolling resistance is replaced with

$$F_{\text{air}} + F_{\text{roll}} = F_0 + F_1v + F_2v^2 + F_3v^3 + F_4v^4.$$

Depending on the sign of $F_{\text{prop}} - F_{\text{res}}$ the simulated vehicle will accelerate or decelerate. If the incline is set to zero the test will simulate driving on a flat road, and the forces the vehicle has to overcome depends on the vehicle parameters and the velocity the simulated vehicle is traveling at.

DRIVING CYCLES

A driving cycle is a speed profile (speed vs time) that can be used to test or certify vehicles regarding exhaust emissions and fuel consumption. Usually the driving cycle is driven at a flat road, i.e. with zero incline. This test mode is an application of the road force simulation where a pre-defined speed profile is to be tracked. During these tests either a driver in the vehicle is shown the profile and tries to follow it or a pedal robot is used to automate the testing.

ROAD PROFILE

A new test mode has been developed which simulates the forces for a road with varying road profile and hence varying incline depending on how far the simulated vehicle has traveled in the driving mission. Figure 8 shows the results of such an experiment where the driver was instructed to drive at highway speed. In the upper figure the vehicle speed is shown. In the lower figure road profile as function of distance is shown.

The speed of the vehicle determines the traveled distance which sets the current incline. Thus, depending on the driver input the distance and incline at a certain time is not necessary the same for another driver on the same driving mission.

This mode is a requirement for projects such as look-ahead control, co-simulation with a moving base simulator and studies of driver feel and behavior. These are new and more complex usages than standard constant speed tests and road force simulations, and thus puts new requirements on interfaces and behavior of the test equipment. Some also require access to internal vehicle control. To develop this new functionality we have collaborated with the dynamometer supplier, automotive companies, the Swedish National Road and Transport Research Institute, and our local Internet service provider.

LOOK-AHEAD CONTROL

A natural continuation of the road profile test mode is to use the system for look-ahead control related research. Look-ahead control using GPS navigation

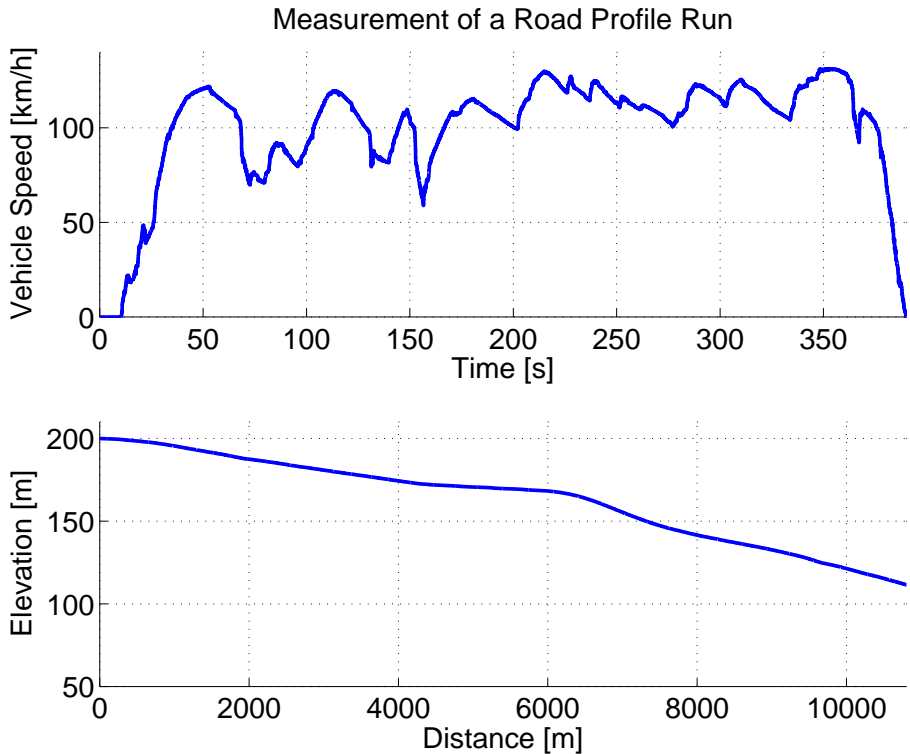


Figure 8: Velocity profile with elevation over sea level from an example measurement in road profile mode.

has previously been used for heavy vehicles where fuel savings are possible if the road topography is known (Hellström et al., 2009, 2010). An interesting prospect is to use the same techniques applied to hybrid electric or plug in hybrid electric vehicles where optimal battery charging strategies can be calculated using road topography, speed limit, traffic lights, and other road information.

Given the simulation possibilities of the vehicle propulsion laboratory such techniques can easily be evaluated for a large variety of situations and it is possible to answer questions such as what is the most relevant information to have access to or how will the algorithm be affected by dense traffic etc.

5 PERFORMED STUDIES

The system has already been used for a number of different projects such as

- NVH-analysis where the drivetrain and engine induced oscillations are analyzed achieving separation from the tire in an attempt to refine a tire pressure indicator system.

- Demonstrating appropriate excitation for modeling and control of co-surge for a 6-cylinder bi-turbo engine.
- Traditional engine mapping made possible for a group of students participating in the Formula student competition, having a slim budget.
- Chassis dynamometer road force co-simulation with a moving base simulator, where a pedal robot replaces the human driver, demonstrating functional interfaces to the lab.

5.1 MODELING OF ENGINE AND DRIVELINE RELATED DISTURBANCES ON THE WHEEL SPEED IN PASSENGER CARS

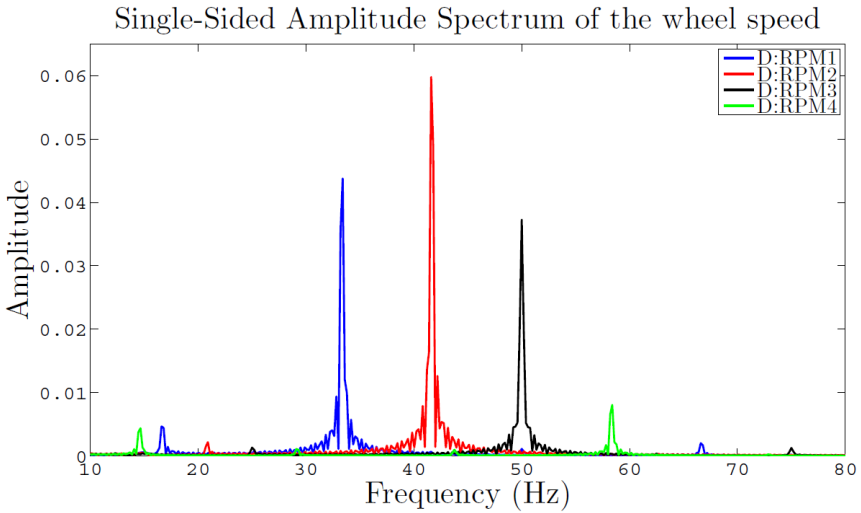
Tire vibrations measured from the wheel speed sensors can be used to monitor tire pressure since the dynamics of the tire depends on the pressure. However, other sources of vibrations, such as the drivetrain are also visible in the sensor data. An interesting problem therefore is to model and decouple the vibrations that origins from the drivetrain.

In cooperation with an industry partner the vehicle propulsion laboratory has been used to investigate how a wheel mounted dynamometer can be used to separate the tire vibrations in an effort to model these drivetrain vibrations (Johansson, 2012). This would not have been possible when using a chassis dynamometer with rolls. Another benefit with the hub-mounted dynamometer is that the body of the vehicle does not need to be fixed to the lab which means that regular cars of the market can be used without modification. For the experiments two different four wheel drive cars, a diesel Audi A4 and a petrol Audi A5, were used.

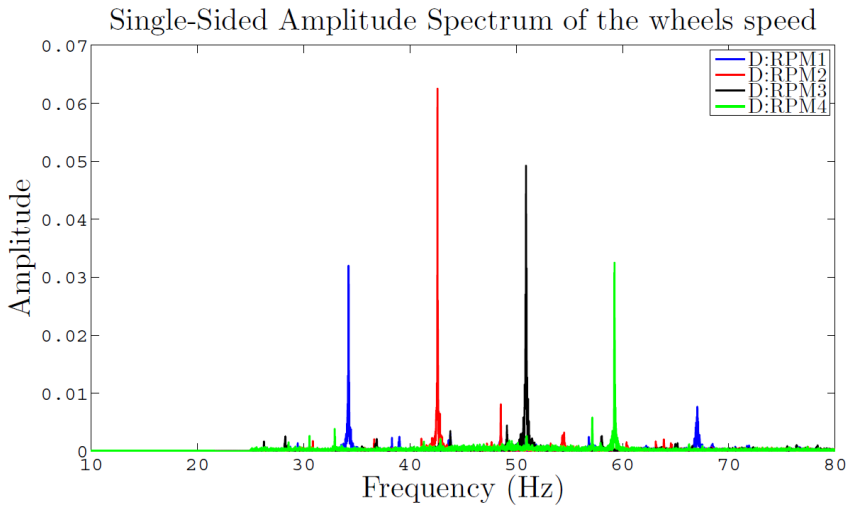
In (Johansson, 2012) the drivetrain is modeled as a series of masses, dampers, and springs and experiments are performed to parametrize the model. An example of a validation of the drivetrain model for the Audi A4 is shown in Figure 9. During these experiments the constant speed mode was used for a number of different engine speeds while the drivetrain oscillations were measured. The engine torque that was used for these experiments was 50 Nm. More details of the project are found in (Johansson, 2012). The fact that Figure 9 shows well defined peaks means that the equipment is appropriate for this type of investigation in terms of its own inertia, control performance, and noise levels.

5.2 MODELING AND CONTROL OF CO-SURGE IN BI-TURBO ENGINES

Bi-turbocharged supercharger configurations can give faster torque response and help to better utilize exhaust energy for V-type engines by allowing more efficient placement of the turbocharger (Thomasson and Eriksson, 2011). In a recent project the propulsion laboratory was used to study, model, and control a special surge phenomenon, co-surge, that can occur in these configurations. An



(a) Spectrum of the **simulated** wheel speed disturbances at different engine speeds for gear four.



(b) Spectrum of the **measured** wheel speed disturbances at different engine speeds for gear four.

Figure 9: Example of model validation for the drivetrain model. Simulated wheel speed disturbances, a), are compared to measured, b), for different engine speeds at fourth gear. (Courtesy of Robert Johansson, c.f. (Johansson, 2012))

example of co-surge is shown in Figure 10 where a 6-cylinder bi-turbo equipped vehicle was forced into co-surge by inducing a small 0.3 s throttle disturbance at time $t=0$. The disturbance causes oscillations in the mass flows of the two air-paths which can be seen in the upper figure.

For the experiments the constant speed mode was used for the dynamometer. Using this operation mode a set of operating points with different engine-speed and load was spanned. The bi-turbocharged engine was mounted in a car together with its auxiliary systems, making it possible to perform experiments and calibrate the control design in a realistic setting. The experiments show that it was possible to excite and study individual components in the car using the equipment in the laboratory. This made the development process efficient. Another benefit to be noticed was the short start-up time of the project compared to a conventional engine test bed. More information about the project can be found in (Thomasson and Eriksson, 2011).

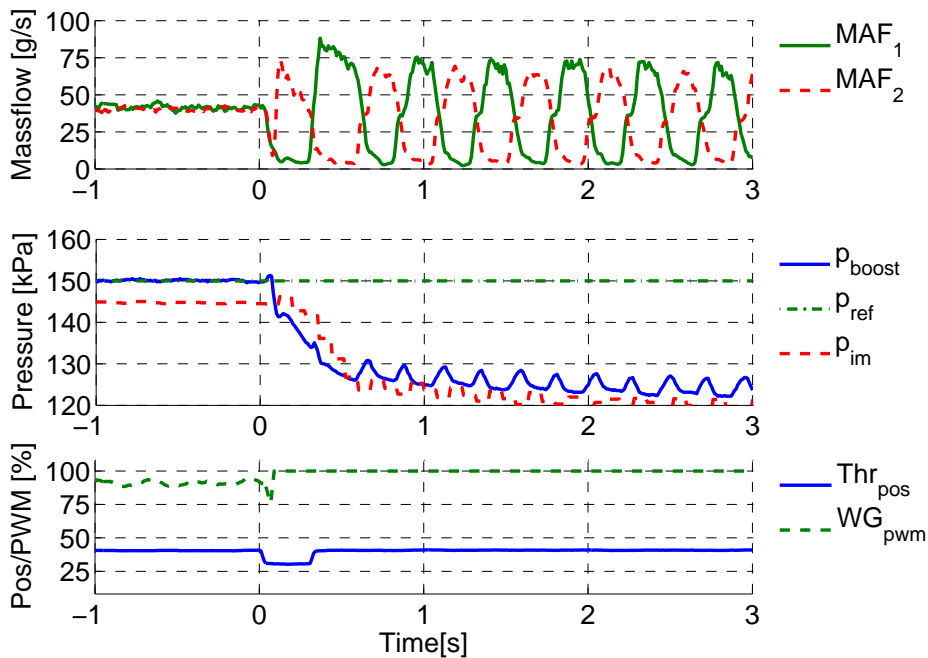


Figure 10: Mass flow rates for the two air-paths (upper), intake manifold and boost pressure (middle), and throttle position (lower). A 0.3 s throttle disturbance at time $t=0$ induces co-surge in the system. The mass flows starts to oscillate and will keep oscillating until the operating point it changed or a controller damps out the oscillations.

5.3 FORMULA STUDENT, MAPPING

The propulsion laboratory has also been used by the newly started Formula student team at Linköping University. The Formula student is a competition where the competing teams develop, design and build a small race car and competes with other universities once a year. The mapping of the engine was performed by measuring the torque at the wheel hubs at different engine speeds. Changes in the ignition timing and amount of fuel injected were executed. The fuel-to-air-ratio, λ value, was measured with an external λ -sensor and the torque was measured at the wheel hubs.

Given a complete vehicle it was beneficial to perform the mapping of the engine with the chassis dynamometer. The reason is that it is low-effort-work compared to constructing appropriate engine mounts and running it in an engine test bed, and even more important for a project with low budget it is significantly more cost-efficient. Another difference is that the complete powertrain is tested instead of only the engine, which can be beneficial sometimes.

5.4 CHASSIS DYNAMOMETER ROAD FORCE CO-SIMULATION WITH A MOVING BASE SIMULATOR

In cooperation with the Swedish National Road and Transport Research Institute, VTI, a hardware-in-the-loop setup with a pedal robot to replace the human driver has recently been investigated (Andersson et al., 2013). The idea is to use co-simulation to let a driver in the VTI moving base simulator, Sim III, experience an actual powertrain instead of the traditional models that are used, and to study the possibilities to enhance the fidelity of the simulator. Another possible benefit from such a setup is that the vehicle in the chassis dynamometer is exposed to more realistic loads because the driver input is likely to be closer to actual driving than when used independently.

In the project a pedal robot, shown in Figure 11, was developed for this purpose. During the experiments the pedal robot was fed driver inputs from Sim III via a low latency dedicated single mode fiber connection and the resulting forces and wheel speeds from the chassis dynamometer were returned to the Sim III simulator.

An actual driving mission using the pedal robot can be seen in Figure 12 where the driver sitting in the moving base simulator Sim III was instructed to drive at highway speeds with varying incline and traffic. At around 180 seconds the driver was exposed to traffic which can also be seen in the upper figure where the speed becomes more varying for the rest of the test. The elevation profile can be seen in the lower left figure and the measured wheel torque from the powertrain can be seen in the lower right figure. More information about this project can be found in (Andersson et al., 2013).

The overall conclusion is that the interfaces and coordination with other systems, such as pedal robot and moving base simulator, work well. This includes measurement and communication systems.



Figure 11: Pedal robot that was used to actuate the gas and brake pedal according to the input from the driver in the Sim III simulator.

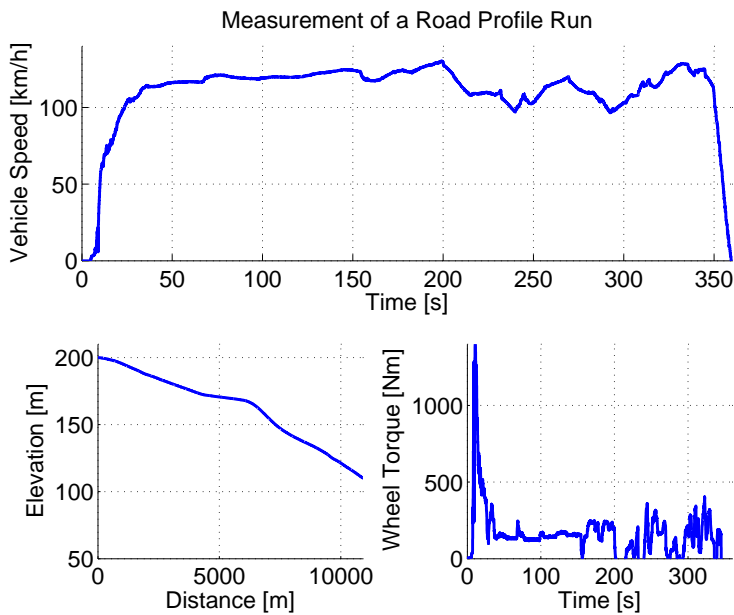


Figure 12: Velocity profile with elevation over sea level and wheel torque from a measurement in road profile mode and driver input from the pedal robot connected with the Sim III simulator. During the launch from zero velocity the high torque originates from low gear and high engine torque.

6 FUTURE PROJECTS AIMS AND GOALS

A natural continuation is development of future test methods for concept evaluation, driving feel, performance, and driver behavior. Specifically we are aiming for the following topics

- Continued development of co-simulation with moving base simulator.
- Behavioral studies.
- Integrated model chain (see below).
- Driving cycle research (see below).

INTEGRATED MODEL CHAIN

In a neighboring laboratory, dynamic vehicle models are used to evaluate vehicle behavior for different purposes (Lundahl et al., 2011; Nickmehr et al., 2012). The aim here is an integrated chain for testing of vehicle concepts consisting of

- Modeling.
- Automatic parameter estimation from measurements.
- Evaluation of driver behavior.

A first step is to automatically parametrize the models using measurements from regular driving while the complete movements, e.g. speed and acceleration, are measured. As a second step the dynamics of these models can be experienced in a moving base simulator, e.g. the previously mentioned Sim III at VTI, as well as in the vehicle propulsion laboratory studying driving feel, driver behavior and performance. Another possible use is to simulate a hybrid powertrain using the parametrized vehicle model to evaluate how a thought hybrid system would have performed in an actual driving mission of a regular car.

DRIVING CYCLE RESEARCH

In another application a pedal robot, e.g. like the one in Figure 11, can be used to eliminate the drivers impact on experiment repeatability. This is interesting for example when following a driving cycle where it is beneficial that the drivers direct impact on the vehicle is eliminated. Here the research focus on test repeatability with respect to driving cycle deviation.

Research questions that need to be answered is for example, how long should a driving cycle be and what should it look like to represent real world driving. Another research topic deals with how to construct a driving cycle to excite specific phenomena, e.g. for control system tuning. Both these examples requires a controlled environment with a predictable driving cycle tracking performance.

7 SUMMARY

The vehicle propulsion laboratory has been operational for about one year. It is still under continuous development both in collaboration with the manufacturer and with vehicular applications. The flexibility of the lab with its wheel mounted configuration yields an opportunity to use regular cars of the market without prior modifications and has proved useful to shorten the start-up times for projects such as the investigation of co-surge for bi-turbocharged V-type engines and for the traditional engine mapping, when used by the Formula student team. The experiments for the co-surge project also show that it was possible to excite and study individual components in the car using the equipment in the laboratory. This made the development process efficient.

Further, the wheel mounted configuration of the dynamometer is advantageous in investigations used to separate the tire vibrations in an effort to decouple the vibrations that origins from the drivetrain. The fact that it is possible to see well defined peaks in the measured data means that the equipment is appropriate for this type of investigation in terms of its own inertia, control performance, and noise levels.

The jointly developed road profile test mode, where topography maps are used together with the road force simulation, is a key component that enables new and more complex usages than standard constant speed tests and road force simulations, and thus puts new requirements on interfaces and behavior of the test equipment. As an example, the road profile test mode is used in the moving base simulator/chassis dynamometer co-simulation project. The overall conclusion is that the interface and coordination with other systems, such as pedal robot and moving base simulator, work well. This includes measurement and communication systems.

The road profile test mode thus yields unique opportunities, such as research on look-ahead control and driving cycle related research, and with infrastructure to neighboring facilities the usefulness of the lab can be extended even further, e.g. as in the co-simulation project.

REFERENCES

- A. Andersson, P. Nyberg, H. Sehammar, and P. Öberg. Vehicle powertrain test bench co-simulation with a moving base simulator using a pedal robot. *SAE International Journal of Passenger Cars - Electronic and Electrical Systems*, 6(1):169–179, 2013.
- M. André. The ARTEMIS European driving cycles for measuring car pollutant emissions. *Science of The Total Environment*, 334-335(0):73–84, 2004.
- C. J. Brace and J. Moffa. Increasing accuracy and repeatability of fuel consumption measurement in chassis dynamometer testing. *Journal of Automobile Engineering*, 223(9):1163–1177, 2009.
- E. Hellström, M. Ivarsson, J. Åslund, and L. Nielsen. Look-ahead control for heavy trucks to minimize trip time and fuel consumption. *Control Engineering Practice*, 17(2):245–254, 2009.
- E. Hellström, J. Åslund, and L. Nielsen. Design of an efficient algorithm for fuel-optimal look-ahead control. *Control Engineering Practice*, 18(11):1318–1327, 2010.
- M. Johanson. Multimedia communication, collaboration and conferencing using alkit confero. Whitepaper, Alkit Communications, 2010. URL http://confero.alkit.se/confero_whitepaper.pdf.
- R. Johansson. Modeling of engine and driveline related disturbances on the wheel speed in passenger cars. Master’s thesis, Linköping University, 2012.
- K. Lundahl, J. Åslund, and L. Nielsen. Investigating vehicle model detail for close to limit maneuvers aiming at optimal control. In *Proceedings of the 22nd International Symposium on Dynamics of Vehicles on Roads and Tracks (IAVSD)*, Manchester, UK, 2011.
- N. Nickmehr, J. Åslund, L. Nielsen, and K. Lundahl. On experimental-analytical evaluation of passenger car ride quality subject to engine and road disturbances. In *Proceedings of the 19th International Congress on Sound and Vibration*, Vilnius, Lithuania, 2012.
- L. Pelkmans and P. Debal. Comparison of on-road emissions with emissions measured on chassis dynamometer test cycles. *Transportation Research Part D: Transport and Environment*, 11(4):233–241, 2006.
- A. Thomasson and L. Eriksson. Modeling and control of co-surge in bi-turbo engines. In *Proceedings of the 19th IFAC World Congress*, Milano, Italy, 2011.
- W. Wang, N. Clark, D. Lyons, R. Yang, M. Gautam, R. Bata, and J. Loth. Emissions comparisons from alternative fuel buses and diesel buses with a chassis dynamometer testing facility. *Environmental Science & Technology*, 31:3132–3137, 1997.

Vehicle Powertrain Test Bench Co-Simulation
with a Moving Base Simulator Using a Pedal
Robot*

B

*Published in *SAE International Journal of Passenger Cars - Electronic and Electrical Systems*, 6(1):169-179, 2013.

Vehicle Powertrain Test Bench Co-Simulation with a Moving Base Simulator Using a Pedal Robot

Anders Andersson^{*}, Peter Nyberg^{**}, Håkan Sehammar^{*} and Per Öberg^{**}

^{}Vehicle Technology and Simulation,
VTI, SE-581 95 Linköping, Sweden.*

*^{**}Vehicular Systems, Department of Electrical Engineering,
Linköping University, SE-581 83 Linköping, Sweden.*

ABSTRACT

To evaluate driver perception of a vehicle powertrain a moving base simulator is a well-established technique. We are connecting the moving base simulator Sim III, at the Swedish National Road and Transport Research Institute with a newly built chassis dynamometer at Vehicular Systems, Linköping University. The purpose of the effort is to enhance fidelity of moving base simulators by letting drivers experience an actual powertrain. At the same time technicians are given a new tool for evaluating powertrain solutions in a controlled environment. As a first step the vehicle model from the chassis dynamometer system has been implemented in Sim III. Interfacing software was developed and an optical fiber covering the physical distance of 500 m between the facilities is used to connect the systems. Further, a pedal robot has been developed that uses two linear actuators pressing the accelerator and brake pedals. The pedal robot uses feedback loops on accelerator position or brake cylinder pressure and is controlled via an UDP interface. Results from running the complete setup showed expected functionality and we are successful in performing a driving mission based on real road topography data. Vehicle acceleration and general driving feel was perceived as realistic by the test subjects while braking still needs improvements. The pedal robot construction enables use of a large set of cars available on the market and except for mounting the brake pressure sensor the time to switch vehicle is approximately 30 minutes.

1 INTRODUCTION

One major part of any vehicle is the powertrain. This is what enables a vehicle to move forward providing energy conversion to torque at the wheels to overcome rolling resistance, aerodynamic drag and/or climbing resistance. The powertrain has also been under a lot of development recently as the environmental demands increase (Chan, 2007). To cope with the increasing demands the amount of hybrid vehicles using multiple sources for energy have increased (Chan, 2007; Offer et al., 2010). This introduces several clever solutions providing good environmental performance at the cost of more complex and expensive systems. It is thus interesting to see how these solutions are perceived by a driver. Also, battery cost is a major issue for hybrid electric and plug-in hybrid electric vehicles and it is therefore interesting to see how the driver behavior influences battery lifetime (Wu et al., 2012). To improve the possibilities to evaluate driver perception of a vehicle powertrain one idea is to use a moving base simulation. In these situations the powertrain is usually simulated using a vehicle model. To enhance the fidelity of the powertrain one possibility is to use a hardware-in-the-loop, HIL, powertrain. This enables a driver in a moving base simulator to experience an actual powertrain and for technicians to try new powertrain solutions while letting a driver run a test in a controlled environment. There exists a lot of HIL setups which would benefit if they could be used cooperatively. Previous work has been done by Ersal et al. (2011, 2012) where an internet distributed setup with an engine was investigated.

In this work we have connected the moving base simulator, Sim III, at the Swedish National Road and Transport Research Institute, VTI, with the vehicle propulsion laboratory, presented in (Öberg et al., 2013), at Linköping University, LiU.

Co-simulating a moving base simulator with a vehicle powertrain test bench using a test vehicle over a network connection is an area where little work has been done although individual parts have been well investigated. Therefore it's interesting to evaluate if this can be used to increase fidelity of current designs even further. The question we here initially investigate is if we think it is possible to obtain a realistic driving experience using a vehicle powertrain test bench in co-simulation with a moving base simulator.

2 EXPERIMENTAL SETUP

The main parts of the experimental setup are the vehicle propulsion laboratory at LiU, the moving base simulator Sim III, the pedal robot used to control the test vehicle in the propulsion laboratory, and the connection between the research facilities at LiU and VTI. In the following section these systems are all described. Further, the synchronization between the vehicle models and the driving mission used for the test driving is discussed.

2.1 CHASSIS DYNAMOMETER LAB

A new chassis dynamometer lab has recently been built at the Division of Vehicular Systems, Linköping University (Öberg et al., 2013), in the vehicle propulsion laboratory a chassis dynamometer setup is installed. The dynamometer provides four wheel motors/generators that can provide both positive and negative torque at the wheels of a vehicle, and a control computer. This control computer can be given road profile data to simulate driving for an installed vehicle. An overview of the lab can be seen in Figure 1.

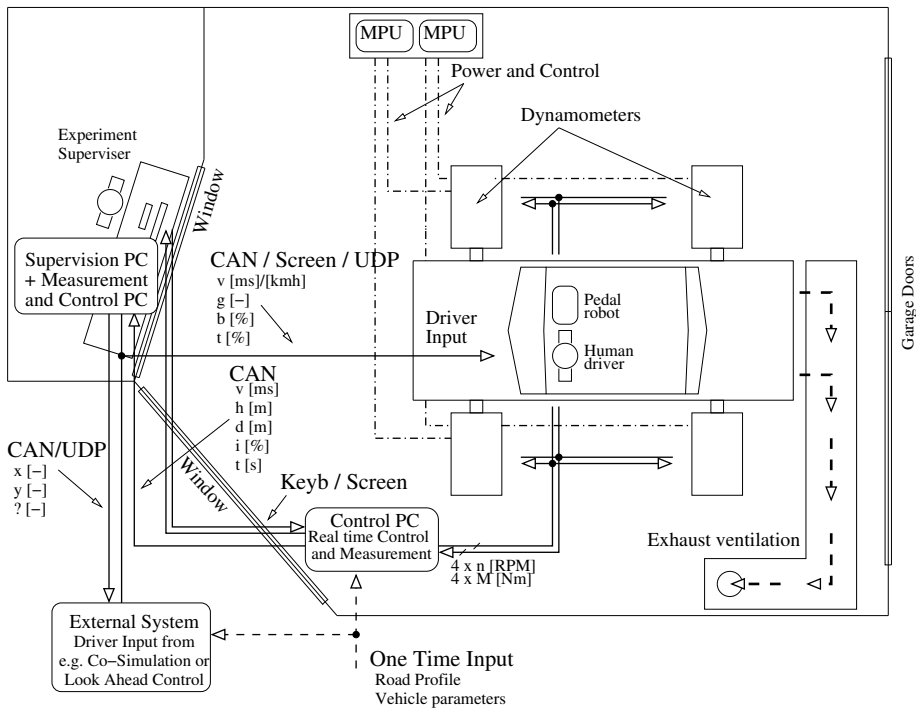


Figure 1: Schematic overview of the propulsion laboratory. The car is driven into the lab through the garage doors on the right and the dynamometers are then mounted to respective wheel hub. Road topography and vehicle parameters are then entered in the chassis dynamometer control PC. During the experiment the measurement and control PC in the control room forwards CAN messages from the chassis dynamometer to an external system via UDP. The external system then returns driver input to a human driver or, as in this case, a pedal robot.

SYSTEM DESCRIPTION

The dynamometer units can operate as both motors and generators depending on the system mode and can thus both brake and propel the vehicle. The dynamometer units are mobile and can be moved to fit different vehicle sizes and configurations, such as 1WD (motorcycles), 2WD, or 4WD vehicles. The vehicle is fit to the dynamometers by removing the driven wheels and mounting the vehicle to the dynamometer using adapter plates directly on the wheel hubs.

In a typical test setup the driver steps into the car as would be the case for a normal driving mission. In another scenario a pedal robot is used, e.g. when connected to an external system as discussed in this work. In both setups the experiments can be directed from the control room and the dynamometer can be controlled either through the Control PC or via CAN remote control which adds for extra safety because the external system can be used to automatically stop the dynamometer.

The outputs of the dynamometer are wheel torque and rotational speed but also vehicle speed and other quantities that can be calculated using the internal vehicle model. The torques are measured using string gauges fit to the drive suspension and the torque measurement accuracy is within 0.1% of measured value.

SYSTEM SETUP

Before starting an experiment a number of vehicle parameters is needed. Depending on operation mode they are

- Axle load in kg, m_a , and effective wheel radius, r_w , for calculation of safety limits
- Gear ratios, $r_{g,i}$, for all gears including the final drive, for calculation of engine speed
- Vehicle mass, m_v , front area, A_f , drag coefficient, c_d , and rolling resistance, c_r , for driving resistance calculation in the road force simulation mode
- Road topography map, including turn radii, for the road.

The chassis dynamometer equipment can be used in a variety of ways depending on the purpose of the experiments. One test mode is constant speed while measuring the torque exerted by the powertrain. In another test mode the forces a vehicle is exposed to during normal driving are simulated, e.g. used when simulating driving cycles. This is also the foundation for the road profile test mode that is used in this work.

ROAD FORCES SIMULATION

The simulated forces that a vehicle has to overcome at the wheels are the aerodynamic drag force F_{air} , the rolling resistance, F_{roll} , the climbing resistance,

F_{climb} , in case that the simulated road is not flat, i.e. has non-zero incline. The propulsion force at the wheels, F_{prop} , produced by the powertrain and the resistance forces determines the acceleration, a , of the mounted vehicle according to following model

$$F_{\text{tot}} = m_v \cdot a = F_{\text{prop}} - F_{\text{res}}$$

$$F_{\text{prop}} = \sum_i \frac{T_{w,i}}{r_w},$$

where m_v is the vehicle mass, F_{prop} the propulsion force calculated from the measured torque on each driven wheel, $T_{w,i}$, and the measured wheel radius r_w which is constant during simulation. The resistance force F_{res} can either be a polynomial function in vehicle speed or a standard model for road resistance

$$F_{\text{res}} = F_{\text{roll}} + F_{\text{air}} + F_{\text{climb}} \quad (1)$$

$$F_{\text{roll}} = c_r \cdot m_v \cdot g$$

$$F_{\text{air}} = c_d \cdot A_f \cdot \frac{\rho_{\text{air}} \cdot (v + v_0)^2}{2}$$

$$F_{\text{climb}} = m_v \cdot g \cdot p,$$

where c_r is the rolling friction coefficient, g the gravitational acceleration constant, ρ_a the density of air, c_d aerodynamic resistance coefficient, A_f the frontal area of the vehicle, p incline of the road, and v_0 is the relative wind speed during the experiment. In case a polynomial function is used the air drag and rolling resistance is replaced with

$$F_{\text{air}} + F_{\text{roll}} = c_0 + c_1 \cdot v + c_2 v^2 + c_3 \cdot v^3 + c_4 \cdot v^4.$$

Depending on the sign of $F_{\text{prop}} - F_{\text{res}}$ the simulated vehicle will thus accelerate or decelerate. If the incline is set to zero these equations will simulate driving on a flat road. The forces the vehicle has to overcome thus depends on the vehicle parameters and the velocity the simulated vehicle is traveling at.

VEHICLE DYNAMICS PARAMETERS

The parameters that are needed for the vehicle dynamics part when calculating braking force for the road simulation are

m_v - Mass of vehicle in kg

A_f - Front area m^2

c_d - Drag coefficient

c_r - Rolling coefficient

Built in parameters are

ρ_{air} - Air density (1.202 kg/m^3 at an altitude of 200 m)

g - Gravitational acceleration (9.81 m/s^2).

TEST VEHICLE

For this study a 2009 Volkswagen Passat Ecofuel DSG was used. This car has a dual clutch semi-automatic transmission and runs on both gasoline and methane. The maximal power of the car is 110 kW (150 hp) for both fuel options. In Figure 2 the car is shown mounted in the vehicle propulsion laboratory. Because it is a front-wheel driven car only the front wheels need to be connected.



Figure 2: Volkswagen Passat that is used in the experiment mounted in the chassis dynamometer of the vehicle propulsion laboratory.

Before the experiments a brake pressure sensor was installed on the main brake cylinder. To be able to mount the pedal robot the driver chair was removed. The parameters that were used for the vehicle are listed in Table 1.

Table 1: Vehicle model parameters used in the study.

Parameter	Value	Unit
m_v	1 401	kg
c_d	0.320	-
A_f	2.0	m ²
c_r	0.01	-
r_w	0.3	m

INPUT AND OUTPUT DURING SIMULATION

During simulation the input to the chassis dynamometer is those that a driver can give, namely

- Accelerator pedal position in the range $[0 - 1]$.
- Brake pedal pressure, measured in the range $[2.98 - 7]$ volts.

The outputs are in form of CAN messages sent either at 10 or 100 Hz. Status messages, such as temperature etc, are sent in 10 Hz and simulation output messages are sent either at 10 Hz or 100 Hz. The outputs available through these CAN messages are summarized in Table 2.

Table 2: Available output signals from the simulator rig.

Signal	Unit	Frequency	Description
n_i	rpm	100 Hz	Wheel speed
T_i	Nm	100 Hz	Wheel torque
v_l	km/h	10 Hz	Longitudinal vehicle speed
v_v	km/h	10 Hz	Vertical vehicle speed
r_{road}	m	10 Hz	Road curvature radius
H	°	10 Hz	Heading, relative origin
h	m	10 Hz	Elevation of road
p	°]	10 Hz	Incline
d_{TP}	m	10 Hz	Distance since start
t_{TP}	s	10 Hz	Time since start
T_i	°C	10 Hz	Dynamometer temperature
$S_{d,i}$	-	10 Hz	Dynamometer status
S	-	10 Hz	System status

2.2 VTI SIMULATOR III

The Swedish National Road and Transport Research Institute, VTI, is an independent research institute in the transport sector. The principal task of VTI is to conduct research and development related to infrastructure, traffic and transport. The institute has technically advanced equipment, and part of this equipment are the driving simulators. For this work, particularly the advanced moving base simulator, VTI Simulator III, or Sim III was used.

Sim III uses state of the art techniques for simulation of road conditions (Bolling et al., 2011) and has earlier been used in, amongst others, studies related to effects of yaw stability at side impact (Andersson and Jansson, 2011). A picture of Sim III can be seen in Figure 3.

The linear motion system of Sim III's has four degrees of freedom and offers both linear and tilt motion at an acceleration of 8 m/s^2 . Realistic lateral motions are obtained by linking the cradle's motion to the vehicle's lateral



Figure 3: Moving base driving simulator Sim III at VTI.

position. Sim III can be rotated 90 degrees to enable studies with focus on acceleration and braking instead of lateral forces.

To give the driver a field of vision of 120 degrees during the simulation six projectors are used and to simulate the rear-view mirrors three LCD displays are used. High-frequency vibrations can be provided using a vibration table. This can be used for example to simulate road unevenness during experiments with rumble strips. Both a passenger car and a truck can be fitted to the simulator and for the purpose of this project a Saab 9-3 cabin was used.

Software for running Sim III is largely developed at VTI. The software consists of algorithms for graphics, sound, simulation kernel, motion queuing, vehicle model and more. In this work the focus is on the vehicle model which is modified to accept inputs from the vehicle propulsion laboratory at LiU. This means that the chassis dynamometer at the propulsion laboratory controls the propulsion of the vehicle during the simulation but that other parts of the simulator is intact providing a realistic environment to the driver.

2.3 PEDAL ROBOT

To control the vehicle speed a pedal robot has been constructed which uses two electrical linear actuators pressing the accelerator and brake pedals. Together with a vehicle with an automatic transmission this setup gives basic control of the vehicle powertrain. The pedal robot control logic has been created using



Figure 4: Pedal robot installed in the Volkswagen Passat test vehicle.

Matlab Simulink with Stateflow and xPC-Target and the pedal robot uses a two-way UDP communication interface to Sim III. The actions taken by the driver in the simulator are sent as command signals to the pedal robot and the pedal robot controller sends status information back to the simulator software. A picture of the pedal robot is shown in Figure 4. As can be seen, the construction is made such that the actuators can be moved sideways and up and down which makes it easily adaptable for different vehicles.

Each actuator is of ball screw type and is driven by a 24 volts DC motor, equipped with an encoder for positioning. The actuator is also equipped with two adjustable circuit breakers defining the maximal and minimal allowed position of the piston. Each actuator has a working range of 300 mm.

ACCELERATOR PEDAL CONTROL

The pressure needed for pushing the accelerator pedal is relatively low and thus the main requirement for the actuator is high speed rather than high dynamic load. The chosen actuator has a dynamic load of 210 N and a maximum speed of 250 mm/s.

When mounting the accelerator pedal actuator the circuit breakers are first adjusted to define the maximum allowed range. The control application then starts with a calibration phase where the actuator is slowly moved up and down between the limits defined by the circuit breakers. In this way the circuit

breakers are used to set the safety limits for the controller. The working range is finally set with a safety marginal of 3 mm to these limits. An important aspect of the calibration process is to adjust the circuit breakers so that the zero position for the accelerator pedal is within the region limited by the safety limit and the position where the pedal does not cause any engine activity.

Once the calibration phase is completed a PI controller, shown in Figure 5, is used. Input to the controller is the desired accelerator position in mm. This position is calculated from the range limits and the input signal which is sent from the simulator at a frequency of 200 Hz.

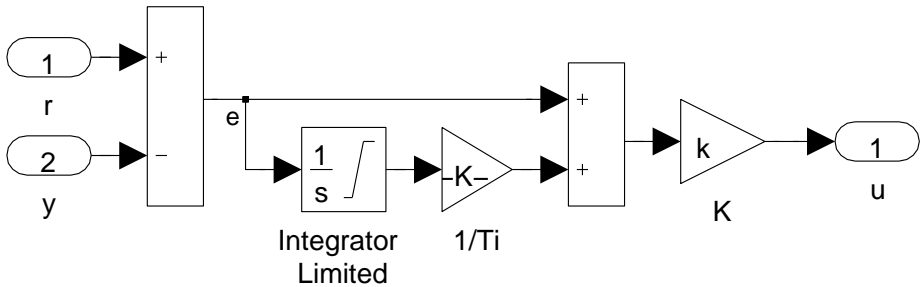


Figure 5: Position control of accelerator pedal with limits on integrator to avoid wind-up using Matlab Simulink.

BRAKE PEDAL CONTROL

The actuator controlling the brake pedal will be subjected to a significant resistance force when a large braking pressure is commanded from the simulator. It is thus desirable that the mounting of the pedal robot in the vehicle is as stiff as possible. For the constructed robot all four front chair screw holes were used to ensure a sufficiently stiff mounting. For this actuator, maximum load has been prioritized and the dynamic load is 420 Nm while the maximum speed is 215 mm/s.

As control signal measured brake pressure in Sim III was scaled linearly between measured brake pressure limits in the Volkswagen Passat test vehicle. The measured maximum and minimum brake pressure in Sim III was thus scaled to measured maximum and minimum brake pressure in test vehicle. In case of measurement spikes the brake pressure measurement was limited to the maximum pressure limit. Zero and maximum pressure in Sim III was measured from 0 kPa to 14000 kPa, and in the test vehicle it was measured from 3 to 7 volts.

As for the accelerator pedal the circuit breakers are first adjusted to define the maximum allowed range of the brake pedal. The brake pedal actuator control application then also starts with a calibration phase where the circuit breakers are used for defining the working range of the actuator. For the brake pedal

control the circuit breakers are adjusted to give maximum and minimum allowed pressure in the brake cylinder of the vehicle. To close the control loop the vehicle has been equipped with a pressure sensor, measuring the pressure in the brake master cylinder. One important aspect of the calibration is to adjust the zero pressure limit so that when the simulator commands zero pressure the brake pedal is not activated. This is necessary because if the pedal is even slightly activated the vehicle's own logic may prevent the car from accelerating.

Once the calibration phase is completed a PI controller for pressure in the main brake cylinder is used. This controller is sufficient when the command signal is greater than zero since this will make the actuator push against the brake pedal. When commanded pressure is zero there is no control of the actuator position and nothing will prevent it from drifting backwards into the circuit breaker. This will cut the power to the actuator for safety reasons. Therefore the pressure controller is complemented by a position controller, which is also a PI controller. This controller uses output from the motor encoder and kicks in when the actuator has no contact with the brake pedal. This way the pedal is prevented from drifting into the circuit breaker.

A problem with the brake pressure measurement is that the voltage switching from the PWM motor control has a negative influence on the measured brake pressure which interferes with the controller. To overcome this problem a second order low-pass filter is used. The filter was tuned to remove the pressure spikes that were present in the pressure signal which introduced a signal delay of approximately 15 ms.

2.4 CONNECTION BETWEEN FACILITIES

To be able to use the powertrain setup at LiU together with the Sim III simulator a connection had to be established between the two facilities. As the physical distance is rather short, approximately 500 meter, an optical fiber link was established which connects the network at the chassis dynamometer facility with the Sim III network. To ensure that no external interference occurred during the simulations this network was closed off by turning off the power to routers connecting hardware which was not used during these experiments. Because UDP has a lower overhead than TCP and because that the need for an acknowledge is not needed when no packet loss is expected UDP was chosen as communication protocol.

2.5 SYNCHRONIZING VEHICLE MODELS

Both the chassis dynamometer in the propulsion laboratory and Sim III need to know the wheel speed of the vehicle. The chassis dynamometer uses the speed for the road force simulation and Sim III needs it for the driver experience.

The chassis dynamometer at the vehicle propulsion lab uses a vehicle model to calculate vehicle speed according to the model in (1). The modeled wheel speed is used as reference and the amount of torque that the powertrain exerts

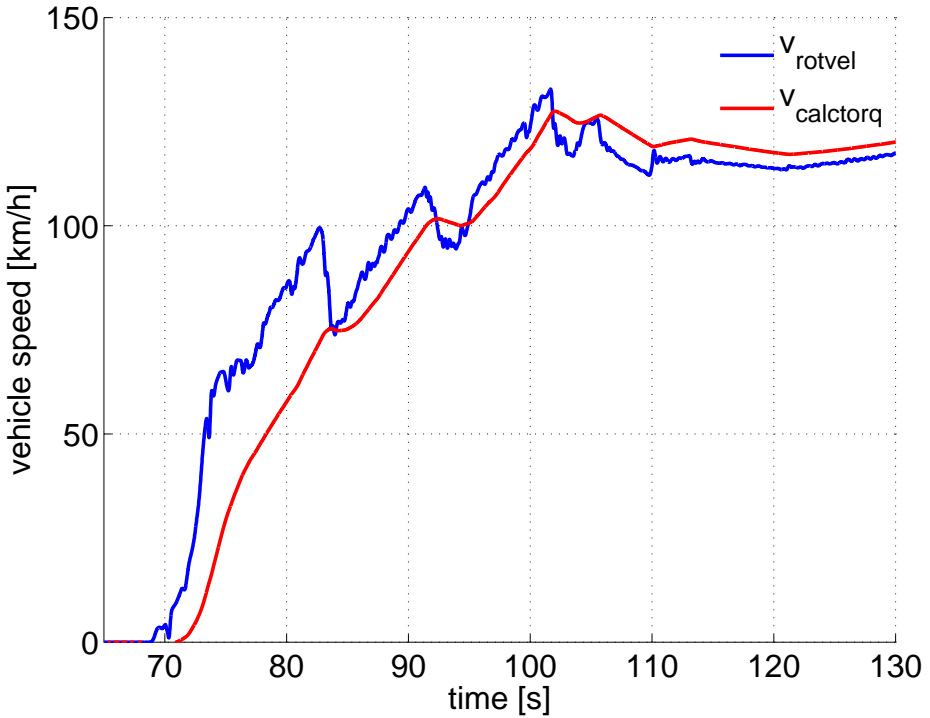


Figure 6: Measured velocity from dynamometers rotational speed compared with calculated speed using (1) from measured dynamometers torque.

at the wheel hubs are measured. Using this torque the vehicle speed is then increased or decreased according to (1).

For the moving base simulator there is thus at least two different ways to calculate vehicle speed. One option is to use the rotational velocity measured at the wheels in the propulsion laboratory and another option is to instead use the measured torque to calculate the acceleration which is then integrated to vehicle speed using the model equations in (1) using the same model parameters as for the dynamometer.

In Figure 6 we show an acceleration phase of the vehicle when starting from stand still on a motorway. Here the velocity is calculated using the two described options. The speed limit on a Swedish motorway is typically 110 km/h. At time 83 s in the data the transmission performs a gear shift and we see a large drop in measured rotational speed. Thus, we see that if we only use the measured rotational speed we get a large variation in speed during the gear shift. If we on the other hand would use measured torque the models deviate due to different implementation choices.

To overcome this model deviation while at the same time suppressing large speed variations due to gear shifts our approach is to use an observer to merge

the two signals. By tweaking the observer gain, K , it is possible to smooth out the speed variation while keeping the two models synchronized. The equations for the vehicle speed using discrete notation is

$$\begin{aligned} \dot{v}[i] &= -c_r \cdot g \cdot \min(v[i-1], 1.0) \\ &\quad + \frac{T_1 + T_2}{m_v \cdot r_w} \\ &\quad - c_d \cdot A_f \cdot \rho_{\text{air}} \cdot \frac{v^2[i-1]}{2 \cdot m_v} \\ &\quad + K \left(\frac{\pi}{30} \frac{n_1 + n_2}{2} r_w - v[i-1] \right) \\ v[i] &= v[i-1] + \dot{v}[i] \cdot \Delta t, \end{aligned}$$

where T_1 and T_2 are torque measured at the chassis dynamometer rig for the front wheels, n_1 and n_2 are measured rotational speed at the chassis dynamometer and Δt is the timestep between samples. Here effects of incline and speed offset due to wind have been neglected.

2.6 DRIVING MISSION

A driving mission with the goal to test the complete setup and at the same time get first impressions feedback was constructed. Other objectives was to evaluate if the obtained performance fulfilled our expectations. The used driving mission consisted of approximately 10 km of driving on a previously measured part of the E4 motorway between Linköping and Norrköping. About 3 km of the drive was without traffic while 7 km was with light surrounding traffic. The height profile of the road is shown in Figure 7 where it can be seen that the motorway is going slightly downwards. The road curvature of the used road segment is small and is thus approximated to be straight. At the start of the driving mission the position for Sim III and the chassis dynamometer are synchronized.

For the initial testing test drivers were recruited at VTI and LiU and their instructions were to maintain a speed between 60 km/h and 140 km/h while trying to get a feeling of the system without having too unnatural behavior. This means that most of the test drivers, even though they were not involved in this work had heard of it, and thus were biased. The large linear motion in Sim III was used for lateral motion and the cylinders were used to present acceleration and deceleration. When a driving mission was complete the test driver was asked to fill in a questionnaire and after that the test leader had an informal discussion until the next test person arrived, which was typically in around 5 minutes.

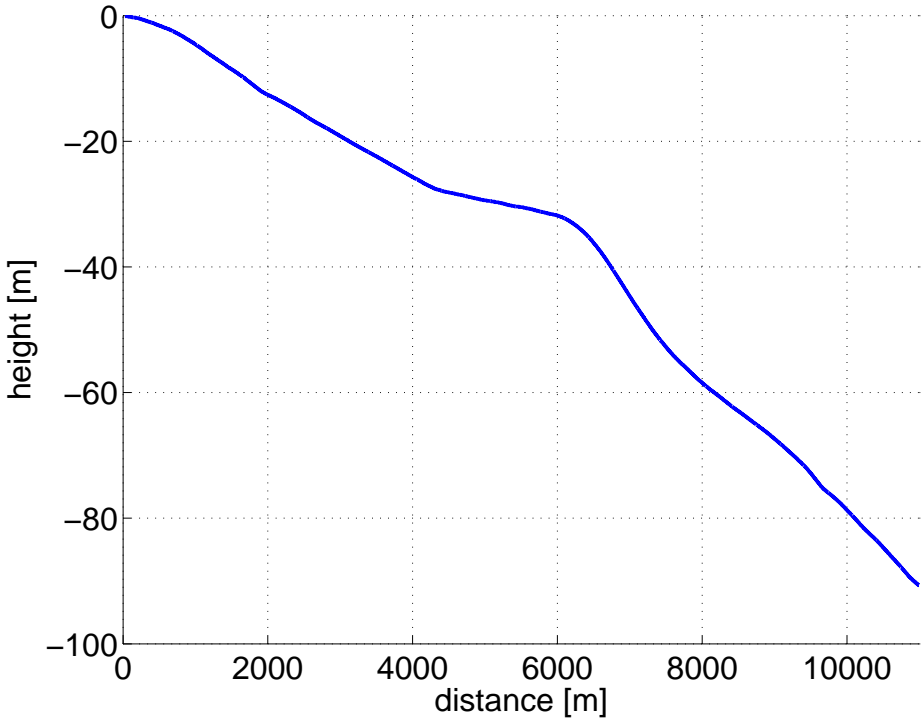


Figure 7: Longitudinal height profile of the used road segment.

3 RESULTS

3.1 NETWORK PERFORMANCE

A round trip time, RTT, test was used to test the performance of the network. A test packet similar to the actual packages sent during simulations was created to ensure that the testing conditions were similar to those of an actual driving mission. The test packets represents actual packets sent from Sim III with some extra data to ensure that the packets had decent sizes, see Table 3.

For the RTT test each packet is timestamped and id-tagged with an increasing counter value before being sent off. This was to ensure that packets were received in order. The packets are then sent at 200 Hz from Sim III, which is the same speed at which the simulator core is running, and upon reception at the vehicle propulsion laboratory they are sent back without modification. When the packet returns to Sim III it is once again timestamped and stored to disc. Typically experiments does not involve driving for to long and about one hour of driving were considered enough as a little above normal. Therefore, during the test one million packets were sent which corresponds to a little more than 83 minutes.

The RTT test programs were running at Linux computers and to ensure

Table 3: Packet structure that was used in the RTT test between the two facilities.

Type	Name
time_t	send_sec
suseconds_t	send_usec
time_t	rcv_sec
suseconds_t	rcv_usec
long	counter
float	data[70]

as low latency as possible the programs ran with higher priority than normal processes. This way the test was performed in the exact same way as would be the case during a driving mission.

Table 4: Statistics for the RTT test between the facilities.

Statistic	Value
Number of Packets	1 000 000
Min delay	0.20 ms
Max delay	2.17 ms
Median delay	0.22 ms
Dropped packets	none
Spikes above 0.5 ms	18

The round trip times for one of these test can be seen in Figure 8 and statistic measures of the delays are shown in Table 4. No packets were received in the wrong order for any of the tests which is the expected result as the largest obtained packet delay was 2.17 ms and a complete simulation loop is 5 ms. 99.9 percent of the packages had a delay of 0.27 ms or faster.

3.2 STEP RESPONSE TESTS OF PEDAL ROBOT

To evaluate the accelerator pedal response time a number of step response tests were performed. The step response tests were about two minutes each and for these test the accelerator pedal was fed reference values of 0, 0.25, 0.75 and 1.0. In Figure 9 five step responses from two different tests are shown on top of each other. The first tests shows a step from 0 (released) to 1 (maximally depressed) and the second shows steps between 0.25 to 0.75 of maximally depressed accelerator pedal.

Step response tests were conducted for the brake as well. For these tests approximately four minutes of step responses were recorded for two different types of step responses, one test between minimum and maximum pressure and one test between 0.25 to 0.75 of maximal brake pressure. Five steps are shown on top each other in Figure 10, where also the two different control strategies

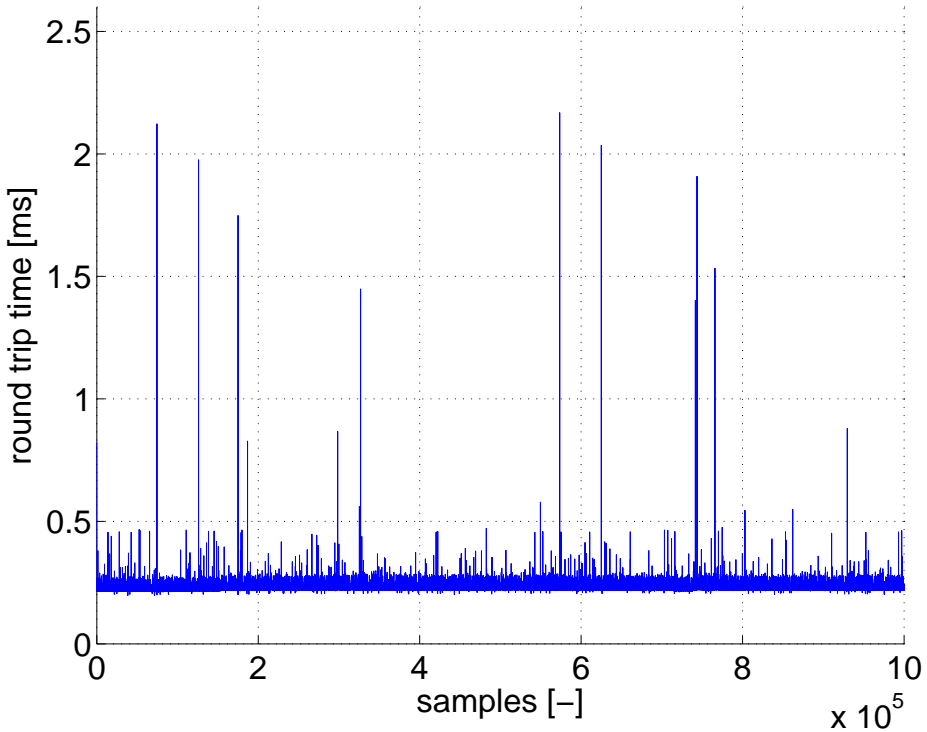


Figure 8: Round trip time, RTT, between the propulsion lab at LiU and Sim III using the fiber optics link.

for the fully released brake pedal and the not fully released brake pressure can be seen.

3.3 RUNNING THE COMPLETE SYSTEM

The study with our driving mission contained five test drivers were data were logged. Here we show data from the different driving missions and summarizes feedback from the test drivers.

ACCELERATOR AND BRAKE PEDAL

The performance of the accelerator and brake pedals is analyzed by evaluating the correspondence between the desired and obtained output. Using these values a control error $\epsilon = u_{ref} - u$ is calculated. Logged data from one of the test drivers is shown in Figure 11 and Figure 12 together with respective control error. As can be seen, both the accelerator and brake pedals closely follows their reference signals. The RMS of the control errors are between $1.87e-4$ to $6.44e-4$ for the accelerator pedal and between $4.82e-2$ to $5.96e-2$ for the brake pedal. As

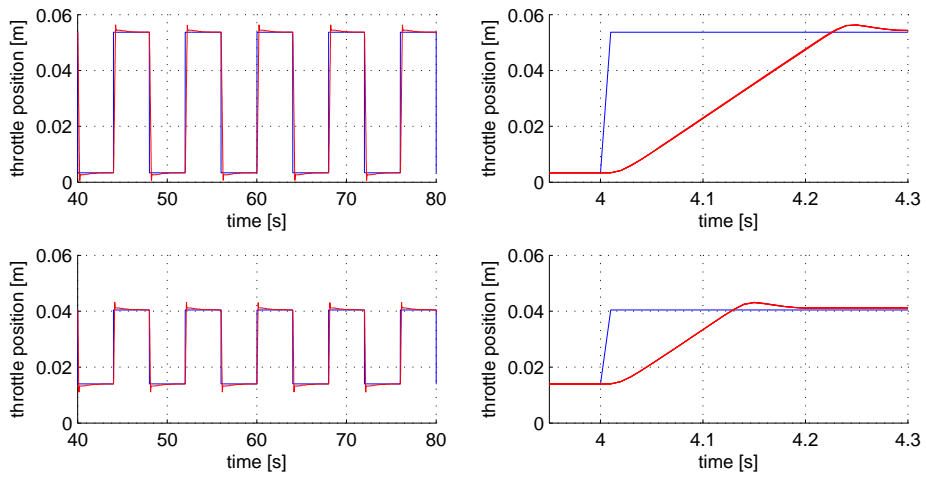


Figure 9: Step response tests made with the accelerator. The steps are from 0 (released) to 1 (maximally depressed) and from 0.25 to 0.75 of maximally depressed accelerator pedal. In the right figures five steps are shown on top of each other.

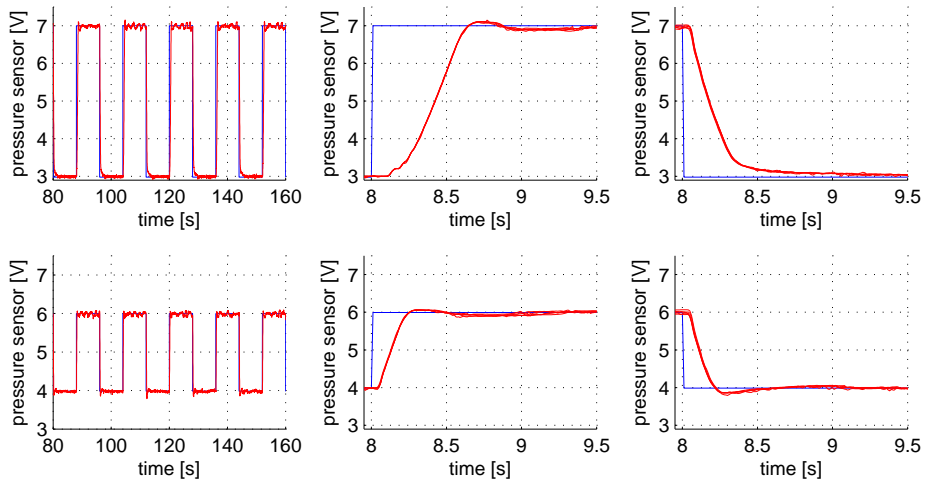


Figure 10: Step response tests made with the brake pedal. Steps are from minimum to maximum brake pressure (upper) and between 0.25 to 0.75 of maximum brake pressure (lower). Note the different control strategy for releasing the brake in the upper rightmost figure.

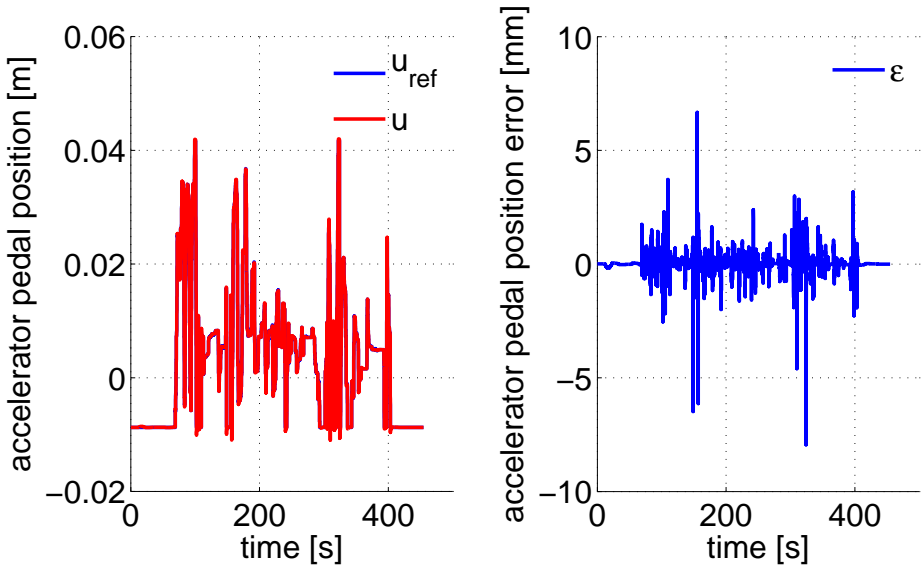


Figure 11: Accelerator pedal position reference value compared with actuated position value for one of the test drivers.

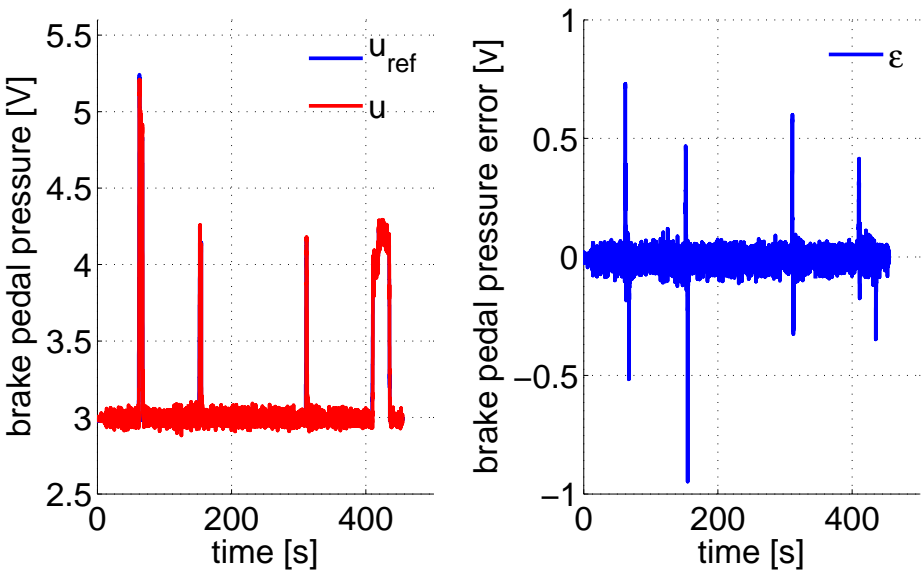


Figure 12: Brake pedal pressure reference value compared with actuated pressure value for one of the test drivers.

the working range of the accelerator pedal is approximately 5 cm this translates to a RMS error of about 1 percent, while for the brake pedal with a working range of 4 V the RMS error is about 1.5 percent. However, because the brake pedal is rarely used during normal driving these values need to be interpreted with care.

For the accelerator pedal, which is used most of the time during driving, the conclusion is that the controller is sufficiently fast while for the brake pedal the RMS is averaged over large periods where the pedal is never used and where the control error is almost zero. The brake pedal RMS therefore measures mostly noise.

VEHICLE RESPONSE IN SIM III

To tune the trade-off for the observer parameter K a few test drives were conducted before the study. In these tests the value of K was adjusted until a reasonable trade-off was obtained. The velocities that were obtained for the chassis dynamometer and Sim III using the chosen K for one of the test drivers driving the test vehicle is shown in Figure 13. Here it can be seen that the

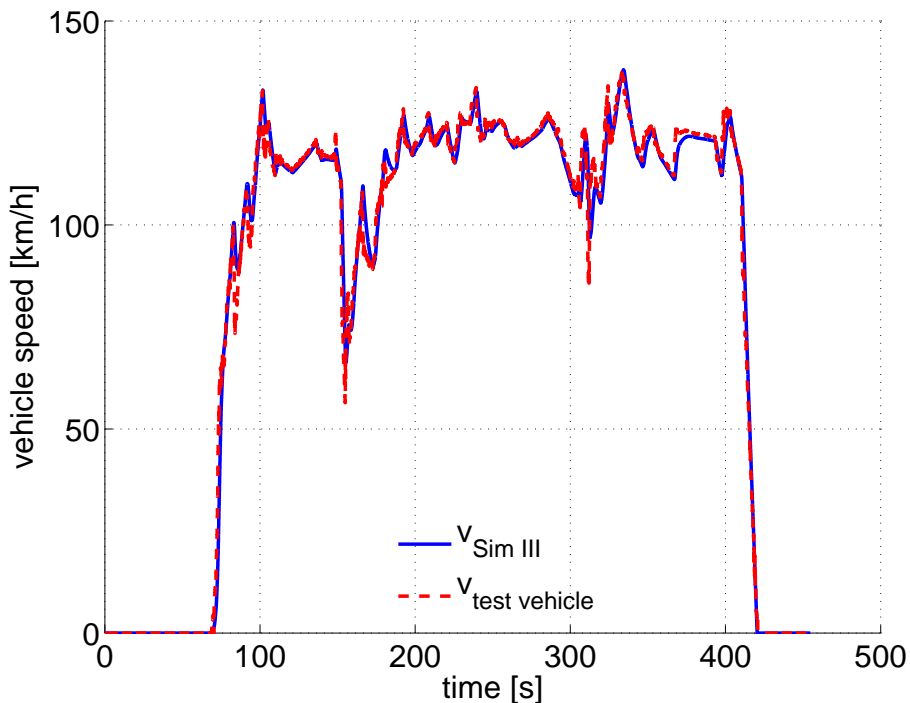


Figure 13: Comparison of the Sim III vehicle speed with the chassis dynamometer vehicle speed for the test vehicle for the chosen K .

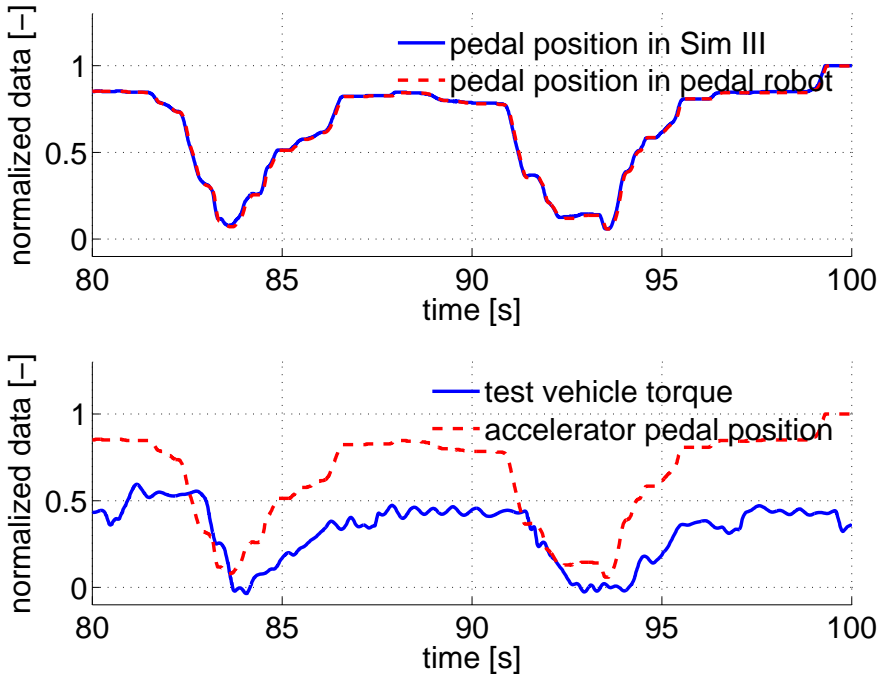


Figure 14: Response times from pedal position in Sim III to pedal robot position (upper) and from pedal robot position to test vehicle torque (lower).

velocity in Sim III is smoother than for the test vehicle, while we also see that the difference in velocity is small. This difference in velocity results in a position error which is approximately 1 percent of driven distance, meaning driving 100 m yields an offset in position by 1 m.

Another important aspect are the time delays for the system. In Figure 14 the time delay from an accelerator pedal change until the pedal robot has actuated desired position is about 0.05 to 0.1 s, which was expected from the step response test. Similar results are obtained for the brake pedal. The time delay from releasing the accelerator pedal, at about 92 s in the figure, until a change in measured torque is about 0.6 s.

TEST DRIVER FEEDBACK

The driver behavior differed between drivers as some drivers were driving between 60 km/h to 140 km/h and some drivers maintained 110 km/h only changing speed due to traffic conditions. This can be seen in the reference values for the accelerator and brake pedal and also in the velocity and acceleration of the vehicle in Sim III.

The general feeling of the vehicle was found sufficiently good by the test

drivers. There were however some complaints of which the main two were

- Lack of engine sound feedback.
- The brakes seemed slow.

The reason for the lack of engine sound is that engine speed was not measured at the propulsion laboratory and hence the sound feedback couldn't be adjusted according to engine speed. Therefore it was decided to rather have no sound than erroneous sound. This is, however, something that will be fixed in future experiments. As a result of the missing sound test drivers probably exaggerated accelerator use.

4 CONCLUSIONS

The connection between the facilities is fast enough for our purposes. The amount of lost packets are none meaning that every packet will reach its destination. The maximum delay is shorter than the simulation loop time which means that data from the chassis dynamometer will always be recent. This conclusion is also drawn when looking at the logged data where the delay from the network is so small compared to other delays that it can not be seen.

The constructed pedal robot works well. This is seen both in the results from the step response test and in the data from the test driving. For the construction, one intention was to minimize the time of switching vehicles and when mounting the pedal robot it was confirmed that even though the front chair had to be removed the mounting took about 30 minutes. As the perception of braking was considered in need of improvement this would be one of the first part to improve along with the engine sound which is most easily implemented.

Data obtained from our driving mission experiment with test drivers show that the complete setup is functional and that the synchronization of the models for the different systems works. For a typical driving mission this initial experiment setup already indicates small, meaning around 1 percent, control errors in the vehicle position and in accelerator pedal position for motorway driving.

Put together, interviews with test drivers and data from the example driving mission shows that the current co-simulation setup has the potential of obtaining a realistic driving experience.

REFERENCES

- A. Andersson and J. Jansson. A moving base simulator investigation of effects of a yaw stability system caused by a side impact. *ASME/Journal of Computing and Information Science in Engineering*, 11(4), 2011.
- A. Bolling, J. Jansson, M. Hjort, M. Lidström, S. Nordmark, H. Sehammar, and L. Sjögren. An approach for realistic simulation of real road condition in a moving base driving simulator. *ASME/Journal of Computing and Information Science in Engineering*, 11(4), 2011.
- C. Chan. The state of the art of electric, hybrid, and fuel cell vehicles. *Proceedings of the IEEE*, 95(4):704–718, 2007.
- T. Ersal, M. Brudnak, A. Salvi, J. Stein, Z. Filipi, and H. Fathy. Development and model-based transparency analysis of an internet-distributed hardware-in-the-loop simulation platform. *Mechatronics*, 21:22–29, 2011.
- T. Ersal, M. Brudnak, J. L. Stein, and H. K. Fathy. Statistical transparency analysis in internet-distributed hardware-in-the-loop simulation. *IEEE/ASME Transactions on Mechatronics*, 17(2), 2012.
- P. Öberg, P. Nyberg, and L. Nielsen. A new chassis dynamometer laboratory for vehicle research. *SAE International Journal of Passenger Cars - Electronic and Electrical Systems*, 6(1):152–161, 2013.
- G. Offer, D. Howey, M. Contestabile, R. Clague, and N. Brandon. Comparative analysis of battery electric, hydrogen fuel cell and hybrid vehicles in a future sustainable road transport system. *Energy Policy*, 38(1):24–29, 2010.
- C. Wu, J. Wan, and G. Zhao. Addressing human factors in electric vehicle system design: Building an integrated computational human-electric vehicle framework. *Journal of Power Sources*, 214:319–329, 2012.

Using Real-World Driving Databases to
Generate Driving Cycles with Equivalence
Properties*

C

*Submitted for journal publication.

Using Real-World Driving Databases to Generate Driving Cycles with Equivalence Properties

Peter Nyberg, Erik Frisk and Lars Nielsen

*Vehicular Systems, Department of Electrical Engineering,
Linköping University, SE-581 83 Linköping, Sweden.*

ABSTRACT

Due to the increasing complexity of vehicle design understanding of driver behavior and driving patterns is becoming more and more important in vehicle design. Therefore large amounts of test driving is performed, which together with recordings of normal driving, results in large databases of recorded drives. A fundamental question is how to make best use of this data to devise driving cycles suitable in the development process of vehicles. One way is to generate driving cycles that are representative for the data, or for a suitable subset of the data e.g. regarding geographical location, driving distance, speed range or regarding many other possible selection variables. Further, to make a fair comparison on two such driving cycles possible, another fundamental requirement is that they should have similar excitation of the vehicle. A key contribution here is an algorithm that combines the two objectives above. A formulation with Markov processes is used to obtain a condensed and effective characterization of the database, and to generate candidate driving cycles. Added to that is a method transforming a candidate to an equivalent driving cycle with desired excitation. The method is a general approach, but is here based on the components of the mean tractive force, MTF, and this is motivated by a hardware-in-the-loop experiment showing the strong relevance of these MTF components regarding fuel consumption. The result is a new method that combines the generation of driving cycles using real-world driving cycles with the concept of equivalent driving cycles.

1 INTRODUCTION

A driving cycle, also called driving schedule, speed profile, or velocity profile is represented by vehicle speed versus time, and an example of a recorded real-world driving cycle can be seen in Figure 1. Driving cycles are used in the automotive industry to evaluate vehicles from different perspectives, and some examples are in exhaust gas emissions tests (Lin and Niemeier, 2002; Fontaras et al., 2014; André, 1996) and in vehicle traffic control (André, 1996; Tong et al., 1999). They are also used as an engineering tool for comparison and design (Kenworthy et al., 1992; Shahidinejad et al., 2010; Stockar et al., 2011), and with increasing complexity of vehicle design this becomes more and more important and creates a strong need for representative driving cycles that can be effectively used in the development process. As an example a common driving cycle, that is used in exhaust gas emissions tests and also heavily used in comparison of vehicles is the New European Driving Cycle, NEDC, which is the certification driving cycle for light-duty vehicles in Europe. It is shown in Figure 2, and it easily seen that it is not a recording of a drive but rather a constructed profile. Regarding the NEDC, the general consensus is that it is not representative of real-world driving (Fontaras and Dilara, 2012; Fontaras et al., 2014; Zaccardi and Le Berr, 2012), partly due to the low levels of acceleration compared to real-world driving. Also, the number of acceleration sequences in the NEDC compared to real-world driving differs, see for example the difference in Figure 1 and Figure 2.

Now, if a vehicle manufacturer focuses only on such a fixed driving cycle during the development and design of a vehicle there are at least two risks. One risk is that the driving cycle is not representative for actual usage of the vehicle. The other risk is that if only one driving cycle is used, then the designs are optimized for this specific driving cycle, and if the driving cycle is not representative for real-world driving there is a considerable risk that the design will be sub-optimal when applied to a similar situation (Schwarzer and Ghorbani, 2013; Kågeson, 1998).

To deal with the abovementioned sub-optimization problem the goal is to have a method that (i) generates new driving cycles that are representative when compared to real-world driving databases, and also (ii) excites the vehicle in a similar way so that any performance comparison made, between the generated cycles, is fair. The problem to solve is then to be able to generate driving cycles that have similar vehicle excitation and also to motivate the excitation measures to use.

1.1 RELATED WORK

Different but related approaches have been reported in the literature. Using mathematical methods to determine which of several different driving cycle that can represent real-world driving has been studied by Zaccardi and Le Berr (2012). Their findings were that five driving cycles could represent a larger set of driving cycles. However, the outcome of one driving cycle is difficult to compare to the

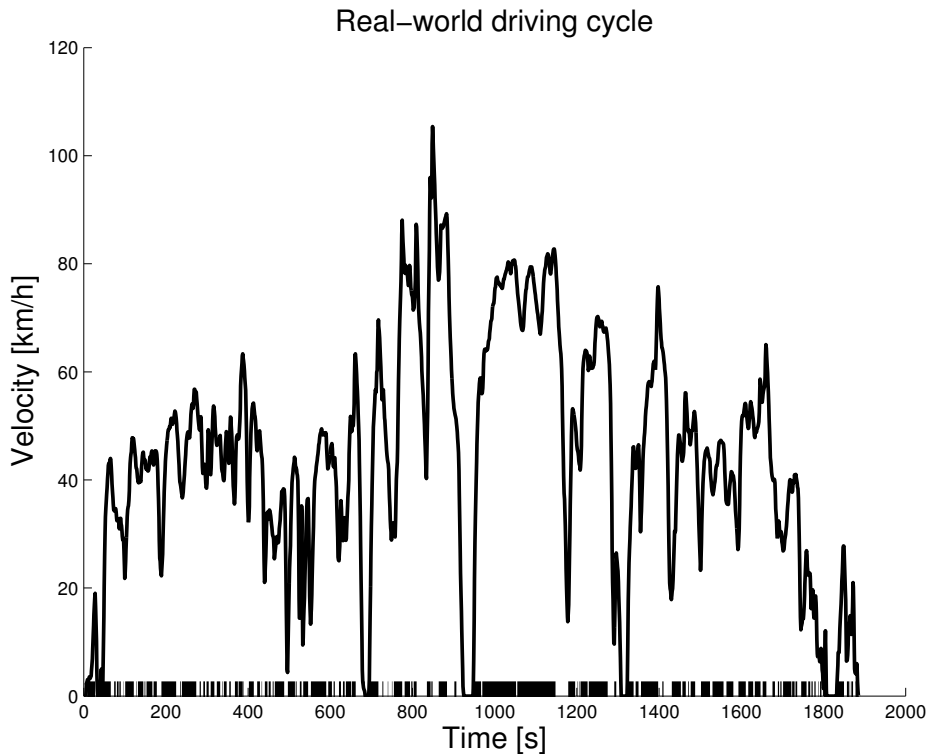


Figure 1: Real-world driving cycle with marked traction regions which shows the instants where the powertrain needs to deliver positive power to the wheels.

outcome of another driving cycle since the vehicle excitation of two different driving cycles can be very different. Thus, a comparison between results from any two driving cycles may not be fair due to that the demand from the driving cycles can be very different.

A common approach of generating driving cycles is the micro-trip approach where a micro-trip is the speed profile between two trailing stops. The approach is to randomly choose micro-trips for different parts of the driving cycle that is to be constructed, see (Tong et al., 1999; Shahidinejad et al., 2010) and the reference therein for more information. Another possibility is the mode-based approach, see (Lin and Niemeier, 2002) and (Ashtari et al., 2014), that generates a driving cycle by iteratively choosing segments of different duration where the aim is to make the speed-acceleration frequency distribution of the generated driving cycle more similar to the real-world driving data. The driving cycle with the best statistical fit is chosen as the final representative.

More recently a Markov chain approach has been used for generating representative driving cycles from real-world driving data in a compact way, see (Lee

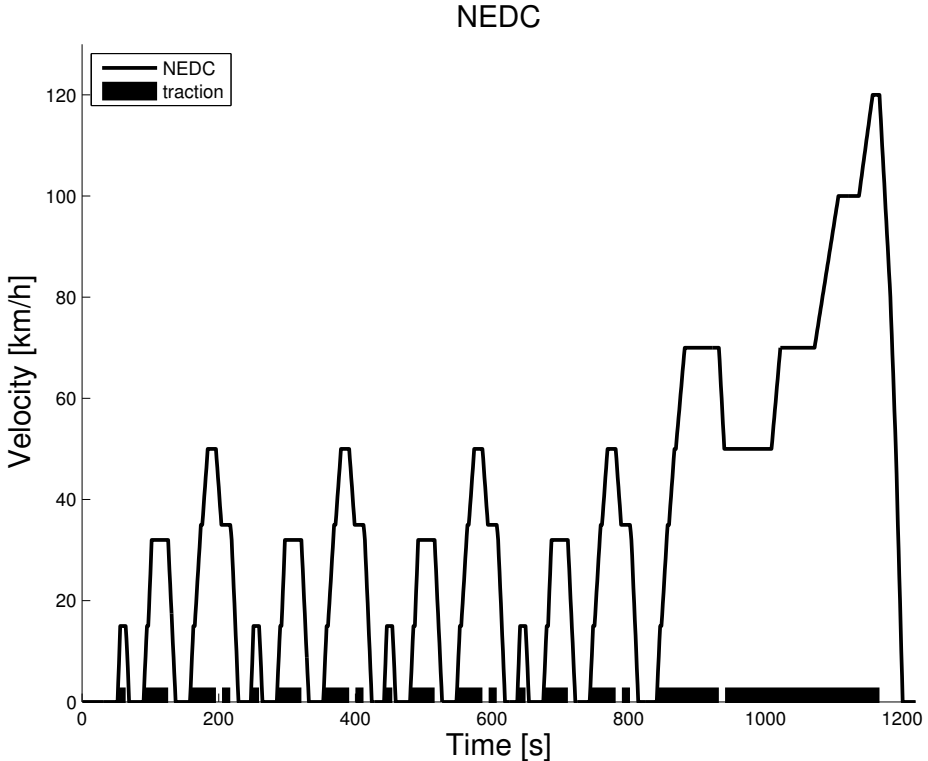


Figure 2: NEDC with marked traction regions which shows the instants where the powertrain needs to deliver positive power to the wheels.

and Filipi, 2011; Gong et al., 2011; Torp and Önnegren, 2013). The database, or a subset of it depending on situation, is used to construct the transition probability matrix of a Markov chain, so that generated driving cycles have the same statistical properties as the recorded data.

1.2 OUTLINE OF IDEAS AND PAPER

To solve the problem of finding representative driving cycles with equivalence properties regarding excitation, the main idea in this paper is to merge the Markov chain approach in (Lee and Filipi, 2011; Torp and Önnegren, 2013), which will be explained in Section 5, with the concept of equivalent driving cycles, that was introduced in (Nyberg et al., 2013). To arrive at an appropriate algorithm there are a number of components to cover. A first question is to determine what excitation measure to use. Since the internal design of the powertrain often is the objective, it is natural to have a measure relating to requirements at the wheels. Here mean tractive force, MTF, and its individual

components are used. These concepts are recalled in Section 2, and the concept of equivalent driving cycles is explained in Section 3. A key contribution in this paper, presented in Section 4, is the experimental verification that it is superior to use the individual components of the MTF, instead of using only the aggregated total MTF. Section 5 presents the framework and algorithms realizing the main idea of generating equivalent driving cycle using Markov chains. In Section 6 the method is illustrated by some examples of generated equivalent driving cycles. Finally, in Section 7 the conclusions of this work are presented.

2 MEAN TRACTIVE FORCE

This section introduces the mean tractive force, MTF, which is also sometimes called specific energy (Lee and Filipi, 2011) or power intensity (Tate et al., 2008). The MTF is described in (Guzzella and Sciarretta, 2007), and is the vehicle's tractive energy at the wheels in a driving cycle, divided by distance traveled. It is a measure on how demanding the driving cycle is to follow for a given vehicle, and the higher MTF the higher demand on the vehicle.

The propulsion force in the longitudinal dynamics, $F(t)$, at the wheels for flat roads consists of aerodynamic drag resistance, F_{air} , rolling friction resistance, F_{roll} , and inertia force, F_{m} , for acceleration or deceleration of the vehicle. The three components are modeled as

$$F(t) = F_{\text{air}} + F_{\text{roll}} + F_{\text{m}} \quad (1)$$

$$F_{\text{air}} = \frac{1}{2} \rho_a c_d A_f v^2(t) \quad (2)$$

$$F_{\text{roll}} = mgc_r \quad (3)$$

$$F_{\text{m}} = ma(t), \quad (4)$$

where ρ_a is the air density, c_d the drag coefficient, and the frontal area of the vehicle is denoted A_f . Further, the vehicle mass is m , g is the gravitational constant and the rolling friction coefficient is c_r . The vehicle speed is $v(t)$ and the acceleration of the vehicle is denoted $a(t)$. An illustration of the abovementioned forces acting on a vehicle is shown in Figure 3 where the vehicle is assumed to be front-wheel-driven. For simplification the road resistance is only depicted on the front wheels even if it would origin also for the rear wheels. The vehicle is assumed to be traveling to the right with a certain acceleration which is indicated by the direction of the force of F_{air} and F_{m} , respectively.

When comparing driving cycles, many measures that have been used previously are based on the whole time interval $\tau = [0, t_{\text{end}}]$ where t_{end} is the final time in the driving cycle. Examples of such measures are the mean speed, standard deviation of acceleration, and percentage of time spent in cruising. A main idea in MTF is to consider the tractive force needed during a driving cycle by the following reasoning. Since the powertrain does not need to provide

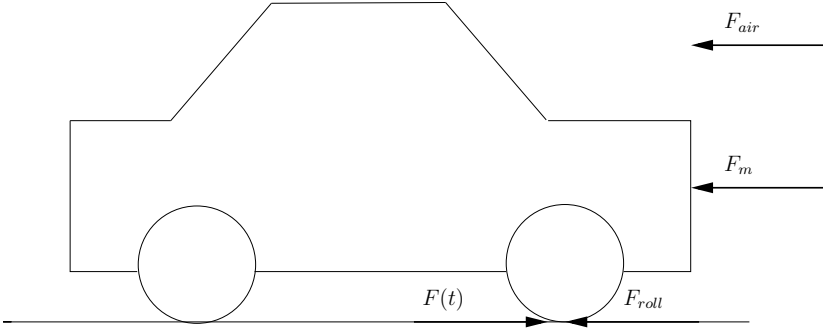


Figure 3: Force diagram of the forces acting on a vehicle at flat road. The vehicle is traveling to the right and the sign of the force $F(t)$ and F_m depends on the level of acceleration/deceleration.

any positive forces to the wheels during coasting regions ($F(t) = 0$) or braking regions ($F(t) < 0$), the traction regions are those when the powertrain need to provide positive power to the wheels ($F(t) > 0$). A driving cycle's MTF, \bar{F}_{trac} , is integrated over the set of intervals $\tau_{\text{trac}} = \{t \in \tau : F(t) > 0\}$, see the marked regions near the x-axis in Figure 1 and Figure 2, and is written as (Guzzella and Sciarretta, 2007)

$$\bar{F}_{\text{trac}} = \frac{1}{x_{\text{tot}}} \int_{t \in \tau_{\text{trac}}} F(t)v(t) dt, \quad (5)$$

where $x_{\text{tot}} = \int_{t \in \tau} v(t) dt$ is the total distance traveled in the driving cycle. Thus, the required power at the wheels are integrated over the set τ_{trac} which yields the energy demand during the traction regions. The tractive energy is then divided by traveled distance and yields the MTF.

From (1) - (5) the MTF can be expressed by the sum of its road resistance components, denoted the MTF components, as

$$\bar{F}_{\text{trac}} = \bar{F}_{\text{air}} + \bar{F}_{\text{roll}} + \bar{F}_m \quad (6)$$

$$\bar{F}_{\text{air}} = \frac{1}{x_{\text{tot}}} \int_{t \in \tau_{\text{trac}}} \frac{1}{2} \rho_a c_d A_f v^3(t) dt = \frac{1}{2} \rho_a c_d A_f \alpha(v(t)) \quad (7)$$

$$\bar{F}_{\text{roll}} = \frac{1}{x_{\text{tot}}} \int_{t \in \tau_{\text{trac}}} mgc_r v(t) dt = mgc_r \beta(v(t)) \quad (8)$$

$$\bar{F}_m = \frac{1}{x_{\text{tot}}} \int_{t \in \tau_{\text{trac}}} ma(t)v(t) dt = m\gamma(v(t)), \quad (9)$$

where driving cycle characterizing measures $\alpha(v(t))$, $\beta(v(t))$, and $\gamma(v(t))$ are

defined as

$$\alpha(v(t)) = \frac{\bar{F}_{\text{air}}}{\frac{1}{2}\rho_a c_d A_f} = \frac{1}{x_{\text{tot}}} \int_{t \in \tau_{\text{trac}}} v^3(t) dt \quad (10)$$

$$\beta(v(t)) = \frac{\bar{F}_{\text{roll}}}{mgc_r} = \frac{1}{x_{\text{tot}}} \int_{t \in \tau_{\text{trac}}} v(t) dt = \frac{x_{\text{trac}}}{x_{\text{tot}}} \quad (11)$$

$$\gamma(v(t)) = \frac{\bar{F}_m}{m} = \frac{1}{x_{\text{tot}}} \int_{t \in \tau_{\text{trac}}} a(t)v(t) dt, \quad (12)$$

where x_{trac} is the distance traveled during the traction regions.

For a given vehicle the vehicle parameters are fixed. Two driving cycles, assuming the air density is constant, have then the same values on the MTF components, \bar{F}_{air} , \bar{F}_{roll} , and \bar{F}_m , if they have the same values on α , β , and γ which are directly dependent on the driving cycle and only affected indirectly by the vehicle parameters which affects τ_{trac} .

3 EQUIVALENT DRIVING CYCLES

To be able to generate driving cycles that are similar, such that a performance comparison between them is fair within the required engineering precision, it is needed to define what similar driving cycle means. Then, the task is to find those characteristics that best define the requirements on the vehicle, and one first reasonable step is to use α , β , and γ from the previous section.

The concept of equivalent driving cycles based on the components of MTF was introduced in (Nyberg et al., 2013) and the definition is

Definition 1. *For a given vehicle, two driving cycles, $v_1(t)$ and $v_2(t)$, are said to be MTF components equivalent or just equivalent for short, denoted $v_1(t) \sim v_2(t)$, if*

$$\begin{aligned} \alpha(v_1(t)) &= \alpha(v_2(t)) \\ \beta(v_1(t)) &= \beta(v_2(t)) \\ \gamma(v_1(t)) &= \gamma(v_2(t)). \end{aligned}$$

Thus, two driving cycles are said to have similar vehicle excitation if the two driving cycles are equivalent according to Definition 1. The definition is of course not limited to the parameters above. Instead, it is open to include more measures in an extended definition, and it is no problem for the algorithms in Section 5 to handle such an extended definition. In this respect the methodology presented in this paper is general.

4 FUEL CONSUMPTION INVESTIGATION

A common performance measure is fuel consumed per distance traveled, which is commonly denoted fuel consumption as in (Fontaras et al., 2009). In (Guzzella and Sciarretta, 2007) the mean tractive force, MTF, is suggested as an indicator of the fuel consumption. To investigate this, an experimental investigation of the fuel consumption has been performed, and the experiments are presented in the following sections.

In our previous work (Nyberg et al., 2014), a simulation study of the fuel consumption was carried out and showed that using the mean tractive force components in a linear regression analysis yields a better prediction of the fuel consumption compared to using the aggregated MTF. That study used a vehicle model that consisted of an ideal drivetrain and the engine was modeled as a Willan's line (Guzzella and Onder, 2010) with frictional and inertia losses. As a natural continuation of that simulation study, this paper takes it a step further and test it on an actual engine in a hardware-in-the-loop-simulation, HILS, setup to see if the results are still valid in a practical application. The experimental investigation is performed in a HILS setup where an engine in a test-cell is used together with a driver model and a vehicle model. The experiment consists of the following steps. First, 100 driving cycles have been generated with a driving cycle generator. Second, these driving cycles have been driven in a HILS setup. Third, the MTF components of the actually driven driving cycle and the corresponding fuel consumption have been used in a regression analysis to investigate the relationship between the mean tractive force, and its components, to the fuel consumption.

4.1 EXPERIMENTAL SETUP

The experimental setup consists of an engine test bench where an engine is coupled to a dynamometer, see Figure 4, where the engine (to the right) and the dynamometer (to the left) are shown. A schematic overview of the setup is shown in Figure 5 and consists of input reference driving cycles, a driver model, the actual engine, and a vehicle model. The speed difference between the reference driving cycle and the vehicle speed, together with a feedforward part, is fed to the driver model to take appropriate actions so that the vehicle will follow the pre-defined reference driving cycle. The driver model actuates the throttle of the actual engine and hence controls the air-path-flow into the cylinders. The torque response of the engine is measured by a dynamometer and serves as input to a vehicle model. The size of the torque will determine the acceleration, and the resulting vehicle speed is the output of the HILS.

GENERATION OF REFERENCE DRIVING CYCLES

Several reference driving cycles are needed in order to conduct the experiments in the HILS setup. In this work the driving cycle generator that is described in

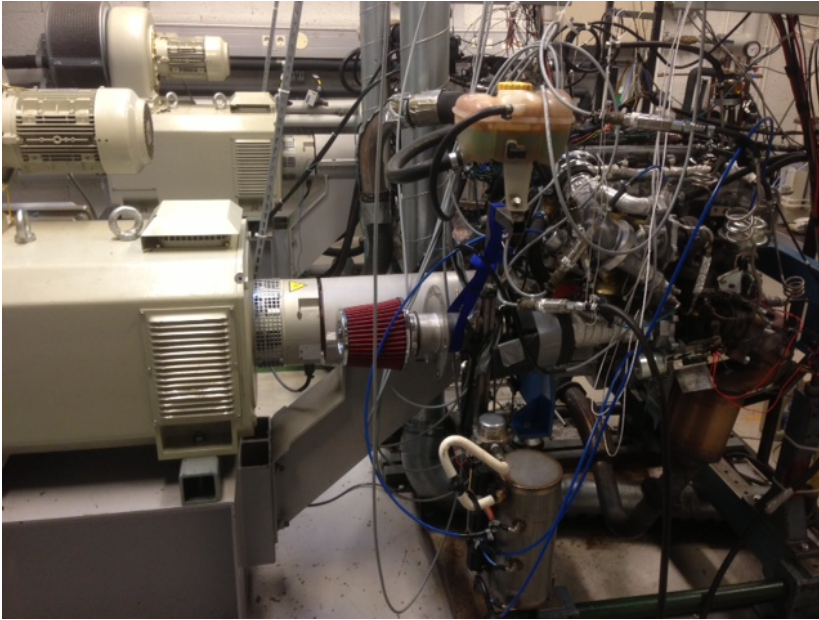


Figure 4: Picture of the engine test stand that has been used in the hardware-in-the-loop simulation. To the left is the dynamometer and to the right the engine is shown.

Section 5.2 has been used. One hundred driving cycles have been generated to be used in the HILS setup.

DRIVER MODEL

The objective of the driver model is to follow the reference driving cycle. The speed difference between the actual speed of the simulated vehicle and the current speed in the reference driving cycle is used to control the throttle position. The driver model is a PI-controller with feedforward part using the reference driving cycle in order to calculate the corresponding torque and throttle angle. The

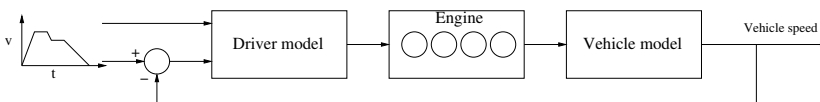


Figure 5: Overview of the hardware-in-the-loop simulation in a forward simulation approach. The input driving cycle (leftmost part of the figure) serve as the reference. Both the feedforward part and the difference between the current vehicle speed and the speed that the reference has are fed to a driver model.

resulting air mass-flow and the corresponding fuel injection by the engine control systems yields a torque response that the engine dynamometer measure.

ENGINE

The engine used is a four cylinder two liters gasoline engine with direct injection. The baseline engine can output 194 kW and 350 Nm but the current engine has somewhat lower performance due to the turbo has been changed. The dynamometer, Schenck Dynas3-LI250, is an asynchronous machine with a rated power of 250 kW, rated speed of 10000 rpm, and a rated torque of 480 Nm. The torque response of the engine is measured by a GIF torque measurement system installed in the dynamometer. The dynamometer and the vehicle model communicates over a RS232 link at 10 Hz. The dynamometer is coupled directly to the engine's flywheel and the speed of the dynamometer, and thus the engine speed, is determined by the current speed of the vehicle and the current engaged gear in the vehicle model. The torque output is then used in the vehicle model to calculate the new speed of the vehicle.

VEHICLE MODEL

The used vehicle model is the same as in (1)-(4) with parameters according to Table 1. For simplification, the drivetrain is assumed to be ideal, and hence there are no losses from the engine to the wheels. The vehicle speed dependent gear-shifting strategy is extracted from the NEDC and includes some hysteresis to avoid frequent gear shifting.

The engine torque output, T_{eng} , is measured by the dynamometer and is used in the vehicle model to calculate the acceleration of the vehicle according to

$$m \cdot a(t) = T_{\text{eng}} \cdot gr_x / r_w - F_{\text{air}} - F_{\text{roll}}, \quad (13)$$

where gr_x is the current gear ratio in the transmission and r_w is the wheel radius in the HILS setup. The F_{air} and F_{roll} are the same as in (2) and in (3) and the parameter values are displayed in Table 1. The acceleration, $a(t)$ in (13), determines the new speed the simulated vehicle will have in the next time step and the dynamometer is set to hold the corresponding new engine speed. The resulting vehicle speed of the simulated vehicle is used together with the reference driving cycle and serves as an input to the driver model.

OUTPUTS OF THE EXPERIMENT

When a complete reference driving cycle has been executed, the actual driven speed profile of the forward simulation is stored and can be seen as an output from the experiment. Another output is the fuel consumption during that speed profile. The fuel consumption is the amount of fuel the control system estimates has been consumed divided by the traveled distance.

Table 1: Parameters for the vehicle model used in the hardware-in-the-loop simulation.

Parameter	Unit	Description
$A_f = 2.15$	[m ²]	Front area
$c_d = 0.4$	[-]	Drag coefficient
$c_r = 0.013$	[-]	Rolling resistance coefficient
$m = 1600$	[kg]	Vehicle mass
$r_w = 0.3$	[m]	Wheel radius
$\rho_a = 1.29$	[kg/m ³]	Air density
$g = 9.81$	[m/s ²]	Gravitational constant
$gr_1 = 9.97$	[-]	First gear ratio
$gr_2 = 5.86$	[-]	Second gear ratio
$gr_3 = 3.84$	[-]	Third gear ratio
$gr_4 = 3.68$	[-]	Fourth gear ratio
$gr_5 = 2.14$	[-]	Fifth gear ratio

One of the 100 driving cycles that were generated required more power than the engine could deliver, and hence it was removed. This yields fuel consumption measurements for 99 driving cycles where the resulting speed profiles were used to calculate the MTF and its components from (6)-(9). A boxplot of the spread in the MTF and its components is seen in Figure 6. The driving cycles that were used have been generated using a Markov chain that is based on real-world driving cycles that are within the category *Short* in Table 3. They consists of many start and stops and have low speeds which are indicated by the high values of \bar{F}_m in (9) and low values of \bar{F}_{air} in (7), respectively, as are shown in Figure 6. The low spread in F_{roll} is normal since the spread is determined by x_{trac}/x_{tot} in (11) and this ratio is not varying much.

4.2 CORRELATION OF THE MTF COMPONENTS TO FUEL CONSUMPTION

The resulting speed profiles and the corresponding fuel consumption will now be used together with the calculated MTF and its components in a linear regression analysis in order to determine if there is a linear relationship between the MTF and its components to the fuel consumption.

The 99 driving cycles that are used in the analysis are split into two halves. The first half consists of 50 driving cycles that are used as estimation data for a linear regression. The response variable is the fuel consumption of the engine during non-idling and the regressors are either the MTF components, \bar{F}_{air} , \bar{F}_{roll} , and \bar{F}_m , or the total MTF, \bar{F}_{trac} . The second half consists of 49 driving cycles that are used as validation data.

The MTF and its components describe traction, so to make the following analysis relevant it is necessary to handle idling properly (5). One alternative

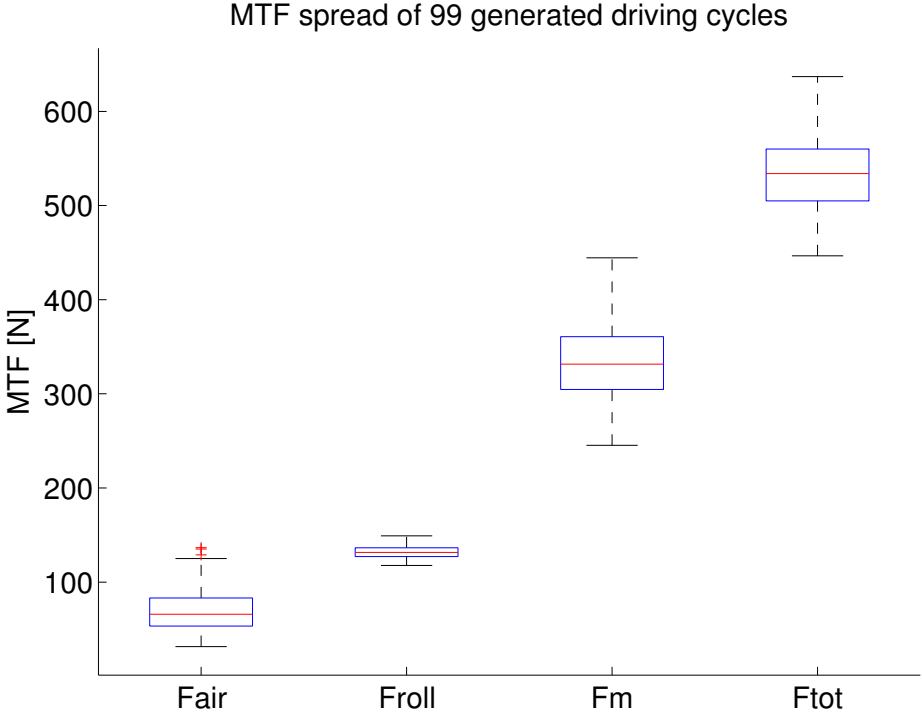


Figure 6: Boxplot that shows the percentile of the MTF components and the aggregated MTF. Each column displays the lowest and highest values with the percentiles 25%, 50%, and 75%. In some cases outliers (labeled as plus-signs) are marked.

would be to use idling time as a regressor. Instead this paper only counts the non-idling parts.

METRIC AND REGRESSION

A metric is needed in order to determine how good the linear regression is to predict the fuel consumption. As a measure of the goodness of fit the r^2 -fit is used and it is defined as

$$r^2 = 1 - \frac{\sum_{i=1}^n (y_i - \hat{y}_i)^2}{\sum_{i=1}^n (y_i - \bar{y})^2}, \quad (14)$$

where y_i is the fuel consumption, \hat{y}_i is the estimated fuel consumption using the linear regression model with coefficients calculated from estimation data, and $\bar{y} = \frac{1}{n} \sum_{i=1}^n y_i$ is the mean value of all $n = 49$ observations or driving cycles in the validation dataset.

The regressors and the fuel consumption are normalized by dividing each value with the maximum value in each variable. These normalized values are

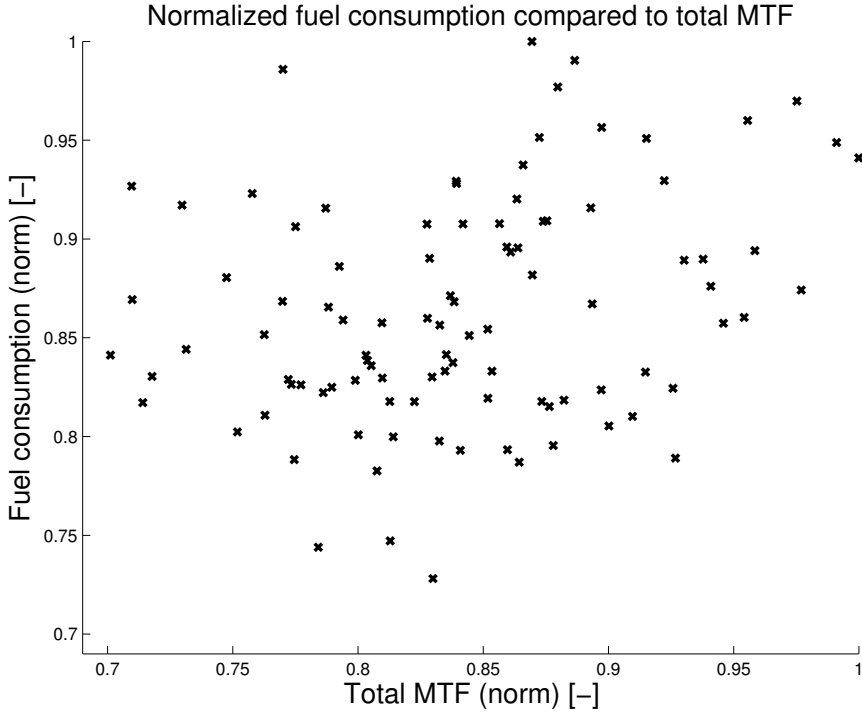


Figure 7: Comparison between normalized fuel consumption and total MTF of 99 driving cycles that have different MTF components.

then used to estimate the parameters in two linear regression where the first one is

$$\hat{y} = b_0 + b_1x_1 + b_2x_2 + b_3x_3, \quad (15)$$

where b_0 is the constant component and b_1 , b_2 , and b_3 are the coefficients for x_1 , x_2 , and x_3 which are the normalized regressors for the MTF components (\bar{F}_{air} , \bar{F}_{roll} , and \bar{F}_{m}). The other linear regression is

$$\hat{y} = b'_0 + b'_1x, \quad (16)$$

where b'_0 is the constant component and b'_1 is the coefficient for x which is the normalized regressor for the total MTF. A comparison between the normalized total MTF and the normalized fuel consumption is seen in Figure 7. As clearly seen the relationship between total MTF and fuel consumption is not proportional and so the correlation is weak.

RESULTS FOR MTF COMPONENTS

The fuel consumption for the non-idling periods for the driving cycles belonging to the validation data are compared to the linear regression models that have been estimated from driving cycles in the estimation data. A comparison between the normalized measured fuel consumption and the estimated fuel consumption using the linear regression models is seen in Figure 8, where the circles correspond to the MTF components as regressors and the triangles correspond to the regressor \bar{F}_{trac} . The estimated parameters in (15) are $(b_0, b_1, b_2, b_3) = (0.3982, -0.2038, 0.3558, 0.3379)$ and in (16) are $(b'_0, b'_1) = (0.6671, 0.2335)$.

The r^2 -fit in (14) for the MTF components and the total MTF are 0.68 and 0.09, respectively. The mean absolute percentage error, $(1/n) \cdot \sum_1^n |(y_i - \hat{y}_i)/(y_i)|$, are 0.026 and 0.048, respectively. The reason for why the linear regression for the total MTF is poor can be seen in Figure 7 which results in the linear regression (16) is mainly depending on the constant term and the amount of MTF does not affect the estimation of the fuel consumption. Compared to the simulation study in (Nyberg et al., 2014) there is a bigger difference when comparing the total MTF and the MTF components. One reason of this is that in the simulation study the efficiency of the engine was depending only on the output torque of the engine and not by the engine speed. The varying efficiency of the engine that depends on both engine torque and engine speed will certainly affect the relationship between MTF, its components and fuel consumption.

The MTF components are thus related to the fuel consumption and driving cycles that have similar values on the MTF components should have similar fuel consumption. The efficiency of the components, the control of the vehicle, auxiliary loads will of course affect the resulting fuel consumption but the variation of the dependence of the driving cycle will be smaller if the MTF components are similar. Thus, the variation in fuel consumption depending on the driving cycle excitation or impact on the vehicle will be less if the MTF components are similar.

Splitting up the MTF into its components compared to using the total MTF gives a r^2 -fit of 0.68 and 0.09 respectively, see also Figure 8. Thus, according to the experiments, the total MTF has too low correlation to the fuel consumption to be trusted, and using the MTF components as equivalence measures between driving cycles is clearly a better choice.

5 DRIVING CYCLE GENERATION

As mentioned in the introduction, the main idea is to have a method that, given a database of real-world driving, generates driving cycles with equivalence properties. An overview of the approach taken is given in Figure 9. The main inspiration for the algorithms in the left part of Figure 9 is the work in (Lee and Filipi, 2011). We use the same fundamental ideas with some slight modifications

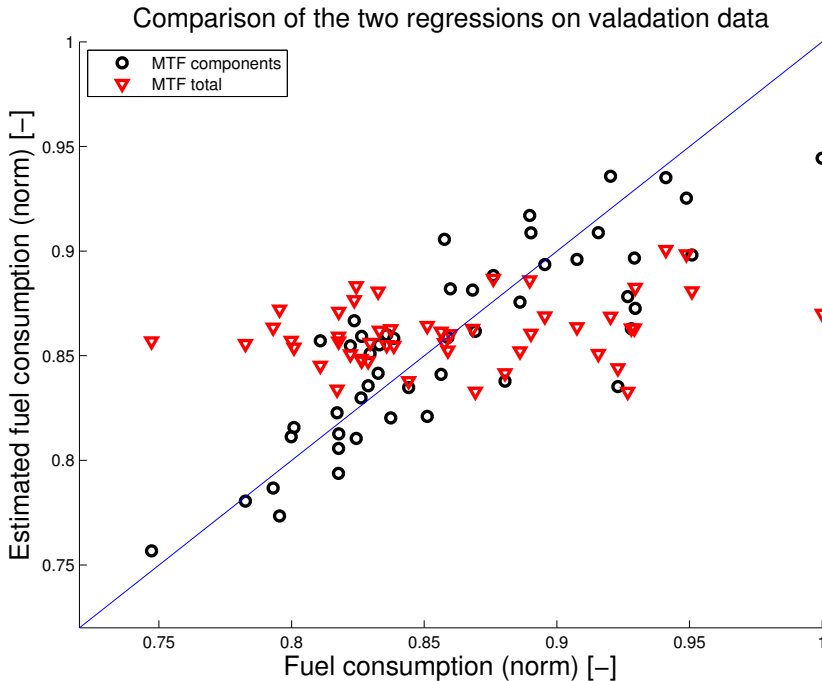


Figure 8: Comparison between the two regressions that estimates the fuel consumption based on the MTF components, $\hat{y} = b_0 + b_1x_1 + b_2x_2 + b_3x_3$ in (15), (circles) or the total MTF, $\hat{y} = b'_0 + b'_1x'_1$ in (16), (triangles).

in the driving cycle generation when using the transition probability matrix. For the selection criterion in the middle of Figure 9 we use a different conceptual background than in their work, and the equivalence transformation in the right part of Figure 9 is a new addition.

The different parts of the algorithm will now be described component by component.

5.1 REAL-WORLD DRIVING CYCLES

Input data to the driving cycle generation are real-world driving cycles that have been measured on instrumented vehicles driving in real traffic. An example of a real-world driving cycle is the one seen in Figure 1, and the data used in this work is a set of 466 drives from a test in the western parts of Sweden. For more details of the real-world driving data see (Torp and Önnegren, 2013). A categorization of driving cycles has been performed by either mean positive velocity, $\bar{v}_{\text{pos}} = \bar{v}(t) : v(t) > 0$, or based on distance traveled in the driving cycle, $x_{\text{tot}} = \int v(t)dt$, which are similar to the categorization used in (Lee and Filipi, 2011). This yields a possibility to generate driving cycles that for example

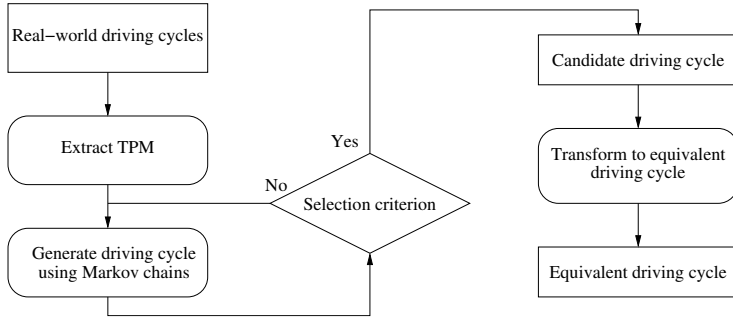


Figure 9: Overview of the method of generating equivalent driving cycles from real-world driving cycles using Markov chains. The selection criterion are that the MTF components shall be similar and the candidate driving cycles are then transformed to equivalent driving cycles.

Table 2: Categorization based on mean positive velocity.

Category	Limits [km/h]	#Cycles
Urban	$0 < \bar{v}_{\text{pos}} \leq 40$	328
Mixed	$40 < \bar{v}_{\text{pos}} \leq 72$	133
Highway	$72 < \bar{v}_{\text{pos}} < \infty$	5

specifically show urban tendencies or highway driving with high speeds.

The chosen limits in the categorization and the number of real-world driving cycles that fit into each category can be seen in Table 2 and in Table 3.

5.2 MARKOV CHAINS AND THE TRANSITION PROBABILITY MATRIX

In order to extract information from the real-world driving cycles and to use it in a compact way, a Markov chain formulation with a transition probability matrix, TPM, is used. Let the state $x_n = (v_n, a_n)$ where v_n and a_n are the current velocity and acceleration, respectively. The Markov property is that the

Table 3: Categorization based on driving distance.

Category	Limits [km]	#Cycles
Short	$0 < x_{\text{tot}} \leq 14$	409
Medium	$14 < x_{\text{tot}} \leq 32$	42
Long	$32 < x_{\text{tot}} < \infty$	15

present state contains all information that conditions the future state

$$\begin{aligned} P(X_{n+1} = x_{n+1} | X_1 = x_1, X_2 = x_2, \dots, X_n = x_n) \\ = P(X_{n+1} = x_{n+1} | X_n = x_n), \end{aligned} \quad (17)$$

which means that the current velocity and acceleration contain all relevant information in order to predict the next state $x_{n+1} = (v_{n+1}, a_{n+1})$. The probability of such a transition from state i to state j is

$$p_{ij} = P(X_{n+1} = j | X_n = i), \quad (18)$$

and p_{ij} is predicted by all such transitions that have occurred in the real-world driving data. All the transition probabilities are stored as a TPM and different categories of real-world driving, see Table 2 and Table 3, can be used to generate different TPMs.

A Markov chain is a stochastic process with the Markov property (17) and here the TPM represents the Markov chain and is used to generate driving cycles. Each element in the matrix corresponds to a certain state and within each element the transition probabilities are stored, which is the probability to jump from one state to another state in the Markov chain. The data have for practical reasons been discretized in steps of 1 km/h and 0.2 m/s² in velocity and acceleration, respectively. An illustration of a TPM is shown in Figure 10 where the sub-matrices contain the transition probabilities to jump from one state to another one. For more information about implementation aspects, see (Lee and Filipi, 2011; Torp and Önnegren, 2013).

Generation of a driving cycle, v , using Markov chains in this paper is the process of initiating the driving cycle with velocity and acceleration of zero ($x_0 = (v_0, a_0) = (0, 0)$) and then randomly choose the next state based on the probabilities, see (18) and Figure 10, in the previously generated TPM. For validation of the Markov property when generating driving cycles and the validation of the used driving cycle generation software, see (Shuming et al., 2013) and (Torp and Önnegren, 2013).

ACCELERATION CONSTRAINTS

Vehicle performance, e.g. available power, can differ between the vehicle that drove the real-world driving cycles, and the one that will drive the generated driving cycle. Therefore, compared to (Lee and Filipi, 2011), this paper uses a constraint on the maximum acceleration in the selection of the next state in the Markov chain as follows.

The HILS setup in Section 4, and especially the engine performance causes acceleration constraints on the generated driving cycle. This means that the generated driving cycles can not have too high acceleration in order for the engine to be able to follow the driving cycle. The real-world driving cycles that are used in this paper had some parts that had too high acceleration compared to the engine performance. To be able to generate driving cycles that have less

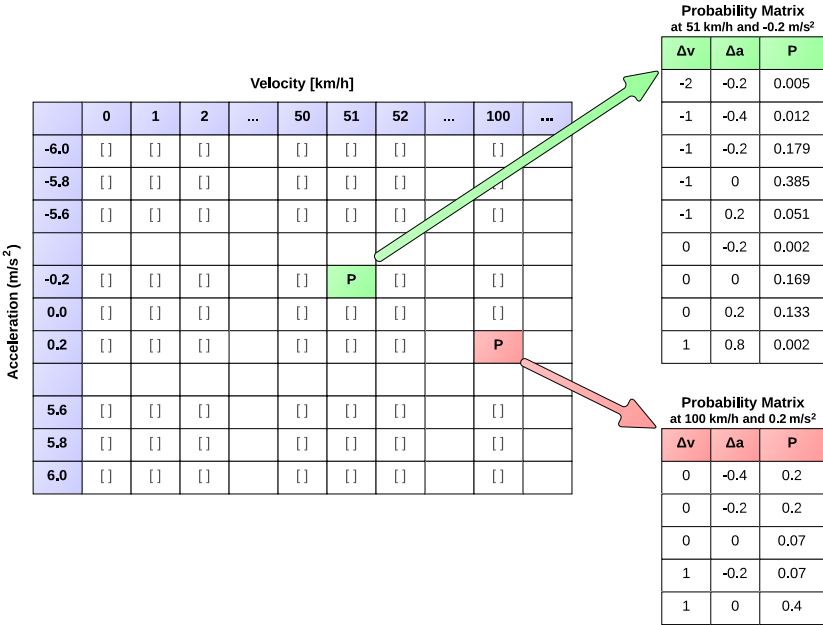


Figure 10: Transition probability matrix which represents the Markov chain. Each element contain the probabilities to jump from a specific state to another. The probabilities are estimated from the occurred transitions in the real-world driving cycles.

demanding acceleration one can either remove those real-world driving cycles from the TPM generation or you can mask those transition in the generation of the driving cycle using some speed-vs-acceleration characteristics. In (André, 2004, Fig. 3) a speed vs acceleration figure of measured real-world driving cycles is shown. A maximum allowed acceleration given vehicle speed was extracted from two points in that figure. The two points were $(v_a, a_a) = (60, 1.2)$ and $(v_b, a_b) = (160, 0.4)$ and the corresponding line between those points gives the maximum allowed acceleration according to $a_{\max} = 1.2 - (1.2 - 0.4) \cdot (v - 60) / (160 - 60)$ for $v \in (60, 160)$. When $v \in (0, 60)$ the maximum acceleration was set to $a_{\max} = 3$. The vehicle speed-vs-acceleration trace (stars) for all generated driving cycles, used in the HILS experiment in Section 4, using this acceleration constraint (solid line) is shown in Figure 11.

STOP CONDITIONS

The generation of the driving cycle will continue until a certain duration in time is achieved and the velocity has reached zero, $v_n = 0$.

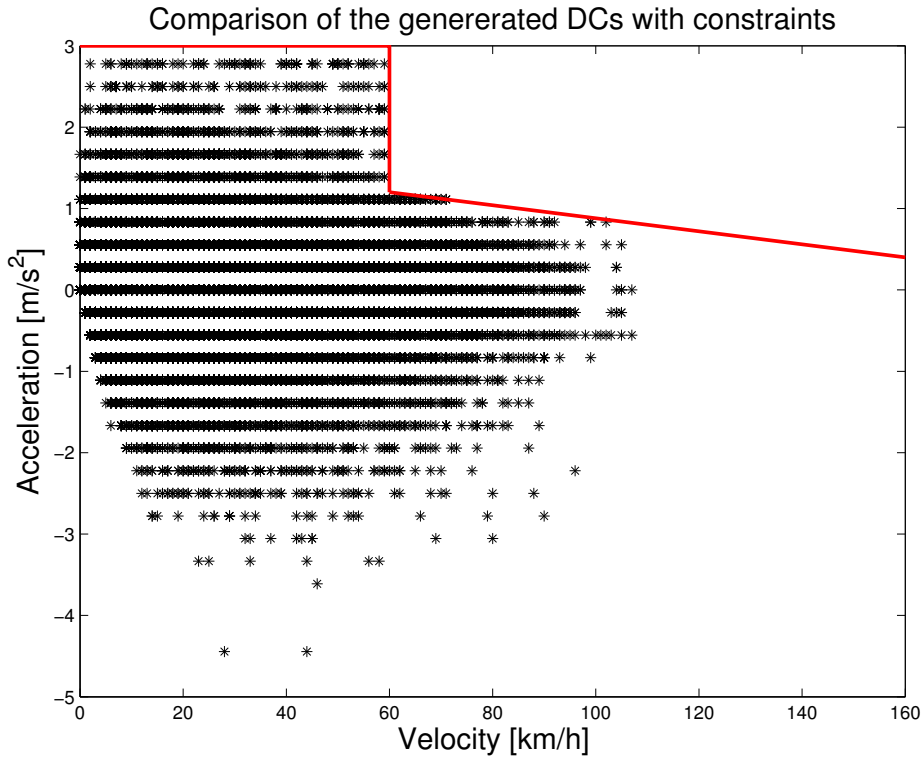


Figure 11: Speed vs acceleration plot from all the generated driving cycles. During the generation the maximum acceleration (solid line) have been considered as can be seen in the figure.

5.3 SELECTION CRITERION

If sufficiently many driving cycles are generated by the TPM constructed from the database, then the generated ensemble will have the same statistical properties as the database. This does not mean that each individual generated drive cycle is representative. As an extreme example, there is a probability that the Markov process stays in the same state, e.g. the idle state, all the time. Therefore there is a need to test if a generated driving cycle is representative, and this is the reason for the selection criterion depicted in Figure 9.

There are different selection criteria that can be used and some examples are statistical measures on key parameters such as velocity, acceleration, time spent in certain modes, number of steps etc. need to be close enough to some values. The approach in (Lee and Filipi, 2011) is to use linear regression in order to determine which parameters that are significant in order to describe the MTF. Principal components analysis, PCA, is used in (Gong et al., 2011) in order to decrease the number of correlated parameters, and in (Torp and Önnegren,

2013) the selection criterion can be changed from different options, from linear regression of the MTF as in (Lee and Filipi, 2011) to PCA as in (Gong et al., 2011).

Relating to Figure 9, the overall function of the selection criterion is that a generated driving cycle, $v = \{v_1, v_2, \dots, v_n\}$ is checked if it fulfills the selection criterion. If the selection criterion is not fulfilled a new driving cycle will be generated. These steps will be repeated until the selection criterion is met. If the generated driving cycle, v , fulfills the selection criterion it has the required characteristics, and is called a candidate driving cycle.

The selection criterion used in this work is that the MTF components shall be similar. That is, the selection criterion is fulfilled if the following holds

$$|1 - \alpha(v)/\alpha'| \leq \psi_\alpha \quad (19)$$

$$|1 - \beta(v)/\beta'| \leq \psi_\beta \quad (20)$$

$$|1 - \gamma(v)/\gamma'| \leq \psi_\gamma, \quad (21)$$

where $\alpha(v)$, $\beta(v)$, and $\gamma(v)$ are calculated from (10)-(12) and α' , β' , and γ' are the desired predetermined values, possibly from an existing driving cycle. The thresholds for respective value are ψ_α , ψ_β , and ψ_γ , where the here chosen values are given in Section 6. The reason for this is that the difference in MTF components should not be too large between the candidate driving cycle and the predetermined values, in order for the transformation step below to work well. Since each transition from one state to another, in the pre-candidate driving cycles, must have occurred in the real-world driving, some values of α' , β' , and γ' can be unfeasible. For example, if $\beta' = 1$, all distance traveled is during traction mode, and if there exist no such possible trace in the TPM, then ψ_β can not be too small to be able to find a candidate driving cycle that pass the selection criterion. Related to this, there is a trade-off between the size of the thresholds (ψ_α , ψ_β , and ψ_γ) and the computational time. With tighter thresholds, the probability to generate a candidate driving cycle within a certain time will go down and vice versa, which directly translates to computational time. The underlying real-world driving cycles also affect the time to generate a candidate driving cycle.

5.4 TRANSFORMATION TO EQUIVALENT DRIVING CYCLES

As a final step in the algorithm, see Figure 9, the candidate driving cycles are transformed to equivalent driving cycles using a three step method presented in (Nyberg et al., 2013).

The equivalent driving cycle, which was defined in Section 3, has the same vehicle excitation regarding the components of the MTF. The three step method iteratively changes a driving cycle until the α , β , and γ are sufficiently close to target values, α' , β' , and γ' that were introduced in the previous section.

Let $\tilde{v} = \{\tilde{v}_1, \tilde{v}_2, \dots, \tilde{v}_n\}$ be the transformed driving cycle, and let ϵ_β , ϵ_γ , and ϵ_α be thresholds for the absolute allowed differences. The final transformation

is performed in three steps as

- 1: The quantity β in (11) is the ratio between traveled distance during traction regions and the total driven distance in the driving cycle. To change the driving cycle such that $|\beta(\tilde{v}) - \beta'| \leq \epsilon_\beta$ the speed points within the traction regions are altered iteratively until the absolute difference between $\beta(\tilde{v})$ and β' is sufficiently small.
- 2: To change F_m and thus γ in (9) when x_{tot} is constant and traction regions are intact the only solution is to change the speed points at the start or end of each traction region according to

$$\begin{aligned}
 \bar{F}_m &= m\gamma = \frac{1}{x_{\text{tot}}} \int_{t \in \tau_{\text{trac}}} m\dot{v}(t)v(t) dt \\
 &= \frac{1}{x_{\text{tot}}} \int_{t \in \tau_{\text{trac}}} \frac{m}{2} \frac{dv^2(t)}{dt} dt \\
 &= \frac{1}{x_{\text{tot}}} \sum_i^{\#trac} \left[\frac{mv^2(t)}{2} \right]_{t_{i,\text{start}}}^{t_{i,\text{end}}}. \tag{22}
 \end{aligned}$$

That is, the MTF component related to vehicle inertia, \bar{F}_m , is the sum of the difference in kinetic energy over all traction intervals. The number of traction intervals is denoted $\#trac$ and each traction interval has its start point, $t_{i,\text{start}}$, and end point $t_{i,\text{end}}$. By iteratively changing the end points it is possible to achieve $|\gamma(\tilde{v}) - \gamma'| \leq \epsilon_\gamma$ as long as ψ_β is small enough in (20).

- 3: Finally, to change the driving cycle to get $|\alpha(\tilde{v}) - \alpha'| \leq \epsilon_\alpha$ while maintaining both $\beta(\tilde{v})$ and $\gamma(\tilde{v})$, is achieved by expanding or contracting of the speed points iteratively within the traction regions (keeping the average speed) in the driving cycle.

5.5 METHOD SUMMARY

To summarize, as illustrated in Figure 9, the method creates a TPM from real-world driving data and generates driving cycles with a certain duration. These pre-candidate driving cycles are regarded as candidate driving cycles, by the selection criterion, if the relative difference between the desired and the current MTF components values are sufficiently small according to (19)-(21). As a final step, the candidate driving cycles are transformed to equivalent driving cycles using the three-step algorithm that was described in the previous section.

6 RESULTS

The methods are illustrated and evaluated using the real-world driving database in Section 5.1 without any additional acceleration constraints. A representative

Table 4: Comparison of parameters of the NEDC, equivalent and candidate driving cycles.

Parameters	NEDC	EqDC _{mixed}	CDC _{mixed}	EqDC _{urban}	CDC _{urban}	EqDC _{short}	CDC _{short}	Unit
MTF comp.	176,175,178	176,175,178	183,173,210	176,175,178	178,172,197	176,175,178	177,172,215	J/m
Distance	11.01	10.52	10.05	5.94	5.47	4.07	3.77	km
Mean pos. vel.	44.66	48.13	45.96	45.70	42.05	33.92	31.39	km/h
Std. vel.	31.03	30.03	31.25	30.57	30.91	29.18	28.98	km/h
Mean pos. acc.	0.59	0.46	0.53	0.41	0.47	0.69	0.54	m/s ²
Std. acc.	0.43	0.71	0.58	0.69	0.52	0.67	0.54	m/s ²
Perc. idle	27	12	12	18	18	24	24	%

driving cycle is to be found for each of the three defined categories *Short*, *Urban*, and *Mixed*, as described in Table 2 and in Table 3. In addition to being representative for its category, the driving cycles are being required to be equivalent to NEDC in the sense defined in Section 3. Any other driving cycle than NEDC could be used, but even if NEDC is not representative for real-world driving it is well known, and therefore a good choice for illustrative purposes.

The notation used is that each of the three resulting equivalent driving cycles, EqDC, first have a corresponding candidate driving cycle, CDC, which is the driving cycle that has been approved by the selection criterion in (19)-(21), as explained in Section 5. To separate between the different EqDC and CDC, the categories *Short*, *Urban*, and *Mixed* are used as subscripts.

The methods from Section 5 are applied to the subset of the driving database categorized as *Mixed* ($40 < \bar{v}_{\text{pos}} \leq 72$ km/h), see Table 2, with the following thresholds $\psi_{\alpha} = 0.06$, $\psi_{\beta} = 0.04$, and $\psi_{\gamma} = 0.24$, see (19)-(21). The generated candidate driving cycle, CDC_{mixed}, seen in Figure 12 (dashed line), has the relative difference compared to the NEDC of 4%, 1%, and 17% for the MTF components (\bar{F}_{air} , \bar{F}_{roll} , and \bar{F}_{m}). The resulting EqDC_{mixed}, after the equivalence transformation step, is also shown in Figure 12 (solid line). It has the relative differences of 0.06%, 0.003%, and 0.001% for the MTF components compared to the NEDC.

Further insights are obtained from Table 4 that shows a comparison of statistical measures between the NEDC, the candidate driving cycle, and the equivalent driving cycles that have been generated. There, the values in the fourth column corresponds to CDC_{mixed} where the MTF components are close but not the same as for the NEDC (second column), see first row. The transformed equivalent driving cycle to NEDC is the EqDC_{mixed} which corresponds to the third column. As seen, the distance is somewhat higher in EqDC_{mixed} compared to CDC_{mixed}, see second row, since the β in (11) needs to be raised in the transformation. As a direct consequence, as the total time is the same, the mean positive velocity is also higher. The current transformation algorithm is applied to traction regions, and hence the idling time is not changed in the transformation step as seen in the table.

In the same way, another equivalent driving cycle to the NEDC has been generated from the category *Urban* ($0 < \bar{v}_{\text{pos}} \leq 40$ km/h), see Table 2. Figure 13 shows a comparison between the equivalent driving cycle (solid line) and the

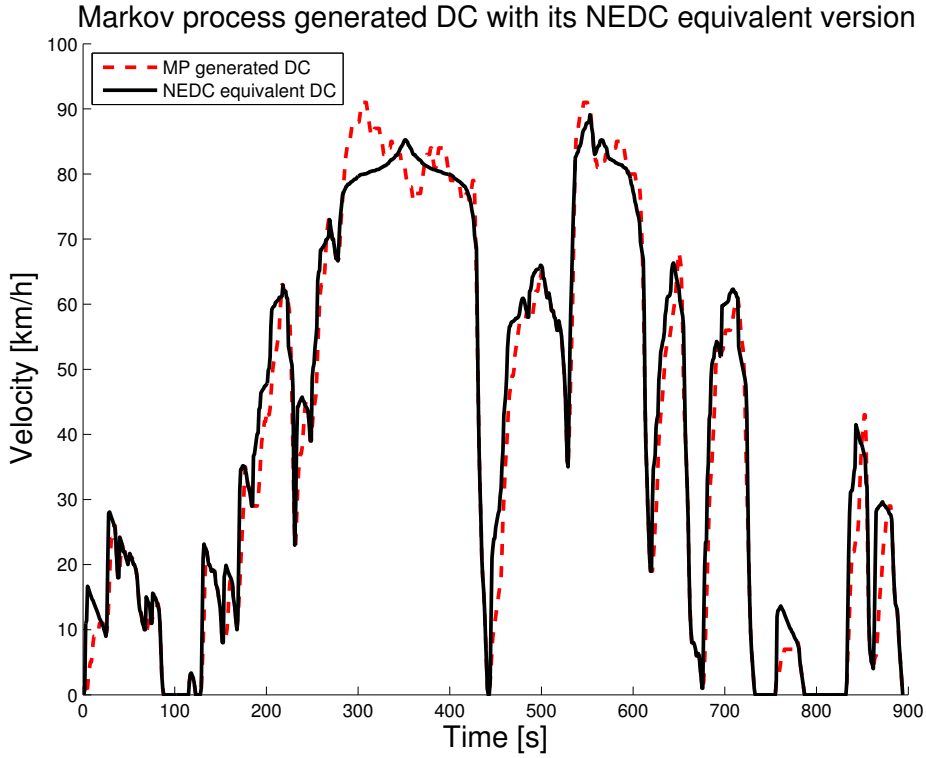


Figure 12: From the category *Mixed* a generated CDC (dashed) with similar MTF components as the NEDC (4%, 1%, and 17% difference), and the transformed EqDC (solid) equivalent to NEDC.

candidate driving cycle (dashed line). As seen in Table 4, the CDC_{urban} has the relative difference compared to the NEDC of 1%, 1%, and 11% for the MTF components and the $EqDC_{urban}$ has the relative differences of 0.03%, 0.002%, and 0.001%.

Finally, from the category *Short* ($0 < x_{tot} \leq 14$ km), see Table 3, Figure 14 shows a candidate and an equivalent driving cycle. The CDC_{short} (dashed line) has the relative difference compared to the NEDC of 1%, 1%, and 21% for the MTF components, and the $EqDC_{short}$ (solid line) has the relative differences of 0.008%, 0.001%, and 0.001%.

The computation time is the sum of the time to find a candidate and the time to do the transformation, and the balance between the two is set by the thresholds in the selection criteria. Here, the chosen values for $\psi_\alpha = 0.06$, $\psi_\beta = 0.04$, and $\psi_\gamma = 0.24$, typically gives that a candidate driving cycle is generated within minutes to hours. The transformation step from a candidate driving cycle to an equivalent driving cycles is typically executed in seconds.

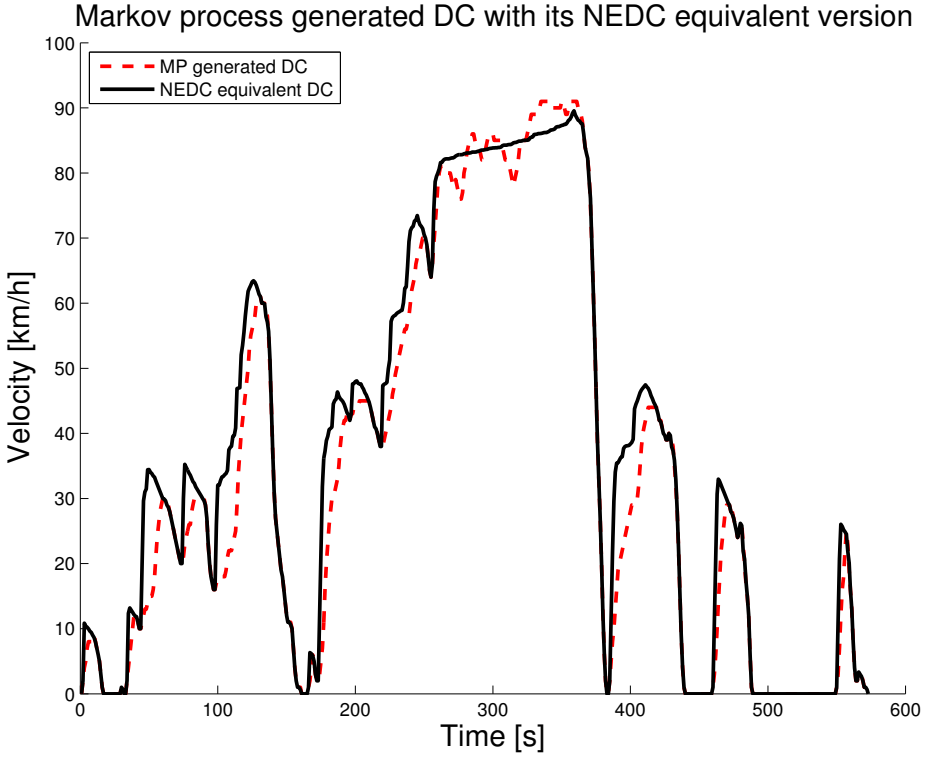


Figure 13: From the category *Urban* a generated CDC (dashed) with similar MTF components as the NEDC (1%, 1%, and 11% difference), and the transformed EqDC (solid) equivalent to NEDC.

6.1 DISCUSSION

In Table 4 the NEDC and all EqDC_{*x*}, with $x \in (\text{mixed}, \text{urban}, \text{short})$, have the same MTF components, i.e. the same $(\bar{F}_{\text{air}}, \bar{F}_{\text{roll}}, \bar{F}_{\text{m}}) = (176, 175, 178)$ J/m. At the same time they have different statistics on other parameters. The mean positive velocity as well as distance are quite different for the equivalent driving cycles and are depending on the underlying TPM and which category the TPM has been generated from.

Another observation from the results above relate to the figures. Even if the resulting equivalent driving cycles have the same vehicle excitation regarding mean tractive force components they can display different types of driving characteristics. For example, the EqDC_{mixed} in Figure 12 is equivalent to the NEDC, seen in Figure 2. The EqDC_{mixed} has more transients and is not as repetitive as the NEDC is constructed to be, so these driving cycles, even though equivalent, look different and exhibit different driver behavior, and still they have the same vehicle excitation regarding the MTF components. It would not have

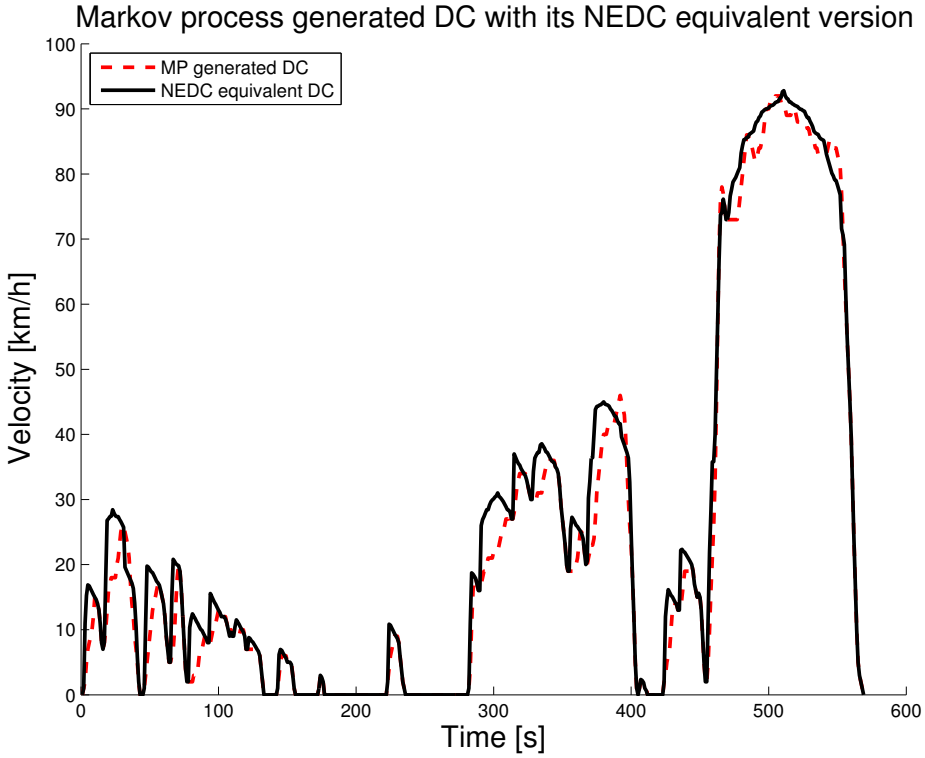


Figure 14: From the category *Short* a generated CDC (dashed) with similar MTF components as the NEDC (1%, 1%, and 21% difference), and the transformed EqDC (solid) equivalent to NEDC.

been feasible to find such equivalent driving cycles manually, so it demonstrates the value to have a systematic method.

7 CONCLUSIONS

A systematic methodology has been developed to generate several driving cycles that are representative compared to a given database of real world driving, and in addition are similar in excitation. A novel part in the generation of driving cycles is to use the individual force components of the mean tractive force instead of only using the aggregated MTF. This is experimentally motivated using a HILS setup with a real engine showing that the fuel consumption estimation is more accurate when the MTF components are considered. Another key novelty is to combine the generation of driving cycles from real-world driving databases using Markov chains with the new concept of equivalence. One may note that the equivalence concept is used both in the selection criterion and in the final

step. The methodology is general in the sense that more selection variables, e.g. like idle time, can be added. The computation time is tractable so that many cycles can be generated if so desired, and because the vehicle excitation can be quantified it is a tractable way to make use of available large databases. The feasibility of the approach was successfully demonstrated in a number of examples, and thus the method is a sound engineering tool for development and testing.

REFERENCES

- M. André. Driving cycles development: Characterization of the methods. In *SAE Technical Paper 961112*, 1996.
- M. André. The ARTEMIS European driving cycles for measuring car pollutant emissions. *Science of The Total Environment*, 334-335(0):73–84, 2004.
- A. Ashtari, E. Bibeau, and S. Shahidinejad. Using large driving record samples and a stochastic approach for real-world driving cycle construction: Winnipeg driving cycle. *Transportation Science*, 48(2):170–183, 2014.
- G. Fontaras and P. Dilara. The evolution of European passenger car characteristics 2000-2010 and its effects on real-world CO₂ emissions and CO₂ reduction policy. *Energy Policy*, 49(0):719–730, 2012.
- G. Fontaras, G. Karavalakis, M. Kousoulidou, T. Tzamkiozis, L. Ntziachristos, E. Bakeas, S. Stournas, and Z. Samaras. Effects of biodiesel on passenger car fuel consumption, regulated and non-regulated pollutant emissions over legislated and real-world driving cycles. *Fuel*, 88(9):1608–1617, 2009.
- G. Fontaras, V. Franco, P. Dilara, G. Martini, and U. Manfredi. Development and review of Euro 5 passenger car emission factors based on experimental results over various driving cycles. *Science of The Total Environment*, 468-469(0):1034–1042, 2014.
- Q. Gong, S. Midlam-Mohler, V. Marano, and G. Rizzoni. An iterative markov chain approach for generating vehicle driving cycles. *SAE International Journal of Engines*, 4(1):1035–1045, 2011.
- L. Guzzella and C. H. Onder. *Introduction to Modeling and Control of Internal Combustion Engine Systems*. Springer, 2010.
- L. Guzzella and A. Sciarretta. *Vehicle Propulsion System: Introduction to Modeling and Optimization*. Springer, 2007.
- J. Kenworthy, P. Newman, and T. Lyons. The ecology of urban driving I - Methodology. *Transportation Research Part A: Policy and Practice*, 26(3): 263–272, 1992.
- P. Kågeson. Cycle-beating and the EU test cycle for cars. *European Fed. for Trans. and Envir. T&E*, 98(3), 1998.
- T.-K. Lee and Z. Filipi. Synthesis of real-world driving cycles using stochastic process and statistical methodology. *International Journal of Vehicle Design*, 57(1):17–36, 2011.
- J. Lin and D. Niemeier. An exploratory analysis comparing a stochastic driving cycle to California’s regulatory cycle. *Atmospheric Environment*, 36(38):5759–5770, 2002.

- P. Nyberg, E. Frisk, and L. Nielsen. Driving cycle adaptation and design based on mean tractive force. In *Proceedings of 7th IFAC Symposium on Advances in Automotive Control*, volume 7, pages 689–694, Tokyo, Japan, 2013.
- P. Nyberg, E. Frisk, and L. Nielsen. Generation of equivalent driving cycles using markov chains and mean tractive force components. In *Proceedings of 19th IFAC World Congress*, volume 19, pages 8787–8792, Cape Town, South Africa, 2014.
- V. Schwarzer and R. Ghorbani. Drive cycle generation for design optimization of electric vehicles. *IEEE Transactions on Vehicular Technology*, 62(1):89–97, 2013.
- S. Shahidinejad, E. Bibeau, and S. Filizadeh. Statistical development of a duty cycle for plug-in vehicles in a North American urban setting using fleet information. *IEEE Transactions on Vehicular Technology*, 59(8):3710–3719, 2010.
- S. Shuming, L. Nan, Z. Yan, H. Chaosheng, L. Li, L. Bingwu, and C. Jingmin. Research on markov property analysis of driving cycle. In *Proceedings of the Vehicle Power and Propulsion Conference (VPPC), 2013 IEEE*, pages 1–5, 2013.
- S. Stockar, V. Marano, M. Canova, G. Rizzoni, and L. Guzzella. Energy-optimal control of plug-in hybrid electric vehicles for real-world driving cycles. *IEEE Transactions on Vehicular Technology*, 60(7):2949–2962, 2011.
- E. Tate, M. Harpster, and P. Savagian. The electrification of the automobile: From conventional hybrid, to plug-in hybrids, to extended-range electric vehicles. *SAE International Journal of Passenger Cars - Electronic and Electrical Systems*, 1(1):156–166, 2008.
- H. Tong, W. Hung, and C. Cheung. Development of a driving cycle for Hong Kong. *Atmospheric Environment*, 33(15):2323–2335, 1999.
- E. Torp and P. Önnegren. Driving cycle generation using statistical analysis and markov chains. Master’s thesis, Linköping University, SE-581 83 Linköping, 2013.
- J.-M. Zaccardi and F. Le Berr. Analysis and choice of representative drive cycles for light duty vehicles - Case study for electric vehicles. *Proceedings of the Institution of Mechanical Engineers, Part D: Journal of Automobile Engineering*, 2012.

Driving Cycle Equivalence and Transformation*

D

*Submitted for journal publication.

Driving Cycle Equivalence and Transformation

Peter Nyberg, Erik Frisk and Lars Nielsen

*Vehicular Systems, Department of Electrical Engineering,
Linköping University, SE-581 83 Linköping, Sweden.*

ABSTRACT

Driving cycles are used in vehicle design, for comparison of vehicles, and also to assess exhaust gas emissions. In a situation with only a few driving cycles would lead to the risk that a test or a design would be tailored to details in a specific driving cycle and thus may risk becoming sub-optimal and non-robust towards real-world driving. A set of driving cycles with desired properties is one solution to this problem, and this paper proposes a novel method for transforming a given driving cycle into a new driving cycle considering equivalence constraints. The approach taken here is to first define equivalence between driving cycles, related to, e.g., vehicle excitation, in order to make fair comparisons of the performance results of driving cycles, and then formulate the driving cycle transformation as a nonlinear program that is solved using general purpose optimization techniques. The method is illustrated by solving different problem instances like transforming a given driving cycle to be equivalent to another driving cycle, where one example is transforming the well-known FTP75 into an equivalent NEDC. A more important example is as a final step in data-driven driving cycle generation. The proposed method is general and a wide range of constraints can be used.

1 INTRODUCTION

A driving cycle is represented by vehicle speed versus time and is supposed to represent typical driving patterns (Nesamani and Subramanian, 2006; Onoda and Emadi, 2004; Wang et al., 2008). The legislative certification driving cycle for type approval for light-duty vehicles in Europe is the New European Driving Cycle, NEDC, which is shown in Figure 1. Driving cycles have mainly been used to assess exhaust gas emissions of vehicles (André, 2004; André et al., 2006; Wang et al., 2000; Fontaras et al., 2009; Fu et al., 2001; Wang et al., 2008; Chan et al., 1995; Zervas and Bikas, 2008; Pelkmans and Debal, 2006), to evaluate different control strategies for vehicles (Pisu and Rizzoni, 2007; Koot et al., 2005; Manzie et al., 2007; Park et al., 2009; Gao et al., 2009; Stockar et al., 2011), in vehicle design and sizing of components (Maxoulis et al., 2004; Hellgren and Jonasson, 2007; Smith et al., 2011; Murgovski et al., 2012; Souffran et al., 2012; Jaafar et al., 2013; Pourabdollah et al., 2013), and also in concept studies (Wolfson and Gower, 1983; Onoda and Emadi, 2004). Driving cycles play a fundamental role in the design of vehicles. The reason for this is that driving cycles yield constraints that vehicles have to satisfy where the cost, fuel consumption, and the pollutant emissions are all dependent on the driving cycle (Liaw and Dubarry, 2007; Durbin et al., 2002; Kean et al., 2003; André and Rapone, 2009; Ericsson, 2000, 2001; Kristensson et al., 2004).

If the vehicle manufacturers focuses only on a single driving cycle during the development and design of a vehicle there is a risk that the design is optimized for this specific driving cycle and the result for another driving cycle may be non-robust and sub-optimal (Tazelaar et al., 2009; Schwarzer and Ghorbani, 2013). Thus, more driving cycles are needed in order to increase the robustness and reduce the risk for sub-optimization. Then, to be able to make a fair comparison of the results it is important that the vehicle have similar excitation, e.g., regarding the forces acting on the vehicle, in the different driving cycles. This leads to the fundamental concept of equivalence, similar but not the same, that was introduced in (Nyberg et al., 2013). The contribution of this paper is a novel method that can transform a given driving cycle into a new driving cycle that (i) excites the vehicle in a similar way, (ii) becomes easier to run in a chassis dynamometer, and (iii) fulfills the imposed constraints, e.g., regarding the maximum acceleration.

How to change or transform a given driving cycle, while considering the drivability, into either a more demanding driving cycle as in (Carlson et al., 2009) or to a less demanding driving cycle, e.g., due to the vehicle cannot meet the acceleration constraints, is not well covered in the literature. For example, in (André et al., 2006) it is proposed that low-powered vehicles shall be tested on other driving cycles than high-powered vehicles since the driving patterns differs due to the difference in engine performance. Given a high demanding driving cycle, how can it be changed to suit a low-powered vehicle. How to adapt a given driving cycle can also be faced in a concept study where the new vehicle design has some limitations so that the currently used driving cycles for

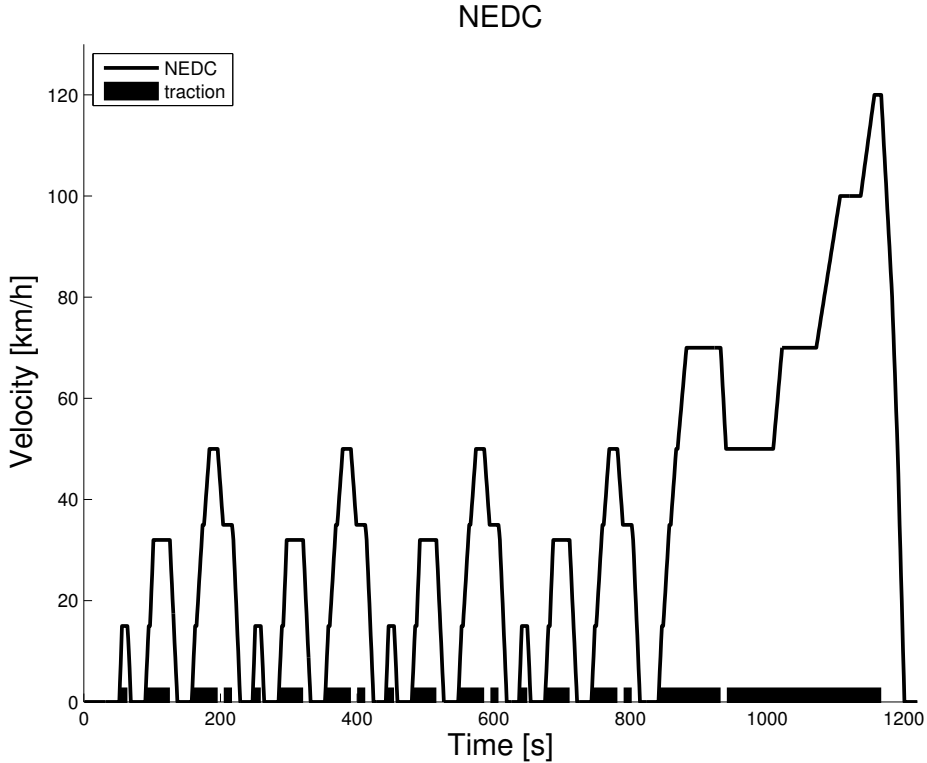


Figure 1: NEDC with marked traction mode regions which indicates the instants where the powertrain needs to deliver positive power to the wheels.

evaluation cannot be used, e.g., due to the required power in the original driving cycles exceeds the maximum power the new powertrain can deliver. Thus, how can a driving cycle be changed using different kind of constraints, and still test the vehicle in a similar way, is an interesting research question. The objective in this paper is to find a general method that can transform a given driving cycle into a new driving cycle that satisfies a number of constraints on either the complete driving cycle or on certain specific partitions of the driving cycle.

1.1 RELATED WORK

The certification driving cycles, such as the NEDC and the FTP75, are often used in comparison of vehicles. However, they are sometimes criticized to not be representative of real-world driving (Zaccardi and Le Berr, 2012; Souffran et al., 2012; Ashtari et al., 2014) since they are not as demanding compared to how vehicles are usually driven. To get a more demanding driving cycle one can either use a driving cycle generator approach or to change the given driving

cycle so it becomes more demanding to follow. Examples of approaches that use the former case are different variants of the micro-trip-approach that is used in (Kent et al., 1978; Tong et al., 1999; André, 2004; André et al., 2006; Wang et al., 2008; Smith et al., 2011; Shahidinejad et al., 2010), the mode-based approaches in (Lin and Niemeier, 2002; Ashtari et al., 2014), and more recently variants of the Markov chain approach that use the vehicle speed and acceleration as states, see (Lee and Filipi, 2011; Gong et al., 2011; Souffran et al., 2012; Nyberg et al., 2014, 2015). The latter case, to change the given driving cycle to a more demanding driving cycle is another option. In (Carlson et al., 2009) a scaling of the UDDS driving cycle (Kruse and Huls, 1973) was used. The vehicle speed in the UDDS was scaled by factors ranging from 1.1 to 1.4 and the time was inversely scaled by the same factors, resulting in an increase of acceleration by up to 96%. Such a scaling results in that the mean speed and acceleration will increase while the driving distance will remain the same. However, other measures like the average power and maximum power are not as clear how much they will increase, resulting in a driving cycle that is more demanding but how much more demanding depends on both the driving cycle and the vehicle's parameters. Instead of scaling of the vehicle speed and the time in the driving cycle it would be beneficial to be able to insert different constraints on the driving cycle so the vehicle excitation of the driving cycle is better controlled during a change.

Our previous work in (Nyberg et al., 2013) proposed algorithms for transforming existing driving cycles while considering equivalence constraints on vehicle excitation. As equivalence measures mean tractive force, MTF, and its components were used. Those algorithms were somewhat limited since (i) only MTF components are considered, (ii) the changed driving cycles have some sharp peaks that reduced the drivability, and (iii) the algorithm could not change the vehicle speed in the non-traction regions in a systematic way. The work in this paper is a continuation of our previous work in (Nyberg et al., 2013) and here a new method is proposed for equivalence transformation of driving cycles. The method can handle general constraints, the drivability in the driving cycle, and enables arbitrary changes in the whole time-interval of the driving cycle.

1.2 OUTLINE

The outline of this paper is as follows. A characterization of the driving cycle is presented in Section 2 together with different measures related to the impact the driving cycle has on the vehicle. In Section 3 a definition of driving cycle equivalence is given and in Section 4 the problem formulation is stated together with three main problems. A key contribution of this paper is the novel method for transforming driving cycles with general equivalence constraints in Section 5. Using the method the problems are solved in Section 6 and finally in Section 7 the conclusions of this paper is presented.

2 CHARACTERIZATION OF DRIVING CYCLES

As mentioned previously the vehicle excitation is important if the comparison of the results in two or more driving cycles shall be fair. To be able to quantify how close two driving cycles are to each other regarding vehicle excitation, a measure is needed. Measures that previously have been used to characterize driving cycles are mostly related to different statistics of the driving cycle such as mean speed, standard deviation of acceleration, mean positive acceleration, and proportion of time spent in different vehicle modes such as acceleration, cruising, deceleration and idling, see for example, (André, 1996; Ericsson, 2000; Lin and Niemeier, 2002). These measures reflect the driving cycle and not specifically the demand on the vehicle that has to follow the driving cycle.

In this paper measures that are based on the impact the driving cycle has on the vehicle will be used instead. The impact that a driving cycle has on a vehicle needs to be quantified, and for that a vehicle model is needed and will be presented in the Section 2.1. In Section 2.2 the vehicle operating modes are defined by a partition of the driving cycle's timeline. Given the vehicle model these modes are determined by the required force at the wheels the powertrain needs to deliver for each given time.

A driving cycle yields demands that the vehicle has to fulfill. For example, the maximum acceleration and the maximum power need to be met by the powertrain if the vehicle shall be able to follow the driving cycle. Further, the power and energy demand in a driving cycle affects the sizing of components for all vehicles, and especially for electric and hybrid vehicles with an energy buffer where, e.g., the battery or electric machine need to be robustly sized. The measures used in this paper are the mean tractive force, MTF, components that are explained in Section 2.3, and power and energy demands that are presented in Section 2.4.

2.1 VEHICLE MODEL

To be able to define measures on the driving cycle's demand on the vehicle, a vehicle model for the longitudinal dynamics is needed. The propulsion force, $F(t)$, at the wheels for flat roads consists of aerodynamic drag resistance, F_{air} , rolling friction resistance, F_{roll} , and inertia force, F_{m} , for acceleration or deceleration of the vehicle. The three components are modeled as in (Guzzella and Sciarretta, 2007)

$$F(t) = F_{\text{air}} + F_{\text{roll}} + F_{\text{m}} \quad (1)$$

$$F_{\text{air}} = \frac{1}{2} \rho_a c_d A_f v^2(t) \quad (2)$$

$$F_{\text{roll}} = mgc_r \quad (3)$$

$$F_{\text{m}} = ma(t), \quad (4)$$

where ρ_a is the air density, c_d the drag coefficient, and the frontal area of the vehicle is denoted A_f . Further, the vehicle mass is m , g is the gravitational constant, and the rolling friction coefficient is c_r . The vehicle speed is $v(t)$ and the acceleration of the vehicle is denoted $a(t)$.

2.2 VEHICLE OPERATING MODES

A driving cycle consists of sequences of different vehicle modes, such as acceleration, cruising, deceleration, and idling mode. These vehicle modes are one possible partitioning of the whole time interval in a driving cycle $\tau = [t_{\text{start}}, t_{\text{end}}]$ where t_{start} and t_{end} are the start and final time in the driving cycle, respectively. The partitioning used in this paper is based on the excitation of the vehicle's powertrain instead of only based on vehicle speed or acceleration. The acceleration, cruising, and deceleration parts are here split into three vehicle operating modes denoted traction, coasting, and braking mode, see (Guzzella and Sciarretta, 2007), which corresponds to the value of the vehicle propulsion force in (1). The three different vehicle operating modes, together with idling, are defined as

$$\tau_{\text{trac}} = \{t \in \tau : F(t) > 0, v(t) \neq 0\} \quad (5)$$

$$\tau_{\text{coast}} = \{t \in \tau : F(t) = 0, v(t) \neq 0\} \quad (6)$$

$$\tau_{\text{brake}} = \{t \in \tau : F(t) < 0, v(t) \neq 0\} \quad (7)$$

$$\tau_{\text{idle}} = \{t \in \tau : v(t) = 0\}, \quad (8)$$

where τ_{trac} is the traction mode region, τ_{coast} is the coasting mode region, τ_{brake} is when the vehicles brakes, and the idling set is denoted τ_{idle} .

The partitioning in (5)-(8) will be used when introducing measures on the driving cycles, in the problem formulation in Section 4, and as important parts in the method explained in Section 5. In the following sections, measures related to vehicle excitation will be presented.

2.3 MEAN TRACTIVE FORCE COMPONENTS

The mean tractive force, MTF, is also sometimes called specific energy (Lee and Filipi, 2011) or power intensity (Tate et al., 2008). The MTF is described in (Guzzella and Sciarretta, 2007), and is the vehicle's tractive energy at the wheels in a driving cycle, divided by distance traveled. It is a measure on how demanding the driving cycle is to follow for a given vehicle, and the higher MTF the higher demand on the vehicle.

A main idea in MTF is to consider the tractive force needed during a driving cycle by the following reasoning. Since the powertrain does not need to provide any positive forces to the wheels during coasting regions ($F(t) = 0$) or braking regions ($F(t) < 0$), the traction regions are those when the powertrain need to provide positive power to the wheels ($F(t) > 0$).

A driving cycle's MTF, \bar{F}_{trac} , is integrated over the set of intervals τ_{trac} as defined in (5) and is written as in (Guzzella and Sciarretta, 2007)

$$\bar{F}_{\text{trac}} = \frac{1}{x_{\text{tot}}} \int_{t \in \tau_{\text{trac}}} F(t)v(t) dt, \quad (9)$$

where $x_{\text{tot}} = \int_{t \in \tau} v(t) dt$ is the total distance traveled in the driving cycle. Thus, the power, $P(t) = F(t)v(t)$, at the wheels are integrated over the set τ_{trac} which yields the energy demand during the traction regions. The tractive energy is then divided by traveled distance and yields the MTF.

From (1) - (4) and (9) the MTF can be expressed by the sum of its components, denoted the MTF components, as

$$\begin{aligned} \bar{F}_{\text{trac}} &= \bar{F}_{\text{air}} + \bar{F}_{\text{roll}} + \bar{F}_{\text{m}} \\ \bar{F}_{\text{air}} &= \frac{1}{x_{\text{tot}}} \int_{t \in \tau_{\text{trac}}} \frac{1}{2} \rho_a c_d A_f v^3(t) dt = \frac{1}{2} \rho_a c_d A_f \alpha(v(t)) \\ \bar{F}_{\text{roll}} &= \frac{1}{x_{\text{tot}}} \int_{t \in \tau_{\text{trac}}} mgc_r v(t) dt = mgc_r \beta(v(t)) \\ \bar{F}_{\text{m}} &= \frac{1}{x_{\text{tot}}} \int_{t \in \tau_{\text{trac}}} ma(t)v(t) dt = m\gamma(v(t)), \end{aligned}$$

where the driving cycle characterizing measures $\alpha(v(t))$, $\beta(v(t))$, and $\gamma(v(t))$ are defined as

$$\alpha(v(t)) = \frac{\bar{F}_{\text{air}}}{\frac{1}{2} \rho_a c_d A_f} = \frac{1}{x_{\text{tot}}} \int_{t \in \tau_{\text{trac}}} v^3(t) dt \quad (10)$$

$$\beta(v(t)) = \frac{\bar{F}_{\text{roll}}}{mgc_r} = \frac{1}{x_{\text{tot}}} \int_{t \in \tau_{\text{trac}}} v(t) dt = \frac{x_{\text{trac}}}{x_{\text{tot}}} \quad (11)$$

$$\gamma(v(t)) = \frac{\bar{F}_{\text{m}}}{m} = \frac{1}{x_{\text{tot}}} \int_{t \in \tau_{\text{trac}}} a(t)v(t) dt, \quad (12)$$

where x_{trac} is the distance traveled during the traction regions.

For a given vehicle the vehicle parameters are fixed. Two driving cycles, assuming the air density is constant, have then the same values on the MTF components, \bar{F}_{air} , \bar{F}_{roll} , and \bar{F}_{m} , if they have the same values on α , β , and γ which are directly dependent on the driving cycle, and only affected indirectly by the vehicle parameters which affects τ_{trac} .

According to Guzzella and Sciarretta (2007) the MTF can be used as an indication value of the fuel consumption. The relationship between the MTF components and the fuel consumption was investigated both in (Nyberg et al., 2014) with a simulation study and in (Nyberg et al., 2015) using a hardware-in-the-loop setup with a real engine. Both studies conclude that the MTF components better characterizes the fuel consumption compared to the aggregated MTF.

2.4 POWER AND ENERGY DEMAND

Hybrid electric vehicles, plug-in electric vehicles and also other types of hybrids do all have one or more degrees of freedom to choose which path the power will come from. This yields a possibility to reduce the fuel consumption by careful design of the powersplit control. However, with the extra degree of freedom comes also sensitivity to the driving cycle, a poor design could lead to even worse fuel consumption. The reason for this is that the weight of the vehicle is usually increased, e.g., from an extra battery and electric machines, and if the control cannot be utilized well enough in the driving cycle the result can be even higher fuel consumption compared to conventional vehicles.

The power and energy demand in a driving cycle influences the design and the overall fuel efficiency of all vehicles and especially of hybrid and electric vehicles. The power and energy measures used in this paper are maximum power, average power, and amount of recuperative energy available. The average power in a driving cycle is here defined as

$$P_{\text{avg}} = \frac{1}{\Delta t_{\text{tot}}} \int_{t \in \tau} F(t)v(t) dt, \quad (13)$$

where the total time in the driving cycle is $\Delta t_{\text{tot}} = t_{\text{end}} - t_{\text{start}}$.

The maximum power is

$$P_{\text{max}} = \max_t F(t)v(t). \quad (14)$$

The available recuperative energy in a driving cycle is equal to the amount of energy that is transformed to heat in the brake discs for a conventional vehicle during a driving cycle and is written as

$$E_{\text{recup}} = - \int_{t \in \tau_{\text{brake}}} F(t)v(t) dt, \quad (15)$$

where the minus sign is to get positive E_{recup} since during braking $F(t) < 0$.

All these measures that have been introduced in this section will be used to illustrate the method that will be presented in Section 5.

3 DRIVING CYCLE EQUIVALENCE

To be able to determine if the vehicle excitation in two driving cycles are equivalent or not it is needed to define what equivalent driving cycles means. This is especially important if it is desired to do a fair comparison of the vehicle performance in different driving cycles, and in this paper it will also be used to show the performance of the method for the driving cycle transformation. Measures on how close a driving cycle is to another driving cycle or a complete driving cycle database are usually different statistics measures of the driving cycle. Examples are the aforementioned, mean speed, standard deviation of

acceleration, and proportion of time in different vehicle modes. A driving cycle that is representative is a driving cycle which statistics are sufficiently close to normal driving, but no formal definition has been given.

In our previous work in (Nyberg et al., 2013) we denoted the term equivalent driving cycles that uses the characterizing measures (10)-(12) and said that for a given vehicle, two driving cycles are equivalent with respect to the MTF components, or the characterizing measures, if these three measures are the same. Where, for a given vehicle means a set of model parameters, $\Omega = \{m, A_f, c_d, c_v, \rho_a, g\}$, used in the vehicle model in (2)-(4). This paper will use an extension of the previous definition of equivalence. Let Γ be a set of measures, $\theta_i \in \Gamma$, where θ_i are different measures, e.g., α in (10) or P_{avg} in (13) and let $\Theta(v(t), \Omega) = (\theta_1(v(t), \Omega), \theta_2(v(t), \Omega), \dots, \theta_n(v(t), \Omega))^T$. The extended definition is

Definition 1. For a given set of model parameters Ω and a set of measures Γ , two driving cycles, $v_1(t)$ and $v_2(t)$, are said to be equivalent with respect to the measures $\theta_1, \theta_2, \dots, \theta_n$, denoted $v_1(t) \sim v_2(t)$, if

$$\Theta(v_1(t), \Omega) = \Theta(v_2(t), \Omega).$$

Using $\Theta(v(t)) = (\theta_1(v(t)), \theta_2(v(t)), \theta_3(v(t)))^T = (\alpha(v(t)), \beta(v(t)), \gamma(v(t)))^T$, where the Ω dependence has been omitted, the extended definition coincides with the previous definition used in (Nyberg et al., 2013, 2014, 2015).

4 PROBLEM FORMULATION

As previously discussed, a set of driving cycles are needed to avoid sub-optimal solutions based on a single driving cycle. This work approaches this problem by transforming a given driving cycle into a new, different, driving cycle but with similar properties such that the results can be compared. Therefore, transformation of a given driving cycle is a key problem in this work. This is motivated by the importance of driving cycles in vehicle design and the lack of existing systematic methods for driving cycle transformation. If the driving cycle shall be followed by an actual vehicle or the driver comfort in the driving cycle is important, the drivability can be an issue and in those cases needs to be dealt with. Developing a general method that can handle a wide range of constraints is the objective in this paper.

4.1 TRANSFORMABLE AND INVARIANT SETS OF THE DRIVING CYCLE

When transforming a given driving cycle, v , it is desired to be able to control which regions that are allowed to change freely and which regions the user have direct control over. Such functionality will increase the usability of the method

and to formalize this, the whole time-interval τ will be split into two sets as

$$\tau = \tau_t \cup \tau_{\text{inv}},$$

where τ_t and τ_{inv} are two disjoint sets. The set τ_t , denoted the transformable set, is where the method is allowed to change the vehicle speed while considering the constraints. The set τ_{inv} is the invariant set for which the vehicle speed in the driving cycle is determined directly by the user. The latter set can, e.g., contain a speed profile segment that shall remain the same during the transformation or if the user wants to incorporate a new speed profile, v_{spec} at τ_{spec} , within the existing driving cycle, which gives $\tau_{\text{spec}} \in \tau_{\text{inv}}$.

The traction and non-traction regions are not changed during the transformation of the driving cycle, that is $\tau_{\text{trac}}(\tilde{v}) = \tau_{\text{trac}}(v)$, where \tilde{v} is the transformed driving cycle. However, the vehicle speed within each region can be changed. The transformable set is in all cases $\tau_t = \tau \setminus \tau_{\text{spec}}$. Note that in (Nyberg et al., 2013) the transformable set was $\tau_t = \tau \setminus (\tau_{\text{idle}} \cup \tau_{\text{coast}} \cup \tau_{\text{brake}} \cup \tau_{\text{spec}}) = \tau_{\text{trac}} \setminus \tau_{\text{spec}}$. This means that the new method is more general compared to the previous method presented in (Nyberg et al., 2013).

The notation will be used in Section 6 where the method will be used to find solutions for the problem instances that will be presented in the next section.

4.2 FUNDAMENTAL PROBLEM AND THREE PROBLEM INSTANCES

As mentioned above, the problem is to transform a given driving cycle into a new driving cycle that fulfills a number of equivalence constraints. This can be formulated into the following problem.

Fundamental Problem: Given a driving cycle $v(t)$, a set of model parameters Ω , and a set of target measures $\Theta' = (\theta'_1, \theta'_2, \dots, \theta'_n)^T$, the fundamental problem is to find a driving cycle $\tilde{v}(t)$ that fulfills $\Theta(\tilde{v}(t), \Omega) = \Theta'$.

This formulation is general and to get specific problems to solve, three problem instances of the fundamental problem will be stated, and corresponds to interesting cases for driving cycle equivalence and transformation. Problems P1 and P2 are the same as in (Nyberg et al., 2013) while Problem P3 is new. Problem P1 is when a certain speed profile segment, v_{spec} at τ_{spec} , is to be incorporated while the characterizing measures are kept constant during the transformation. In Problem P2 the vehicle excitation is changed to another driving cycle's and becomes equivalent with respect to the characterizing measures. A third problem, denoted Problem 3, considers in addition to the characterizing measures also measures on vehicle power and amount of energy in the recuperation regions.

PROBLEM P1

Given a driving cycle $v(t)$, a set of model parameters Ω , and a set of target measures $\Theta' = \Theta(v(t), \Omega) = (\alpha', \beta', \gamma')^T$. Find $\tilde{v}(t) \neq v(t)$ so that (i) $\Theta(\tilde{v}(t), \Omega) = \Theta'$ and (ii) $\tilde{v}(t) = v_{\text{spec}}(t)$, $t \in \tau_{\text{spec}}$.

Another problem is when a driving cycle is given, but it is desired to change the vehicle excitation of the driving cycle. This can be achieved by changing the MTF components and thus changing the characterizing measures to new desired target values of $\Theta' = (\alpha', \beta', \gamma')^T$. The problem formulation is the following.

PROBLEM P2

Given a driving cycle $v(t)$, a set of model parameters Ω , and a set of target measures $\Theta' = (\alpha', \beta', \gamma')^T$. Find $\tilde{v}(t)$ so that $\Theta(\tilde{v}(t), \Omega) = \Theta'$.

The target characterizing measures could be the values for another driving cycle $v_2(t)$, that is $\Theta' = \Theta(v_2(t), \Omega) = (\alpha', \beta', \gamma')^T$, and the resulting driving cycle, $\tilde{v}(t)$, would then be equivalent in those measures to $v_2(t)$, according to Definition 1 in Section 3.

The third and final problem is when, in addition to consider the characterizing measures, also have equivalence constraints on the average power, P'_{avg} , and the amount of recuperative energy, E'_{recup} , in the driving cycle.

PROBLEM P3

Given a driving cycle $v(t)$, a set of model parameters Ω , and a set of target measures $\Theta' = (\alpha', \beta', \gamma', P'_{\text{avg}}, E'_{\text{recup}})^T$. Find $\tilde{v}(t)$ so that $\Theta(\tilde{v}(t), \Omega) = \Theta'$.

5 METHOD: NUMERICAL OPTIMIZATION APPROACH

From the problem formulation the transformed driving cycle, $v = (v_1, v_2, \dots, v_n)$, needs to fulfill a number of equality constraints that can be formulated as $h_i(v, \Omega, \Theta') = 0$. Feasibility aspects such as that the driving cycle shall not cause the vehicle to exceed the maximum acceleration or that the vehicle operating regions shall be intact, can be formulated as inequality constraints as $g_j(v, \Omega) \leq 0$. Finding a method that can fulfill these constraints is sufficient with respect to the problem formulation, i.e., the problem is to solve

$$h_i(v, \Omega, \Theta') = 0 \quad (16)$$

$$g_j(v, \Omega) \leq 0, \quad (17)$$

with respect to v . The solution to (16)-(17) is typically not unique and there are several possibilities to find a feasible solution. One approach in our previous paper (Nyberg et al., 2013) was based on iterating the equations after a stochastic selection process and value modification followed by sorting. Another method, proposed now, is to also consider drivability of the resulting driving cycle. To do this, i.e., to also consider the smoothness of the driving cycle this paper introduces a cost function, $f(v)$, that allows minimizing of the vehicle jerk.

Using this, the transformation of the driving cycle can be formulated as a nonlinear program, NLP, with linear and nonlinear constraints and each

optimization variable corresponds here to a specific vehicle speed in the driving cycle. The optimization can be formulated as

$$\begin{aligned}
& \min f(v) \\
& \text{where } f : R^n \rightarrow R \\
& \text{s.t.} \\
& h_i(v) = 0 \\
& g_j(v) \leq 0,
\end{aligned} \tag{18}$$

where the dependence of the model parameters Ω and the target measures in Θ' have been omitted.

The outline of this section is as follows. The constraints related to the vehicle operating modes in driving cycles, maximum acceleration constraints, and constraints regarding the characterizing measures will be formulated first. This is followed by the different power and energy constraints and constraints on the speed profile. Then the cost function that is minimized is formulated. Finally there is a summary and a discussion of the method.

5.1 CONSTRAINTS FOR KEEPING THE TRACTION AND NON-TRACTION REGIONS

The vehicle operating modes that were introduced in Section 2 are specified before the optimization starts. For example, if the vehicle shall remain in traction the vehicle speed cannot decrease too much from one vehicle speed point to next one in the driving cycle.

One way to characterize traction regions is to calculate the vehicle coasting speed, v_{coast} , which is determined by (1) and comparing it to the vehicle speed in the driving cycle. Using $\dot{v}(t) = a(t)$ and $F(t) = 0$, the vehicle coasting speed is determined by

$$\begin{aligned}
0 &= F_{\text{air}} + F_{\text{roll}} + F_{\text{m}} \Rightarrow \\
\dot{v}_{\text{coast}}(t) &= -\frac{1}{2m} \rho_a c_d A_f v_{\text{coast}}^2(t) - c_r g \\
&= -k_1^2 v_{\text{coast}}^2(t) - k_2^2 \Rightarrow \\
v_{\text{coast}}(t, v(t_{k-1})) &= \frac{k_2}{k_1} \tan(\arctan(\frac{k_1}{k_2} v(t_{k-1})) - \\
& \quad k_1 k_2 \cdot (t - t_{k-1})).
\end{aligned} \tag{19}$$

For driving cycles specified in discrete time and given an initial speed $v(t_{k-1})$ in the driving cycle, the vehicle is in traction mode at time t_k if $v(t_k) > v_{\text{coast}}(t_k, v(t_{k-1}))$, otherwise the vehicle is in coasting mode if $v(t_k) = v_{\text{coast}}(t_k, v(t_{k-1}))$, or in braking mode if $v(t_k) < v_{\text{coast}}(t_k, v(t_{k-1}))$.

That is, if the traction regions, τ_{trac} in Section 2, shall remain intact in the driving cycle the following constraints need to be fulfilled for all $t_i \in \tau_{\text{trac}}$

$$\begin{aligned} v_{\text{coast}}(t_i, v_{i-1}) &< v_i \Rightarrow \\ -v_i + v_{\text{coast}}(t_i, v_{i-1}) &< 0, \end{aligned} \quad (20)$$

where $v_i = v(t_i)$. Each point in traction yields such an inequality as $\mathbf{g}_1(v) = (g_1(v), g_2(v), \dots, g_{n_{\text{trac}}}(v)) < 0$ where n_{trac} is the number of vehicle speed points that are in traction.

Each point in the non-traction regions, $j \notin \tau_{\text{trac}}$, gives a corresponding inequality as

$$\begin{aligned} v_j &\leq v_{\text{coast}}(t_j, v_{j-1}) \Rightarrow \\ v_j - v_{\text{coast}}(t_j, v_{j-1}) &\leq 0, \end{aligned} \quad (21)$$

which leads to $n_{\text{non-trac}}$ number of inequality constraints where $n_{\text{non-trac}}$ is the number of speed points not in traction, $\mathbf{g}_2(v) = (g_{n_{\text{trac}}+1}(v), g_{n_{\text{trac}}+2}(v), \dots, g_{n_{\text{trac}}+n_{\text{non-trac}}}(v)) \leq 0$ where $n_{\text{trac}} + n_{\text{non-trac}} = n$ is the number of speed points in the driving cycle.

5.2 CONSTRAINTS FROM MAXIMUM ACCELERATION

For a given vehicle, let v_i and $a_{\text{max}}(v_i)$ be the vehicle speed and its corresponding maximum acceleration for the vehicle at that speed, respectively. Since the powertrain can only deliver limited power to the wheels the next vehicle speed, v_{i+1} , in the driving cycle, cannot cause the vehicle to exceed the maximum acceleration. This is formulated as

$$\begin{aligned} \frac{v_{i+1} - v_i}{\Delta t} &\leq a_{\text{max}}(v_i) \Rightarrow \\ v_{i+1} - (v_i + a_{\text{max}}(v_i)\Delta t) &\leq 0, \end{aligned} \quad (22)$$

where Δt is the sampling time of the driving cycle, that is the time between two speed points, and in this paper $\Delta t = 1$.

This means that there are additional n number of inequalities, one for each vehicle speed point, $\mathbf{g}_3(v) = (g_{n+1}(v), g_{n+2}(v), \dots, g_{2n}(v)) \leq 0$.

The vehicle's maximum acceleration $a_{\text{max}}(v_i)$ depends on the engine performance, on the vehicle parameters such as vehicle mass, and on the efficiency of the components. However, this paper uses a simplified expression of the maximum acceleration as used in (Nyberg et al., 2014) which reflects the maximum acceleration seen in normal driving as presented in (André, 2004, Fig. 3). The maximum acceleration used is

$$a_{\text{max}}(v_{\text{km/h}}) = \begin{cases} 3 & \text{if } v \in (0, 60] \\ 1.2 - 0.8 \cdot \frac{v_{\text{km/h}} - 60}{100} & \text{if } v \in (60, 160). \end{cases}$$

Note that the unit for vehicle speed is here expressed in km/h and not in m/s that is used in the other constraints. The unit for a_{max} is m/s^2 .

Corresponding constraints regarding the maximum deceleration can also be used and it is trivial to add it if needed. However, no maximum deceleration constraints are used in this paper.

5.3 CONSTRAINTS FROM VEHICLE EXCITATION

As described in Section 2 the MTF components are proportional to the driving cycle characterizing measures, α , β , and γ in (10) - (12), and are here always used as measures on vehicle excitation. Given target values on $(\alpha', \beta', \gamma')$, possibly from an existing driving cycle, the equality constraints for the vehicle excitation will be formulated in the following sections.

CONSTRAINT ON α

Given a target value of α' , the driving cycle needs to fulfill the following equality in order to fulfill the constraint

$$\begin{aligned} \frac{1}{x_{tot}} \int_{t \in \tau_{\text{trac}}} v(t)^3 dt &= \alpha' \Rightarrow (\text{discrete}) \\ \frac{\sum_{i \in \tau_{\text{trac}}} v_i^3 \Delta t}{\sum v_i \Delta t} - \alpha' &= 0 \Rightarrow \\ h_1(v, \tau_{\text{trac}}, \alpha') &= 0, \end{aligned} \quad (23)$$

where $x_{tot} = \sum v_i \Delta t$, and $i \in \tau_{\text{trac}}$ are all indices that the corresponding vehicle speed point is in traction, see (19).

CONSTRAINT ON β

Given a target value of β' , the driving cycle needs to fulfill

$$\begin{aligned} \frac{1}{x_{tot}} \int_{t \in \tau_{\text{trac}}} v(t) dt &= \beta' \Rightarrow (\text{discrete}) \\ \frac{\sum_{i \in \tau_{\text{trac}}} v_i \Delta t}{\sum v_i \Delta t} - \beta' &= 0 \Rightarrow \\ h_2(v, \tau_{\text{trac}}, \beta') &= 0. \end{aligned} \quad (24)$$

CONSTRAINT ON γ

Given a target value of γ' , the driving cycle needs to fulfill

$$\begin{aligned}
& \frac{1}{x_{\text{tot}}} \int_{t \in \tau_{\text{trac}}} \dot{v}(t) \cdot v(t) dt = \gamma' \Rightarrow \\
& \frac{1}{x_{\text{tot}}} \int_{t \in \tau_{\text{trac}}} \frac{1}{2} \cdot \frac{dv^2(t)}{dt} dt - \gamma' = 0 \Rightarrow (\text{discrete}) \\
& \frac{\sum_i^{\#trac} \left[\frac{v(t)^2}{2} \right]_{t_{i,start}}^{t_{i,end}}}{\sum v_i \Delta t} - \gamma' = 0 \Rightarrow \\
& h_3(v, \tau_{\text{trac}}, \gamma') = 0, \tag{25}
\end{aligned}$$

where $\#trac$ is the number of traction regions, $t_{i,start}$ and $t_{i,end}$ are the start and end points in each traction region, respectively. The numerator is proportional to the difference in kinetic energy for all traction regions.

Note that the abovementioned equality constraints are calculated for the whole driving cycle and give three equality constraints, h_1 , h_2 , and h_3 corresponding to the characterizing measures of the driving cycle.

5.4 POWER AND ENERGY RECUPERATION CONSTRAINTS

To be able to solve Problem P3 in Section 4 additional constraints considering power and energy recuperation need to be added. Two power constraints together with a constraint on the amount of recuperative energy in the driving cycle will now be formulated.

POWER CONSTRAINTS

The power in each time-point in a driving cycle can be calculated from the relationship $P(t) = F(t) \cdot v(t)$ in (9). A constraint that the maximum power in (14) shall not exceed a certain maximum value, P'_{\max} , is formulated as

$$\begin{aligned}
& \max_t F(t) \cdot v(t) \leq P'_{\max} \Rightarrow (\text{discrete}) \\
& \max_i F(v_i) \cdot v_i - P'_{\max} \leq 0 \Rightarrow \\
& g_{2n+1}(v, \tau, P'_{\max}) \leq 0, \tag{26}
\end{aligned}$$

where $F(t) = F(v(t))$.

Assume that the average power in (13) shall be a certain value P'_{avg} . This yields an equality constraint as

$$\begin{aligned}
& \frac{1}{\Delta t_{\text{tot}}} \int_{t \in \tau} F(t) v(t) dt = P'_{\text{avg}} \Rightarrow (\text{discrete}) \\
& \frac{\sum_i F(v_i) v_i \Delta t}{t_{\text{end}} - t_{\text{start}}} - P'_{\text{avg}} = 0 \Rightarrow \\
& h_4(v, \tau, P'_{\text{avg}}) = 0. \tag{27}
\end{aligned}$$

RECUPERATION ENERGY CONSTRAINT

Assume that a driving cycle with target recuperative energy of E'_{recup} , see (15), is wanted. This yields the following equality constraint

$$\begin{aligned}
 & - \int_{t \in \tau_{brake}} F(t)v(t)dt = E'_{recup} \Rightarrow (discrete) \\
 & - \sum_{i \in \tau_{brake}} F(v_i)v_i\Delta t - E'_{recup} = 0 \Rightarrow \\
 & \quad h_5(v, \tau_{brake}, E'_{recup}) = 0.
 \end{aligned} \tag{28}$$

5.5 CONSTRAINTS ON THE SPEED PROFILE

Since the optimization variables are vehicle speed points in a driving cycle the nature of driving cycles limits the possible search space for the optimization variables. The lower bound is at least $v_i \geq 0$ and the upper bound can be set to the maximum speed, v_{max} , of the vehicle, that is $v_i \leq v_{max}$.

These bounds can be changed to solve certain problems. For example, assume that the idle set, τ_{idle} , shall be the same before as after the transformation. To achieve this the lower and upper bound can be set to the same value as $lb(t \in \tau_{idle}) = ub(t \in \tau_{idle}) = v(t \in \tau_{idle}) = 0$ where lb and ub are the lower and upper bound, respectively, and where v is the original driving cycle. This will ensure that the solver will output a driving cycle with the specified trajectory.

The same reasoning can be used to incorporate a certain speed profile segment, v_{spec} at τ_{spec} , as in Problem P1 in Section 4. Using $lb(t \in \tau_{spec}) = ub(t \in \tau_{spec}) = v_{spec}(t \in \tau_{spec})$. If a valid solution is found the requested speed profile will have been incorporated within the driving cycle.

5.6 COST FUNCTION

As discussed below, there are many possible choices of cost function to minimize but in this paper the used cost function is

$$f(v) = \|\ddot{v}\|_2^2. \tag{29}$$

Since $\ddot{v} = d^2v/dt^2$ is the jerk, the rate of change of acceleration, the optimization minimizes the jerk and thus gives a smooth driving cycle that increases the drivability. The cost function in (29) is used for all the problem instances in this general nonlinear optimization.

5.7 METHOD SUMMARY AND DISCUSSION

Formulating the driving cycle transformation as an NLP is an effective way to include constraints, like on the vehicle speed, as well as measures on the whole driving cycle. The equality constraints h_i in (18) can be used together

with Definition 1 where two driving cycles are equivalent with respect to some measures if these measures are identical for the two driving cycles. The inequality constraints are more of the type that the driving cycle shall be feasible, e.g., by not exceeding the maximum acceleration as formulated in (22) or keeping the traction and non-traction regions as in (20) and (21). Regarding the cost function it should first be recalled that it is an alternative to the equation based approach in (Nyberg et al., 2013). Further, that there are many possible alternatives for cost functions where one can think of variations that have more or less of a smoothing character. Here, the cost function used is the vehicle jerk which yields driving cycles that are smooth and thus have good drivability. Still, since the NLP formulation is general there are many more alternatives for cost functions to explore.

6 RESULTS

To illustrate the proposed methodology, the three problem instances that were introduced in Section 4 will be solved. Given a driving cycle, v , and a set of vehicle parameters according to Table 1, the optimization formulation in (18) will be used with different constraints.

Table 1: Parameters for the vehicle model.

Parameter	Unit	Description
$A_f = 2.15$	$[\text{m}^2]$	Frontal area
$c_d = 0.4$	$[-]$	Drag coefficient
$c_r = 0.013$	$[-]$	Rolling resistance coefficient
$m = 1600$	$[\text{kg}]$	Vehicle mass
$\rho_a = 1.29$	$[\text{kg}/\text{m}^3]$	Air density
$g = 9.81$	$[\text{m}/\text{s}^2]$	Gravitational constant

When solving Problem P1, the vehicle excitation regarding the MTF components shall remain the same while a specified speed profile for a certain sub-interval will be incorporated within the NEDC. When solving Problem P2, different driving cycles will have their vehicle excitation changed to another vehicle excitation with respect to the MTF components. The examples in this paper are to transform the NEDC and FTP75 to have the same vehicle excitation as each other. Additionally, a real-world driving cycle will also be transformed to be equivalent to NEDC. When solving Problem P3 additional constraints on the maximum power, average power and amount of energy for recuperation will be considered in the optimization. In that case the given driving cycle will be the NEDC and the output driving cycle will be a transformed variant of NEDC that fulfills the additional constraints.

For all problem instances presented here the traction and non-traction regions will be retained and for illustrative reasons the idling regions have remain unchanged during the transformations. The maximum acceleration will be

considered by using $a_{\max}(v_i)$ as defined in Section 5.2. That is, the constraints (20) - (22) will be used in all the problem instances. The use of the other constraints, listed in (23)-(28) will vary from problem instance to problem instance.

The problems have been solved in Matlab with its function `fmincon` using an interior-point solver. The maximum functions evaluations was set to 30000 and each problem instances takes around 1-2 minutes to solve using a standard computer that has an Intel quad-core CPU of 2.66 GHz and a memory of 3.7 GB.

6.1 INCORPORATING A SPEED PROFILE - P1

Given the NEDC, assume that a designer wants to incorporate a different speed profile segment starting at time $t = 1072$. The segment, v_{spec} at $\tau_{\text{spec}} = [1072, 1088]$, to be incorporated within the NEDC, contains an acceleration from 70 to 120 km/h which corresponds the normal maximum acceleration in Section 5.2. This will result in that the acceleration performance of the vehicle that follows the new driving cycle will be tested harder, but for reasons of comparison the excitation should be the same. In Figure 2 the resulting driving cycle, \tilde{v} , from the optimization is shown as the solid line. The dashed line corresponds to NEDC and the difference in vehicle speed for the incorporated speed profile is clearly visible. These driving cycles are equivalent with respect to the characterizing measures. For vehicle parameters according to Table 1 the NEDC have the following characterizing measures $(\alpha_{\text{NEDC}}, \beta_{\text{NEDC}}, \gamma_{\text{NEDC}}) = (317.1, 0.86, 0.11)$ and the equivalent version with the incorporated speed profile have a difference of $(1.3 \cdot 10^{-5}, 9.6 \cdot 10^{-5}, 0.02)$ % in the characterizing measures. Thus, a negligible difference compared to the NEDC.

The total distance traveled, x_{tot} , is higher in \tilde{v} but the two cycles are still equivalent with respect to the characterizing measures since the optimization raised the vehicle speed in the equivalent version of NEDC to compensate the change in x_{tot} .

COMPUTATIONAL COMPLEXITY

The sampling time is one second and since the length of the NEDC is 1220 seconds and each vehicle speed in traction and non-traction is considered this results in 1220 different inequality constraints. Each speed point shall not exceed the maximum acceleration resulting in additional 1220 different inequality constraints. Three equality constraints were here used h_1 , h_2 , and h_3 from (23)-(25). The numbers of optimization variables are equal to the length of the driving cycle, that is 1220. However, 333 of these are in idle and additional 17 speed points originates from the incorporated speed profile. This results in that the number of optimization variables that the method can change freely, considering the constraints, are 870 in this case and there are 2400 inequality and 3 equality constraints to fulfill.

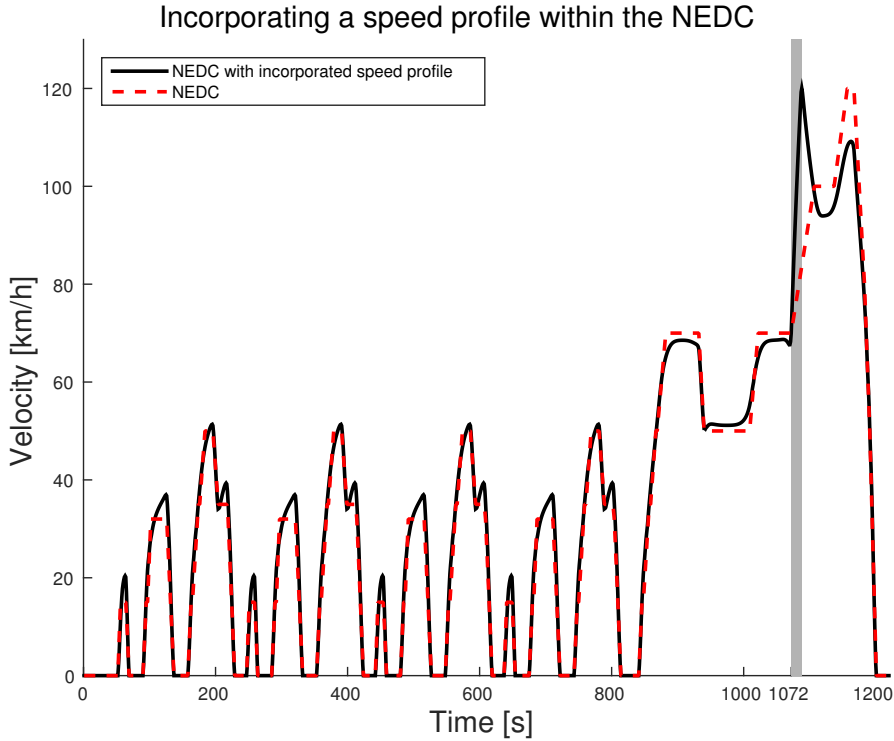


Figure 2: NEDC (dashed) with an NEDC equivalent version (solid) with respect to the characterizing measures where a specified speed profile, v_{spec} , have been incorporated and is highlighted at $\tau_{\text{spec}} = [1072, 1088]$.

6.2 TRANSFORMATION TO EQUIVALENT DRIVING CYCLES - P2

For illustrative purposes, the certification driving cycles, FTP75 and NEDC, will be transformed to a corresponding equivalent counterpart of each other, and thus be a solution for Problem P2. A more important use of P2 is as a component in data-driven driving cycle generation. Therefore, in addition, a generated real-world driving cycle from the driving cycle generator presented in (Nyberg et al., 2014) will be transformed to be equivalent to NEDC.

TRANSFORMING FTP75 TO NEDC

Originally, for vehicle parameters according to Table 1 the FTP75 have the following characterizing measures $(\alpha_{\text{FTP75}}, \beta_{\text{FTP75}}, \gamma_{\text{FTP75}}) = (223.3, 0.79, 0.15)$. The corresponding values for NEDC and also the target values in the optimization are $(\alpha', \beta', \gamma') = (\alpha_{\text{NEDC}}, \beta_{\text{NEDC}}, \gamma_{\text{NEDC}}) = (317.1, 0.86, 0.11)$. This means that the constraints in (23) - (25), $h_1(v, \tau_{\text{trac}}, \alpha') = 0$, $h_2(v, \tau_{\text{trac}}, \beta') = 0$, and $h_3(v, \tau_{\text{trac}}, \gamma') = 0$ will be used together with the constraints in (20) - (22).

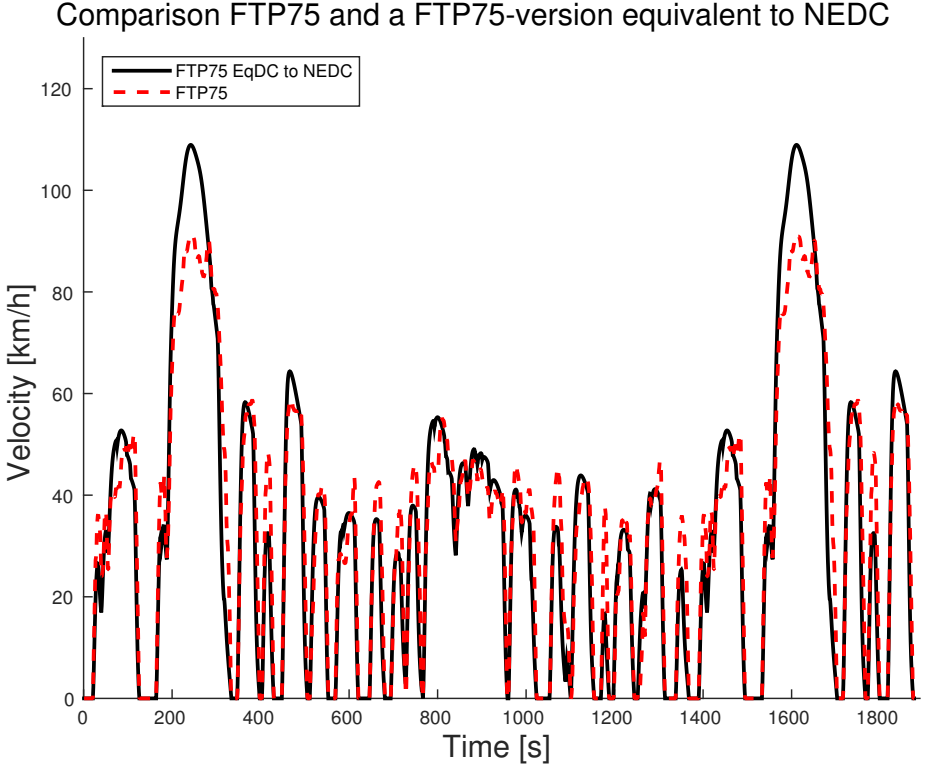


Figure 3: FTP75 (dashed) and its equivalent version to NEDC (solid).

The resulting driving cycle, \tilde{v} , from the optimization is shown in Figure 3. The dashed line corresponds to the FTP75 and the solid line correspond to \tilde{v} that is equivalent to NEDC, respectively. Since both α and β need to be raised in the transformation the vehicle speed in the traction region need to be raised which can be seen by the increase in vehicle speed in the figure. Due to the transient behavior in the FTP75 the value of γ is quite high and reflects that the driving cycle contains more accelerations followed by a coasting or braking region compared to the NEDC. The difference in the characterizing measures between the transformed FTP75 and NEDC are $(3.5 \cdot 10^{-5}, 2.8 \cdot 10^{-5}, 0.0054)$ %. The minimization of the cost function yields a minimization of the jerk in the driving cycle which is seen in the figure as the FTP75 has more changes in acceleration compared to the output from the optimization.

TRANSFORMING NEDC TO FTP75

Here the NEDC will be transformed to be equivalent to FTP75. The resulting equivalent version is seen in Figure 4 where the dashed line is the NEDC and

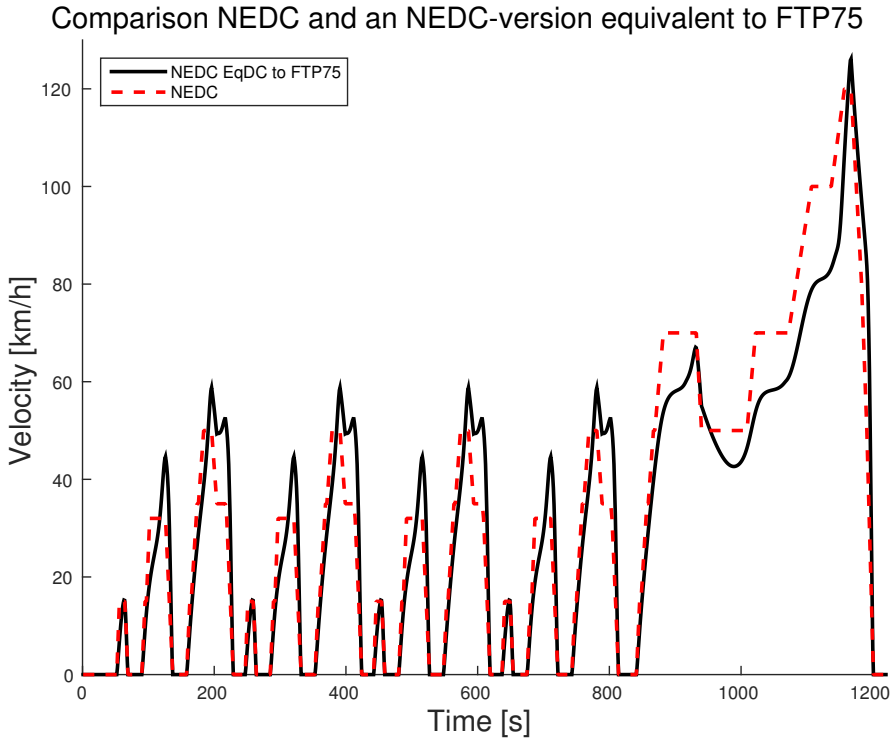


Figure 4: NEDC (dashed) and its equivalent version to FTP75 (solid).

the solid line is a driving cycle that is equivalent to FTP75.

Even if the mean speed in the FTP75 is higher than in the NEDC, (34.1 vs 33.6 km/h) the vehicle excitation constraints in (23) - (25) only consider vehicle speed in traction. To fulfill the constraints the vehicle speed need to be reduced during the traction regions, as can be seen have been done in the figure. The resulting driving cycle, \tilde{v} , have the following characterizing measures $(\alpha, \beta, \gamma) = (223.3, 0.79, 0.15)$ and the deviation compared to the target values are $(1.6 \cdot 10^{-4}, 1.3 \cdot 10^{-4}, 2.8 \cdot 10^{-4}) \%$.

The minimization of the jerk is even more visible in this case. The driving cycle is smooth with fewer sharp edges compared to the NEDC.

REAL-WORLD DRIVING CYCLE

An important application of the method is to be used as a component in driving cycle generation tools where the generated driving cycle in addition to be representative to the database is desired to have equivalence properties. As an example, with the data-driven driving cycle generator in (Nyberg et al., 2014) a real-world driving database has been used to generate a driving cycle that

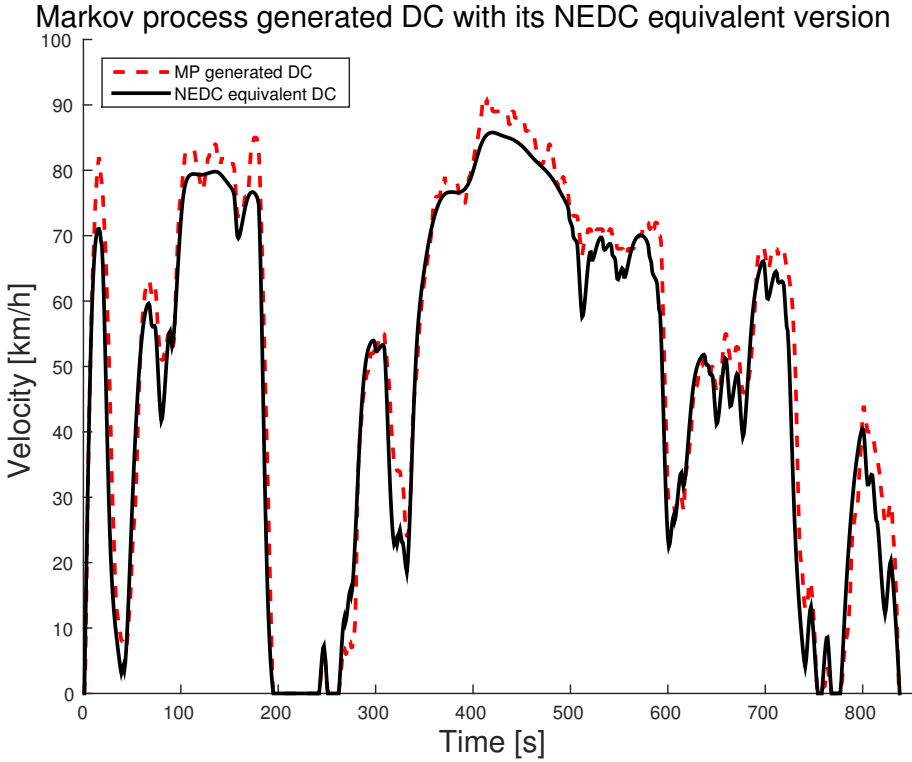


Figure 5: A generated driving cycle (dashed) and its corresponding NEDC equivalent version (solid).

is representative for the data in the database. In a next step it is desired for this driving cycle to be equivalent to NEDC, i.e. to have the same excitation as NEDC. The generated driving cycle has the following characterizing measures $(\alpha, \beta, \gamma) = (332.0, 0.855, 0.111)$. That driving cycle can be seen in Figure 5 as the dashed line. Then the method has been applied and the resulting driving cycle, that is equivalent to NEDC, is the solid line in the figure. Compared to the generated driving cycle the equivalent driving cycle is much smoother and is equivalent to NEDC. The differences in the characterizing measures between the resulting driving cycle (solid line) in the figure and the NEDC are $(2.2 \cdot 10^{-4}, 0.01, 0.009)$ %.

6.3 CHANGING THE POWER AND ENERGY IN A DRIVING CYCLE - P3

When solving Problem P3, power and energy constraints also need to be considered. It will be illustrated by keeping the characterizing measures while the

average power, maximum power, and amount of recuperative energy will be changed in the NEDC. The additional constraints used here are (23)-(28).

NEDC WITH POWER AND RECUPERATION CONSTRAINTS

The amount of recuperate energy in NEDC for a vehicle with parameters according to Table 1 is $E_{\text{recup}} = 1.33$ MJ, the maximum power is $P_{\text{max}} = 41.8$ kW, and the average power is $P_{\text{avg}} = 3.66$ kW.

Using the methodology the NEDC is transformed to a driving cycle that has 20% higher available recuperation energy, that is $E'_{\text{recup}} = 1.597$ MJ while the power constraints are set to $P'_{\text{max}} = 40$ kW and $P'_{\text{avg}} = 4.0$ kW, respectively.

The resulting driving cycle, \tilde{v} , from the optimization is seen in Figure 6. To get more available recuperation energy the vehicle needs to brake harder in the braking regions and increasing the average power causes a raise in the vehicle speed and thus the traveled distance. This has to be compensated by the method to fulfill the constraints regarding vehicle excitation in (23)-(25). The resulting driving cycle, \tilde{v} , have the following measures, $P_{\text{max}} = 38.81$ kW, $P_{\text{avg}} = 4.000$ kW, and $E_{\text{recup}} = 1.597$ MJ. For the average power and amount of recuperative energy, which are equality constraints the deviation are 0.0027 % and 0.009 %, respectively, which are negligible differences. The difference in the characterizing measures between the solid line in Figure 6 and the NEDC (dashed line) are (0.006, $1.6 \cdot 10^{-6}$, 0.05) %.

In conclusions, non-trivial equivalence transformations are conveniently performed in one optimization problem.

7 CONCLUSIONS

Driving cycles play a fundamental role in vehicle design and are therefore important in the vehicle development process. We have presented a novel method to transform a given driving cycle to a new driving cycle that fulfills a number of constraints. The constraints used can for example be related to the excitation of the vehicle, be that certain speed profile segments shall be incorporated within the existing driving cycle, or that the vehicle operating regions shall be intact during the transformation. In this paper vehicle excitation mainly regards the mean tractive force components, but can also include other types of measures such as average power or amount of recuperation energy in the braking regions. The transformation of the driving cycle was formulated as a nonlinear program where the optimization variables are the vehicle speed points in the driving cycle. By using vehicle jerk as cost function the drivability of the driving cycle is simultaneously increased. An algorithm in Matlab was implemented and to illustrate the method, equivalence among driving cycles was defined and three problems were formulated and solved.

The novel method is general, easy to use, and not restricted to the constraints used in this paper. The level of modification can be controlled and directed to

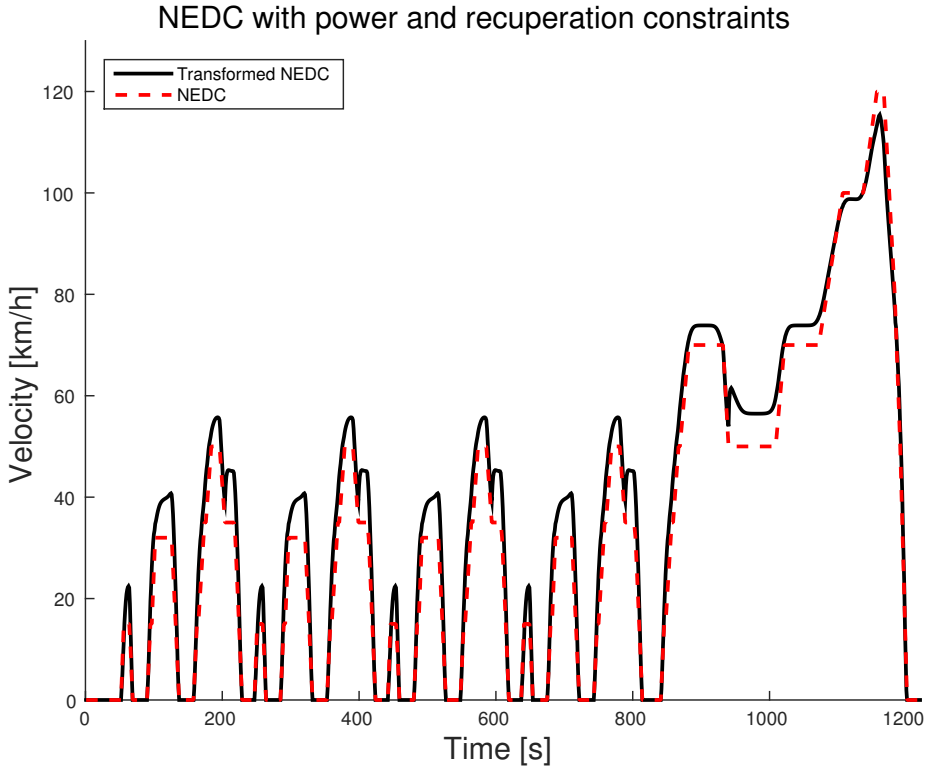


Figure 6: NEDC (dashed) together with a transformed NEDC (solid) that have different measures regarding the amount of recuperation, maximum power and average power.

parts of the driving cycle of specific interest. The method shows great potential and versatility, and solved every problem within a few minutes. The authors foresee that the method will be used in future driving cycle design, to test the robustness and sensitivity of the controls of the vehicle, and as a component in data-driven driving cycle generation with equivalence properties.

In conclusion, for a wide set of useful equivalence formulations for driving cycles, approaching the important problem of similar but not the same, the nonlinear program with jerk as cost function effectively gives solutions to real-world problems. The method is straightforward to use together with data-driven methods for finding representative driving cycles, and all in all it gives an effective engineering tool for all these problems.

REFERENCES

- M. André and M. Rapone. Analysis and modelling of the pollutant emissions from European cars regarding the driving characteristics and test cycles. *Atmospheric Environment*, 43(5):986–995, 2009.
- M. André. Driving cycles development: Characterization of the methods. In *SAE Technical Paper 961112*, 1996.
- M. André. The ARTEMIS European driving cycles for measuring car pollutant emissions. *Science of The Total Environment*, 334-335(0):73–84, 2004.
- M. André, R. Joumard, R. Vidon, P. Tassel, and P. Perret. Real-world European driving cycles, for measuring pollutant emissions from high- and low-powered cars. *Atmospheric Environment*, 40(31):5944–5953, 2006. 13th International Symposium on Transport and Air Pollution (TAP-2004).
- A. Ashtari, E. Bibeau, and S. Shahidinejad. Using large driving record samples and a stochastic approach for real-world driving cycle construction: Winnipeg driving cycle. *Transportation Science*, 48(2):170–183, 2014.
- R. Carlson, H. Lohse-Busch, M. Douba, and N. Shidore. Drive cycle fuel consumption variability of plug-in hybrid electric vehicles due to aggressive driving. In *SAE Technical paper 2009-01-1335*, Detroit, USA, 2009.
- C. Chan, C. Nien, C. Tsai, and G. Her. Comparison of tail-pipe emissions from motorcycles and passenger cars. *Journal of the Air and Waste Management Association*, 45(2):116–124, 1995.
- T. D. Durbin, R. D. Wilson, J. M. Norbeck, J. Miller, T. Huai, and S. H. Rhee. Estimates of the emission rates of ammonia from light-duty vehicles using standard chassis dynamometer test cycles. *Atmospheric Environment*, 36(9):1475–1482, 2002.
- E. Ericsson. Variability in urban driving patterns. *Transportation Research Part D: Transport and Environment*, 5(5):337–354, 2000.
- E. Ericsson. Independent driving pattern factors and their influence on fuel-use and exhaust emission factors. *Transportation Research Part D: Transport and Environment*, 6(5):325–345, 2001.
- G. Fontaras, G. Karavalakis, M. Kousoulidou, T. Tzankiozis, L. Ntziachristos, E. Bakeas, S. Stournas, and Z. Samaras. Effects of biodiesel on passenger car fuel consumption, regulated and non-regulated pollutant emissions over legislated and real-world driving cycles. *Fuel*, 88(9):1608–1617, 2009.
- L. Fu, J. Hao, D. He, K. He, and P. Li. Assessment of vehicular pollution in China. *Journal of the Air and Waste Management Association*, 51(5):658–668, 2001.

- J.-P. Gao, G.-M. G. Zhu, E. G. Strangas, and F.-C. Sun. Equivalent fuel consumption optimal control of a series hybrid electric vehicle. *Proceedings of the Institution of Mechanical Engineers, Part D: Journal of Automobile Engineering*, 223(8):1003–1018, 2009.
- Q. Gong, S. Midlam-Mohler, V. Marano, and G. Rizzoni. An iterative markov chain approach for generating vehicle driving cycles. *SAE International Journal of Engines*, 4(1):1035–1045, 2011.
- L. Guzzella and A. Sciarretta. *Vehicle Propulsion System: Introduction to Modeling and Optimization*. Springer, 2007.
- J. Hellgren and E. Jonasson. Maximisation of brake energy regeneration in a hybrid electric parallel car. *International Journal of Electric and Hybrid Vehicles*, 1(1):95–121, 2007.
- A. Jaafar, B. Sareni, and X. Roboam. A systemic approach integrating driving cycles for the design of hybrid locomotives. *IEEE Transactions on Vehicular Technology*, 62(8):3541–3550, 2013.
- A. Kean, R. Harley, and G. Kendall. Effects of vehicle speed and engine load on motor vehicle emissions. *Environmental Science and Technology*, 37(17):3739–3746, 2003.
- J. Kent, G. Allen, and G. Rule. A driving cycle for Sydney. *Transportation Research*, 12(3):147–152, 1978.
- M. Koot, J. Kessels, B. de Jager, W. Heemels, P. van den Bosch, and M. Steinbuch. Energy management strategies for vehicular electric power systems. *IEEE Transactions on Vehicular Technology*, 54(3):771–782, May 2005.
- A. Kristensson, C. Johansson, R. Westerholm, E. Swietlicki, L. Gidhagen, U. Wideqvist, and V. Vesely. Real-world traffic emission factors of gases and particles measured in a road tunnel in Stockholm, Sweden. *Atmospheric Environment*, 38(5):657–673, 2004.
- R. E. Kruse and T. A. Huls. Development of the federal urban driving schedule. In *SAE Technical Paper 730553*, 1973.
- T.-K. Lee and Z. Filipi. Synthesis of real-world driving cycles using stochastic process and statistical methodology. *International Journal of Vehicle Design*, 57(1):17–36, 2011.
- B. Liaw and M. Dubarry. From driving cycle analysis to understanding battery performance in real-life electric hybrid vehicle operation. *Journal of Power Sources*, 174(1):76–88, 2007.
- J. Lin and D. Niemeier. An exploratory analysis comparing a stochastic driving cycle to California’s regulatory cycle. *Atmospheric Environment*, 36(38):5759–5770, 2002.

- C. Manzie, H. Watson, and S. Halgamuge. Fuel economy improvements for urban driving: Hybrid vs. intelligent vehicles. *Transportation Research Part C: Emerging Technologies*, 15(1):1–16, 2007.
- C. N. Maxoulis, D. N. Tsinoglou, and G. C. Koltsakis. Modeling of automotive fuel cell operation in driving cycles. *Energy Conversion and Management*, 45(4):559–573, 2004.
- N. Murgovski, L. Johannesson, J. Sjöberg, and B. Egardt. Component sizing of a plug-in hybrid electric powertrain via convex optimization. *Mechatronics*, 22(1):106–120, 2012.
- K. Nesamani and K. Subramanian. Impact of real-world driving characteristics on vehicular emissions. *JSME International Journal, Series B: Fluids and Thermal Engineering*, 49(1):19–26, 2006.
- P. Nyberg, E. Frisk, and L. Nielsen. Driving cycle adaption and design based on mean tractive force. In *Proceedings of 7th IFAC Symposium on Advances in Automotive Control*, volume 7, pages 689–694, Tokyo, Japan, 2013.
- P. Nyberg, E. Frisk, and L. Nielsen. Generation of equivalent driving cycles using markov chains and mean tractive force components. In *Proceedings of 19th IFAC World Congress*, volume 19, pages 8787–8792, Cape Town, South Africa, 2014.
- P. Nyberg, E. Frisk, and L. Nielsen. Using real-world driving databases to generate driving cycles with equivalence properties. 2015. Submitted for journal publication.
- S. Onoda and A. Emadi. PSIM-based modeling of automotive power systems: Conventional, electric, and hybrid electric vehicles. *IEEE Transactions on Vehicular Technology*, 53(2):390–400, March 2004.
- J. Park, Z. Chen, L. Kiliaris, M. Kuang, M. Masrur, A. Phillips, and Y. Murphey. Intelligent vehicle power control based on machine learning of optimal control parameters and prediction of road type and traffic congestion. *IEEE Transactions on Vehicular Technology*, 58(9):4741–4756, 2009.
- L. Pelkmans and P. Debal. Comparison of on-road emissions with emissions measured on chassis dynamometer test cycles. *Transportation Research Part D: Transport and Environment*, 11(4):233–241, 2006.
- P. Pisu and G. Rizzoni. A comparative study of supervisory control strategies for hybrid electric vehicles. *IEEE Transactions on Control Systems Technology*, 15(3):506–518, May 2007.
- M. Pourabdollah, N. Murgovski, A. Grauers, and B. Egardt. Optimal sizing of a parallel PHEV powertrain. *IEEE Transactions on Vehicular Technology*, 62(6):2469–2480, 2013.

- V. Schwarzer and R. Ghorbani. Drive cycle generation for design optimization of electric vehicles. *IEEE Transactions on Vehicular Technology*, 62(1):89–97, 2013.
- S. Shahidinejad, E. Bibeau, and S. Filizadeh. Statistical development of a duty cycle for plug-in vehicles in a North American urban setting using fleet information. *IEEE Transactions on Vehicular Technology*, 59(8):3710–3719, 2010.
- R. Smith, S. Shahidinejad, D. Blair, and E. Bibeau. Characterization of urban commuter driving profiles to optimize battery size in light-duty plug-in electric vehicles. *Transportation Research Part D: Transport and Environment*, 16(3):218–224, 2011.
- G. Souffran, L. Miegerville, and P. Guerin. Simulation of real-world vehicle missions using a stochastic markov model for optimal powertrain sizing. *IEEE Transactions on Vehicular Technology*, 61(8):3454–3465, 2012.
- S. Stockar, V. Marano, M. Canova, G. Rizzoni, and L. Guzzella. Energy-optimal control of plug-in hybrid electric vehicles for real-world driving cycles. *IEEE Transactions on Vehicular Technology*, 60(7):2949–2962, 2011.
- E. Tate, M. Harpster, and P. Savagian. The electrification of the automobile: From conventional hybrid, to plug-in hybrids, to extended-range electric vehicles. *SAE International Journal of Passenger Cars - Electronic and Electrical Systems*, 1(1):156–166, 2008.
- E. Tazelaar, J. Bruinsma, B. Veenhuizen, and P. van den Bosch. Driving cycle characterization and generation, for design and control of fuel cell buses. *World Electric Vehicle Journal*, 3(1), 2009.
- H. Tong, W. Hung, and C. Cheung. Development of a driving cycle for Hong Kong. *Atmospheric Environment*, 33(15):2323–2335, 1999.
- Q. Wang, H. Huo, K. He, Z. Yao, and Q. Zhang. Characterization of vehicle driving patterns and development of driving cycles in Chinese cities. *Transportation Research Part D: Transport and Environment*, 13(5):289–297, 2008.
- W. Wang, D. Lyons, N. Clark, M. Gautam, and P. Norton. Emissions from nine heavy trucks fueled by diesel and biodiesel blend without engine modification. *Environmental Science and Technology*, 34(6):933–939, 2000.
- R. Wolfson and J. Gower. The role of computer modeling and simulation in electric and hybrid vehicle research and development. *IEEE Transactions on Vehicular Technology*, 32(1):62–73, Feb 1983.
- J.-M. Zaccardi and F. Le Berr. Analysis and choice of representative drive cycles for light duty vehicles - Case study for electric vehicles. *Proceedings of the Institution of Mechanical Engineers, Part D: Journal of Automobile Engineering*, 2012.

E. Zervas and G. Bikas. Impact of the driving cycle on the NO_x and particulate matter exhaust emissions of diesel passenger cars. *Energy and Fuels*, 22(3): 1707–1713, 2008.

Linköping Studies in Science and Technology, Dissertations
Division of Vehicular Systems
Department of Electrical Engineering
Linköping University

- No 1** Magnus Pettersson, *Driveline Modeling and Control*, 1997.
- No 2** Lars Eriksson, *Spark Advance Modeling and Control*, 1999.
- No 3** Mattias Nyberg, *Model Based Fault Diagnosis: Methods, Theory, and Automotive Engine Applications*, 1999.
- No 4** Erik Frisk, *Residual Generation for Fault Diagnosis*, 2001.
- No 5** Per Andersson, *Air Charge Estimation in Turbocharged Spark Ignition Engines*, 2005.
- No 6** Mattias Krysanter, *Design and Analysis of Diagnosis Systems Using Structural Methods*, 2006.
- No 7** Jonas Biteus, *Fault Isolation in Distributed Embedded Systems*, 2007.
- No 8** Ylva Nilsson, *Modelling for Fuel Optimal Control of a Variable Compression Engine*, 2007.
- No 9** Markus Klein, *Single-Zone Cylinder Pressure Modeling and Estimation for Heat Release Analysis of SI Engines*, 2007.
- No 10** Anders Fröberg, *Efficient Simulation and Optimal Control for Vehicle Propulsion*, 2008.
- No 11** Per Öberg, *A DAE Formulation for Multi-Zone Thermodynamic Models and its Application to CVCP Engines*, 2009.
- No 12** Johan Wahlström, *Control of EGR and VGT for Emission Control and Pumping Work Minimization in Diesel Engines*, 2009.
- No 13** Anna Pernestål, *Probabilistic Fault Diagnosis with Automotive Applications*, 2009.
- No 14** Erik Hellström, *Look-ahead Control of Heavy Vehicles*, 2010.
- No 15** Erik Höckerdal, *Model Error Compensation in ODE and DAE Estimators with Automotive Engine Applications*, 2011.

- No 16** Carl Svärd, *Methods for Automated Design of Fault Detection and Isolation Systems with Automotive Applications*, 2012.
- No 17** Oskar Leufvén, *Modeling for Control of Centrifugal Compressors*, 2013.
- No 18** Christofer Sundström, *Model Based Vehicle Level Diagnosis for Hybrid Electric Vehicles*, 2014.
- No 19** Andreas Thomasson, *Modeling and Control of Actuators and Co-Surge in Turbocharged Engines*, 2014.
- No 20** Emil Larsson, *Model Based Diagnosis and Supervision of Industrial Gas Turbines*, 2014.
- No 21** Andreas Myklebust, *Dry Clutch Modeling, Estimation, and Control*, 2014.
- No 22** Tomas Nilsson, *Optimal Predictive Control of Wheel Loader Transmissions*, 2015.